Investigation on Synthesis: Structure & Characterization of Some Novel Copper (II) and Iridium (III) complexes: Biological activities and DFT studies

THESIS SUBMITTED FOR THE

DEGREE OF DOCTOR OF PHILOSOPHY (SCIENCE)

OF

JADAVPUR UNIVERSITY

JANUARY, 2025

By

SUPRIYA DEBNATH

DEPARTMENT OF CHEMISTRY

JADAVPUR UNIVERSITY

JADAVPUR

K0LKATA-700032

INDIA

2025

Prof. Kajal Krishna Rajak,
Professor,
Department of Chemistry

JADAVPUR UNIVERSITY
KOLKATA - 7 0 0 0 3 2, I N D I A
E-mail:
kajalk.rajak@jadavpuruniversity.in
Mobile: +91-9830905167

CERTIFICATE FROM THE SUPERVISOR

This is to certify that the thesis entitled **"Investigation on Synthesis: Structure & Characterization of Some Novel Copper (II) and Iridium (III) complexes: Biological activities and DFT studies"** submitted by **Mr. Supriya Debnath** who got his name registered on **30.01.2018 (Index No: 7/18/Chem./25)** for the award of **Ph.D. (Science) degree** of **Jadavpur University**, is absolutely based upon his own work under my direct supervision and that neither this thesis nor any part of it has been submitted for either any degree / diploma or any other academic award anywhere before.

Date: ---------- 15th January 2025

Kajal Krishna Rajak

(Prof. Kajal Krishna Rajak)

Signature of the Supervisor & date with seal

Department of Chemistry
Jadavpur University
Kolkata 700 032

Dr Kajal Krishna Rajak
Professor of Chemistry
Jadavpur University
Kolkata-700032

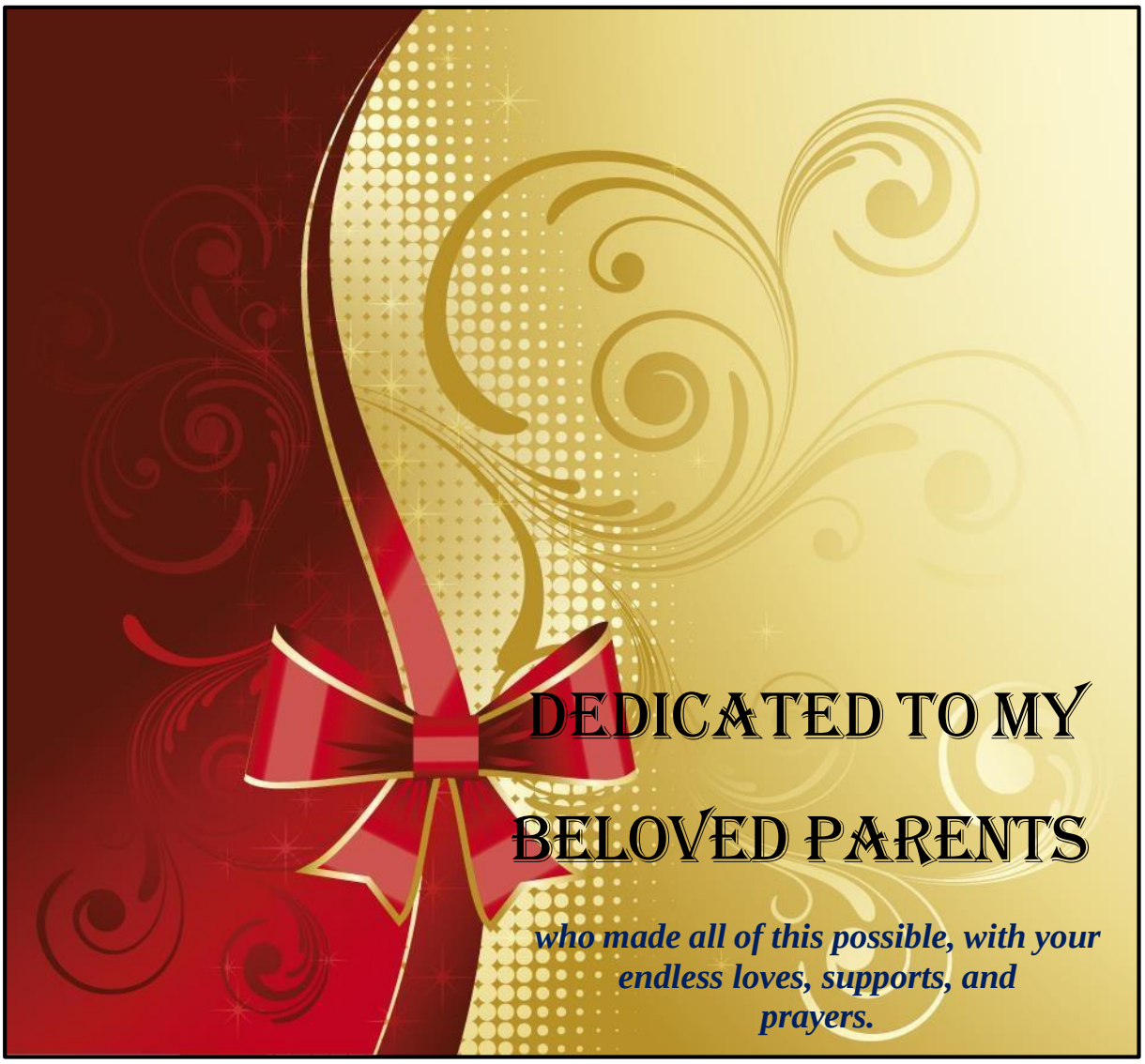
DEDICATED TO MY
BELOVED PARENTS
who made all of this possible, with your endless loves, supports, and prayers.

Preface

The work presented in this thesis entitled **''Investigation on Synthesis: Structure & Characterization of Some Novel Copper (II) and Iridium (III) complexes: Biological activities and DFT studies''** was initiated in January, 2018 and have been carried out in the Department of Chemistry, Jadavpur University.

The thesis consists of five chapters which are summarized below.

Chapter 1 contains summary of the work presented in this thesis with short description of the physical methods and equipment employed.

Chapter 2 describes the synthesis and characterization of a heteroleptic iridium(III) complex, $[Ir(2\text{-}ppy)_2(L)]PF_6$ with a ligand bearing azo (N=N) linkage. Here the azo-ligand is coordinated to iridium(III) center as monoanionic bidentate N,O-donors. Molecular structures of both the ligand and complex were confirmed by single-crystal X-ray diffraction. The ground and excited-state geometries, absorption, and emission properties of the iridium(III) complex were further examined by DFT and TD-DFT methods. The complex exhibits a blue- violet emission band at 395 nm with quantum yield (Φ) 0.06. Experimental and theoretical studies support the fact that the nature of emission is an admixture of ^{3}IL and ^{3}MLCT state.

Chapter 3 deals with the synthesis and characterization of an iridium(III) complex of composition $[Ir(2\text{-}ppy)_2(L)]PF_6$. Here, the iridium centre is bound to neutral bidentate N, N donating sites of the ligand (L), where the azo part of L is not involved in chelation. The ligand and complex are characterized by elemental analysis, NMR spectroscopy, ESI-MS mass spectrometry, FTIR, UV–Vis and luminescence spectroscopic techniques. The ligand structure and the geometry around iridium centre of complex $[Ir(2\text{-}ppy)_2(L)]PF_6$ is confirmed by the single-crystal X-ray diffraction (XRD) method. DFT studies were also performed to support the experimental aspects of the complex as well as electronic distribution in molecular orbitals of various energy states. The complex exhibits blue emission band at 428 nm with quantum yield (Φ) 0.136. Further, in vitro analysis of the anticancer activity of the complex was studied mainly with the MCF - 7 cell line. The results showed that the complex have good IC_{50} values when compared to the standard drug cisplatin.

Chapter 4 describes synthesis and characterization of a copper(II) complex of composition $[(L)_2Cu]$. The ligand HL binds the Cu(II) centre in bidentate (N,O) fashion being uninegative

anion by the way of phenolic proton dissociation during chelation. The complex was characterized by spectroscopic studies. X-Ray structures of $[(L)_2Cu]$ was determined to confirm the molecular species unequivocally. The photoluminescence properties of the ligand and complex were studied. Oxidation of benzyl alcohol using the newly synthesized complex as catalyst has been studied.

Chapter 5 deals with the synthesis and characterization of a new copper(II) complex, which was derived from the reaction of $Cu(OAc)_2$. H_2O with 2-hydroxy-5-methyl-3-(((4-((E)-phenyldiazenyl)phenyl)imino)methyl) ligand (HL_1). The ligand reacted with copper acetate to afford the new complexes of composition $[(L_1)_2Cu]$ where it binds the Cu(II) centres in bidentate (N, O) fashion. The complexes were characterized by analytical and spectroscopic studies. X-ray structures of $[(L_1)_2Cu]$ was determined to confirm the molecular species unequivocally.

Acknowledgements

"P. G. Science Building

Ground floor, Kajal Krishna Rajak Research Lab"

The last six years were like a difficult and long test, which directed me to look over my scientific ability. While taking it, I struggled with myself not to give it up several times. This dissertation would not have been possible without the help of so many people in different way throughout my research carrier. Now I want to acknowledge those persons who played a role directly or indirectly for the successful completion of my thesis.

First and foremost, I would like to thank my supervisor, Prof. Kajal Krishna Rajak, for taking me into his lab and assigning such a challenging project to me. I also like to express my sincere gratitude to him for the continuous support, encourage and to give me confidence for my research and Ph.D. study. I am grateful for the advice and the training that he provides for me to be prepared for anything in my future endeavors and I am greatly proud of being a member of his group. I could not have imagined having a better advisor and mentor for my Ph.D. study.

I would also like to thank the Inorganic Chemistry faculty members at Jadavpur University, specially, present Dean of Science Prof. Chittaranjan Sinha, present Head, Department of Chemistry, Prof. Kajal Krishna Rajak, and Prof. Partha Roy, Sectional in-charge, Inorganic Chemistry for their kind cooperation and encouragement. I am also thankful to Prof. Samaresh Bhattacharya, Prof. Kaushikisankar Pramanik, Prof. Sujoy Baitalik, Prof. Subratanath Koner, Department of Chemistry, Jadavpur University, for providing me their laboratory facilities whenever required. I also sincerely

appreciate the constant encouragement of all the faculty members and non-teaching staffs. I am also thankful to collaborator, Dr. Nabendu Murmu, CNCI, Kolkata and his research groups (Aritri Bhattacharjee and Rahul Naskar) for helping me in my research work.

This journey would not have been possible without the support of my seniors: Dr. Sankar Prasad Parua, Dr. Amit Maity, Dr. Sohini Basuroy and Dr. Debopam Sinha. I am also grateful to the other members of my research group: Tapashi di, Mitali, Roumi, Uday, Sneha and Biswajit. The important discussions with them, dinners, outings to the short trips, general help and friendship were all greatly appreciated. I will never forget the beautiful memories and the difficulty that we shared together.

This journey would not have been complete if there was no Mihir da. To say thank you is a gross understatement.

It is a genuine pleasure to express my appreciation to my close friends for their support and encouragement during the last six years. I am indebted to my JU friends Shantanu, Writabrata, Deblina and Subarna for helping me with data analysis of my research work. I also want to express my heartfelt thanks to some of my very close friends Sayana, Rakesh, Gopal, Sagnik da, Rahul (Pantha), Shantanu (Leja), Santanu (Nuntu), Suraj (Mama), Milan (Mili), Bappa, Prasun, Mohana, Bishu, Rauth, Biman da, Tema da, Dipu da, Sona da, Deep da, Soumik da, Aradhita di and Aparajita di for providing me the company and support through every step of this journey. They were always beside me during the happy and hard moments to push me and motivate me. Without their support this journey would not be smooth and pleasant.

Finally, No thanks can be enough to acknowledge the people who mean a lot to me, my parents, Ma and Baba, for showing faith in me and giving me liberty to

choose what I wanted. I salute you all for the selfless love, care, pain and a lots of sacrifice you did to shape my life. They provide me always both the moral as well as emotional support in my life and prayers on my behalf. I would never be able to pay back the love and affection showered upon by my parents. Also I want to express a heartfelt gratitude to my dear bro Chandan, Sekhar da and sister Soma di for their selfless love, care, support and valuable prayers which contributed a lot for completion of my thesis.

I would like to thank everybody who was important to the successful insight of the thesis, as well as expressing my apology that I could not mention personally one by one.

I am also thankful to DST Inspire fellowship for the last five years to carry out my research work smoothly. I am also thankful to the authorities of the Jadavpur University for allowing me to use the necessary infrastructure.

Finally, I would like to thank the almighty for his blessing to journey of completion of my thesis.

Supriya Debnath

Department of Chemistry
Jadavpur University
Kolkata– 700 032, India.

CONTENTS

Chapter 1

Introduction

1.1 Preamble

1.1.1 Transition Metals

Transition metals are designated as those elements which have partially filled *d* orbitals. The *d*-block elements in groups 3–12 are transition elements. In addition to being of academic interest, Beyond scholarly pursuits, transition-metal complexes are valuable in today's world in a variety of fields, such as medication design, molecular electronics, biological activity, antitumor activity, light-emitting diodes, and photoelectric devices. Among the transition metals, iridium and copper have been preferred for interest of the present work.

1.1.2 Chemistry of Iridium

The chemical element iridium, represented by the symbol Ir, has atomic no. 77 with electronic configuration $[Xe]4f^{14}5d^{7}6s^{2}$. It belongs to the platinum group and is a highly hard, brittle, silvery-white transition metal. The two isotopes that are found naturally are mass numbers 191 and 192, with a relative abundance of 37.3% and 62.7%, respectively. The latter is the more prevalent of the two. Numerous organometallic compounds containing iridium are employed in research and industry catalysis.

Iridium has oxidation states ranging from +VI to +I; however, the most prevalent oxidation states in complexes are +III (d^6) and +I (d^8). Ir(III) complexes typically have an octahedral molecular geometry and are diamagnetic (low-spin), while Ir(I) complexes are often square planar. The amazing characteristics of iridium(III) metal centres, including their excellent photophysical capabilities, high photo-chemical and thermal stability, synthetic plasticity, and extensive application in light-harvesting and electroluminescent devices, have garnered significant interest.[1-10]

Phosphorescence emitters in organic light-emitting diodes (OLEDs) and, more recently, light-emitting electrochemical cells (LECs) are the primary areas of potential use for iridium complexes.[5,7,11,12] Additional uses include a range of technological areas such as sensing,[13] photoinduced reduction of H_2O to H_2,[14] multiphoton excitation for up-converted lasing, 3D data storage, and optical power limiting.[15-19] Iridium complexes belong to one of the most promising classes of anticancer activities.

Numerous cyclometalated iridium compounds that are monovalent frequently exhibit intriguing photophysical characteristics. As a result, there has been a lot of interest in this

field. Because of the long luminescence lifetimes, octahedral d^6 low-spin Ir(III) tricarbonyl complexes have been the subject of extensive research.[20-28] The iridium(III) complexes that coordinate with cyclometalating ligands have drawn a lot of interest because of their photochemical and photophysical properties.[29-31] These iridium(III) complexes have a mixed low energy excited state that includes intraligand (IL) $^3\pi-\pi^*$ excited states and low lying metal-to-ligand charge transfer (^{3}MLCT) states.[32,33] Due to strong spin-orbit coupling, resulting improved singlet-triplet mixing of cyclometalated metal complexes are powerful phosphorescent emitters having long-lived excited states.[32,33] Luminescent sensors and materials for OLED devices can be simply designed using such techniques.[34] The photochemical and photophysical features of the Ir(III) complexes can be fine-tuned by modifying the chromophoric, bidentate schiff bases, or azo ligands by conjugation in the ligand moiety.

Currently, iridium has garnered significant attention because of its electroluminescent properties, which can be utilised in the development of molecular electronic devices. Iridium(III) complexes exhibit a significant affinity for light-emitting phenomena, attributed to their robust spin-orbit coupling and the presence of rich triplet state excited states. However, by designing various Schiff base and azo ligand types with extended conjugations, as well as various cyclometalated ligands like 2-phenylpyridine, 2-phenylquinoline, and 2-benzo(h)quinoline, the structures of iridium complexes can be investigated in terms of both photophysical and electrochemical properties. Additionally, azo ligand complexes can be used as studies of cis-trans isomerism.

1.1.3 Chemistry of Copper

The Latin word "cuprum" is where the word "copper" originates. Copper is a soft, ductile metal with great electrical and thermal conductivity. In its zero oxidation state, copper has the electronic structure $[Ar]4s^13d^{10}$. It has atomic and covalent radii of 1.96 and 1.28 Å, respectively. Two significant copper isotopes, ^{63}Cu and ^{65}Cu, have relative abundances of 69.15 and 30.85%, respectively.

After iron and zinc, copper, an essential trace metal, is the most prevalent element in the human body.[35,36] Human blood has 1.0 ppm of copper, while the Earth's crust contains 50 ppm. Numerous enzymes that include copper ions serve as cofactors and sustain a range of

biological processes, including metabolism and cellular activity.[37,38] Copper is needed for key enzymes in human metabolism. Copper makes a noteworthy and important contribution to medicinal chemistry. This is because human blood plasma, a biological fluid, has a high affinity for binding copper ions.[39,40] Numerous illnesses, including Parkinson's disease, cardiovascular disorders, anaemia, and Menke's disease, are brought on by copper deficiency.[41-44] Once more, consuming too much of it poisons the body. Additionally, this leads to a number of illnesses, including Alzheimer's and Wilson's.[44,45] Therefore, it is essential to recognize copper, ideally at physiological pH. A common element, copper has a special function in coordination chemistry. Numerous coordination complexes are formed by it.[46-56] Copper coordination complexes often have octahedral, tetrahedral, or square planar geometries.

Much emphasis has also been paid to studies of mononuclear copper complexes in order to prepare new molecular-based magnetic materials and demonstrate the magneto structural connection. Additionally, a new area of basic research for a deeper comprehension of their behaviour is the theoretical study of such complexes.

1.1.4 Schiff Bases Ligands

Schiff bases are a significant ligand class that has attracted unwavering attention. They provide structural versatility and have consequences for a variety of application areas. In our present work, we consider several kinds of Schiff base ligands. Significant parts of copper (II) and Ir (III) chemistry have been enhanced by the design, synthesis, and subsequent use of these ligands. In 1864, Hugo Schiff made the first report on the preparation of Schiff base condensate.[57] **Scheme 1.1** illustrates the general synthesis pathway of a Schiff base. The nitrogen atom of an azomethine group in a Schiff base ligand has the ability to attach a metal ion. Schiff bases that have an azomethine group and one or more donor centres can also function as polydentate ligands. Several investigations have shown the exceptional biological and chemical significance of the lone pair of electrons on the nitrogen atom in a sp^2 hybrid orbital of the azomethine group.[58-60] Sprung[61], Sollenberger and Martin[62] have contributed to the development of Schiff base ligand chemistry. The variety of coordination sites, forms, functions, and sensitivity of this class of ligands makes them incredibly adaptable. All of

these characteristics combine to make them an intriguing class of ligands in coordination chemistry.

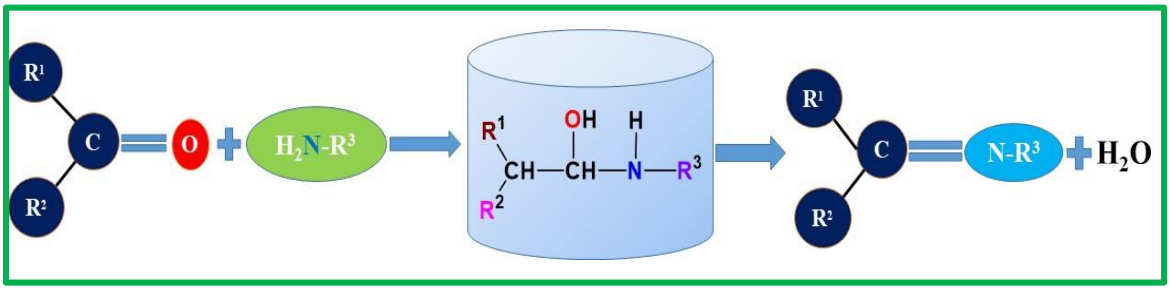

Scheme 1.1. Synthetic scheme of Schiff base formation [R^1, R^2 and R^3 are alkyl groups].

1.1.5 Aromatic Azo Ligands

Compounds with the functional group R−N=N−R′, where R and R′ can be either aryl or alkyl, are known as azo ligands. Compared to alkyl azo compounds, aryl azo compounds are more stable. Azo coupling processes, which are essentially electrophilic substitution reactions, are used to create the aromatic azo ligands or azo compounds. The azo moiety in the azo compound essentially stays in the trans isomer, but it may also undergo photochemical conversion to the cis isomer. The primary source of coordination in azo compounds is the - N=N- moiety towards the metal centre. This coordination through the nitrozen atom's low- lying, empty π* orbital, makes the azo compound a redox active ligand.

Moreover, the azo ligands are of special importance in chemical research due to the azo compound's flexible coordination. In addition to coordination through the nitrogen of the N=N bond, the azo compound's additional donor sites increase its flexibility with regard to coordination with the metal ion in metal ligand complexes. The -N=N- group in azo compounds is part of an extended delocalised electron system involving the aromatic rings, called a chromophore. This kind of chromophore in specific compounds is of greater interest to us. We are interested in this particular chemistry because this chromophore produces significant photophysical activity. In that chromophore, the pendant azo moiety experiences photophysical switching, also known as photoirradiated cis-trans isomerism, and the photoisomerization process of azo compounds is currently receiving a lot of attention.

The main focus of this thesis has been the synthesis and characterisation of several complexes of iridium (III) and copper (II) with coordinating bidentate ligands C, N, and O, N. Our

research also includes detailed theoretical explorations of all the structural and photophysical aspects.

1.2 Summary of the present work

The goal of the present work is to synthesise and characterise novel complexes of iridium (III) and copper (II) with various polydentate Schiff bases and azo ligands, as well as to examine their significant structural and photophysical characteristics. Chapter-wise brief discussion about this work is given below.

1.2.1 Chapter 2

This chapter describes the preparation of a heteroleptic iridium (III) complex with a ligand bearing azo (N=N) linkage, where the azo-ligand is coordinated to iridium(III) center as monoanionic bidentate N,O-donors. The structures of the ligand and complex $[Ir(2\text{-}ppy)_2(L)]PF_6$ were confirmed by X-ray crystallography. The study reveals that the complex displays photophysical properties having intense photoluminescence in relatively shorter wavelength region. The ground and excited-state geometries, absorption, and emission properties of the iridium(III) complex were further examined by DFT and TD-DFT methods.

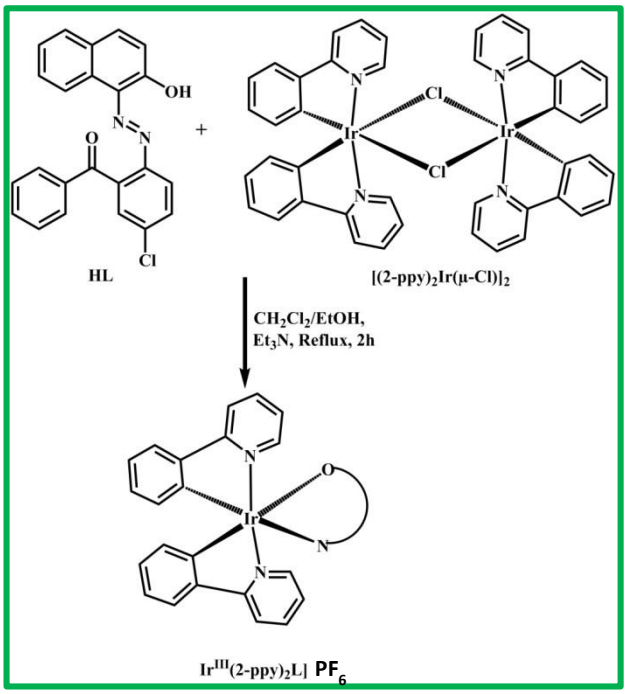

1.2.2 Chapter 3

In this chapter, a novel quinolone based Schiff base ligand and corresponding tris-cyclometalated iridum complex have been synthesized and investigated. Here, the iridium centre is bound to neutral bidentate N, N donating sites of the ligand (HL). The ligand and complex are characterized by elemental analysis, NMR spectroscopy, ESI-MS mass spectrometry, FTIR, UV–Vis and luminescence spectroscopic techniques. The ligand structure and the geometry around iridium centre of complex $[Ir(2\text{-}ppy)_2(L)]PF_6$ is confirmed by the single-crystal X-ray diffraction (XRD) method. DFT studies were also performed to support the experimental aspects of the complex as well as electronic distribution in molecular orbitals of various energy states.

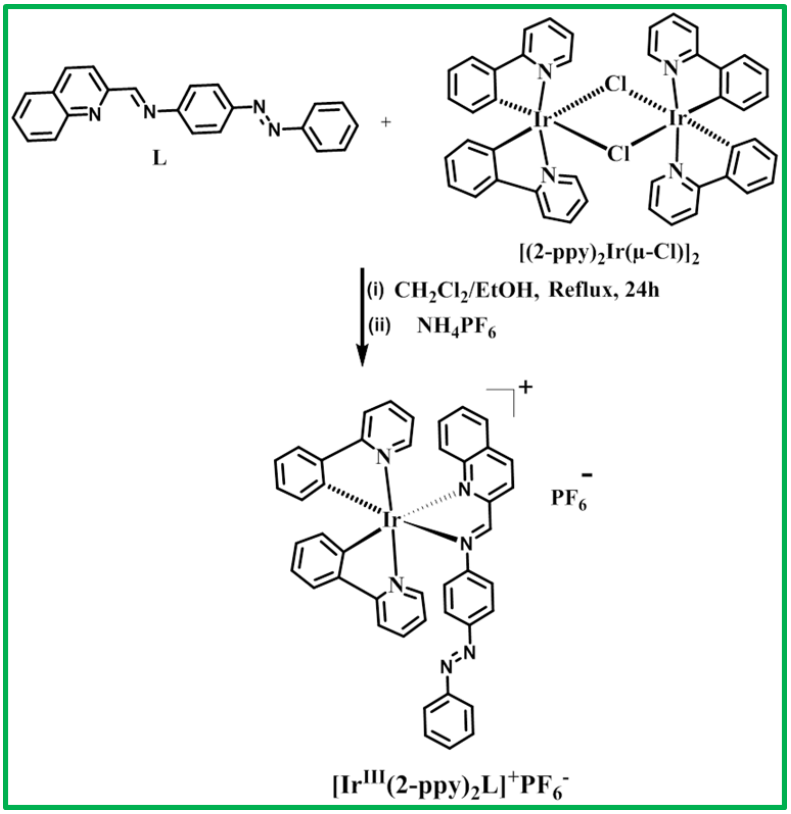

1.2.3 Chapter 4

This chapter deals with the synthesis and characterization of Schiff base copper(II) complex incorporating N, O donor ligand. The structure of the complex $[(L)_2Cu]$ was confirmed by X-ray crystallography. The complex was also characterized by various spectroscopic studies. As application, the synthesized $[(L)_2Cu]$ complex have been used as catalyst in the oxidation of

benzyl alcohol to benzaldehyde. In addition, we have also examined the fluorescence properties of the ligand and complex.

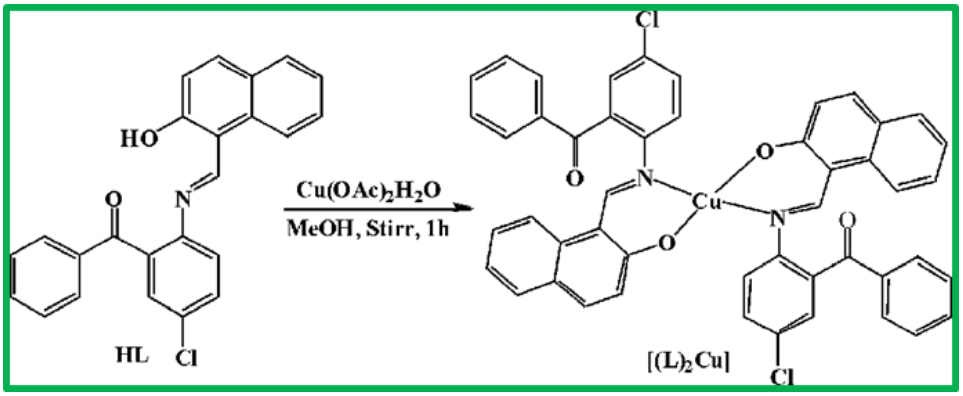

1.2.4 Chapter 5

This chapter illustrates the synthesis and characterization of a mononuclear Cu(II) complex. Here, the ligand reacted with copper acetate to afford the new complexes of composition $[(L_1)_2Cu]$, where it binds the Cu(II) centres in bidentate (N, O) fashion. X-ray structure of $[(L_1)_2Cu]$ was determined to confirm the molecular species unequivocally. The redox behaviour was also determined using EPR spectroscopy. Theoretical calculation was employed to support the experimental data.

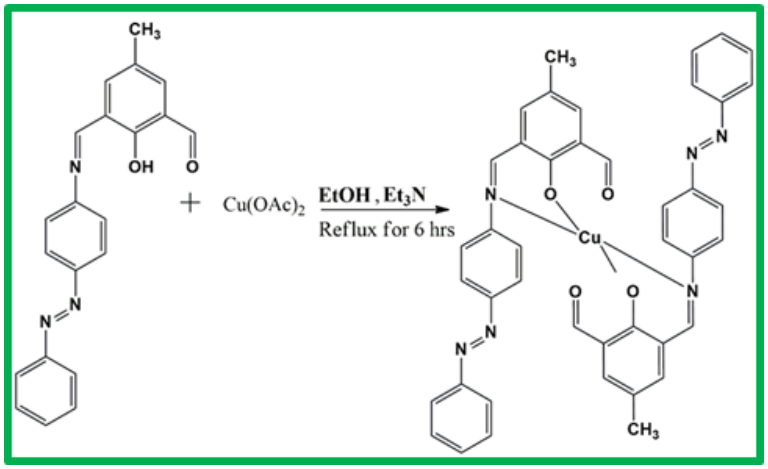

1.3 Physical Measurements

Various physical methods have been employed for the characterization and elucidation of the properties of the synthesized compounds and these are described in the subsequent chapters. These are briefly described below.

1.3.1 Elemental Analysis

The C, H, N content of the samples were determined with the help of a Perkin-Elmer 2400 Series II elemental analyzer which utilizes thermal conductivity data for gas (CO_2, H_2O, N_2) analysis. The sample (1.5-2.5 mg) was introduced into the combustion cell usually at a temperature in the range of 900–980 ºC. For combustion, pure oxygen was used and pure helium was used as the driving gas.

1.3.2 Infrared Spectra

IR spectra were recorded in KBr disk with the help of a Perkin-Elmer L-0100 spectrometer.

1.3.3 Electronic Spectra

Electronic spectra were recorded on Perkin-Elmer LAMBDA EZ-301 and a LAMBDA 25 UV/VIS spectrometer (190-1100 nm). A matched pair of quartz cells of path length 1 cm was used.

1.3.4 Electrochemical Measurements

A CHI-620A electrochemical analyzer was used for electrochemical measurements. All experiments were performed under pure nitrogen atmosphere at 295 and 298 K. The potentials are referenced to the standard calomel electrode (SCE) without junction correction. A three-electrode system consisting of a planar Beckman model 39273 platinum inlay working electrode, platinum wire auxiliary electrode and a saturated calomel electrode (SCE) were used. In every case, care was taken to obtain a flat current-voltage base line over the required voltage range in the absence of the relevant electroactive species.

1.3.5 Fluorescence Spectra

The emission data were collected on Horiba Fluoromax-4 fluorescence spectrometer. For all luminescence measurements excitation and emission slit width of 5 nm were used. Cells are same as that of the electronic spectra.

1.3.6 Quantum yields Measurements

Quantum yields of the complexes were determined in freeze-pump-thaw-degassed solutions of the complexes by a relative method using Quinine Sulfate in the same solvent as the standard.[63] The quantum yields were calculated using eq 1,[64]

$$\Phi_r = \Phi_{std} \frac{A_{std}}{A_r} \frac{I_r}{I_{std}} \frac{\eta_r^2}{\eta_{std}^2} \quad (1)$$

Where Φ_r and Φ_{std} were the quantum yields of unknown and standard samples (Φ_{std} = 0.08951 (at 298 K) in CH_3CN at λ_{ex}= 450 nm), A_r and A_{std} (<0.1) were the solution absorbances at the excitation wavelength (λ_{ex}), I_r and I_{std} were the integrated emission intensities, and η_r and η_{std} were the refractive indices of the solvent. Experimental errors in the reported luminescence quantum yields were about 10%.

1.3.7 TCSPC Measurements

Time correlated single photon counting (TCSPC) measurements were carried out for the luminescence decay of complexes in a suitable solvent. For TCSPC measurement, the photoexcitation was made at 450 nm using a picosecond diode laser (IBH Nanoled 07) in an IBH Fluorocube apparatus. The fluorescence decay data were collected on a Hamamatsu MCP photomultiplier (R3809) and were analyzed by using IBH DAS6 software.

1.3.8 Mass Spectra

Electrospray ionization mass spectrometry (ESI-MS) spectra of the samples were recorded on a Micromass Qtof YA 263 mass spectrometer.

1.3.9 NMR Spectra

^1H and ^{13}C NMR spectra were recorded in mainly $CDCl_3$, CD_3CN and DMSO-d_6 with the help of Bruker FT 300 MHz spectrometer and Bruker FT 400 MHz spectrometer, respectively using tetramethylsilane (TMS) as an internal standard depending upon the solubility of the products. Signals are assigned to individual protons on the basis of chemical shifts, spin-spin structure and substituent effects. The atom-numbering scheme used for ^1H and ^{13}C was same as that used in the crystallography.

1.3.10 Crystallographic Studies

The X-ray intensity data were collected on Bruker AXS SMART APEX CCD diffractometer (Mo Kα, λ = 0.71073 Å) at 293 K. The detector was placed at a distance 6.03 cm from the crystal. Total 606 frames were collected with a scan width of 0.3° in different settings of φ. The data were reduced in SAINTPLUS[65] and empirical absorption correction was applied using the SADABS package.[66] Metal atom was located by Patterson Method and the rest of the non-hydrogen atoms were emerged from successive Fourier synthesis. The structures were refined by full matrix least-square procedure on F^2. All non-hydrogen atoms were refined anisotropically. All calculations were performed using the SHELXTL V 6.14 program package.[67] Molecular structure plots were drawn using the Oak Ridge thermal ellipsoid plot (ORTEP).[68]

R1, wR2 and goodness-of-fit (GOF) are given by the following equations **2**, **3** and **4** respectively.

$$R1 = \Sigma \left| \left| F_o \right| - \left| F_c \right| \right| / \Sigma \left| F_o \right| \quad \text{..... (2)}$$

$$wR2 = [\Sigma[w(F^2 - F^2)^2] / \Sigma[w(F^2)^2]]^{1/2} \quad \text{.....(3)}$$

$$GOF = S = [\Sigma[w(F^2 - F^2)^2] / (n - n_p)]^{1/2} \quad \text{.....(4)}$$

n_o =number of reflections

n_p = total number of parameters refined

Specific details for each compound will be given in the concerned chapter.

1.3.11 DFT Study and Computational Details

All the quantum mechanical calculations were performed with the Gaussian 09W software package.[69] GaussSum 2.1 program[70] was used to calculate the molecular orbital contributions from groups or atoms. Figures showing MOs, NTOs and the difference density plots were prepared by using the Gauss View 5.1 software. All the calculations were carried out in IBM Intellistation Z Pro 922892A machine and Super-micro Super-server work station. The geometrical structures of the singlet ground state (S_0) and the lowest lying triplet excited state (T_1) were optimized by the DFT[71] method with B3LYP exchange correlation functional[72,73] approach. The geometry of the complexes was fully optimized in solution phase without any symmetry constraints. For H we used 6-31(g) basis set and the 6-31+G(d)[74] basis set for C, N, O, and Cl atoms for the optimization of the ground state geometries.

The vibrational frequency calculation was also performed for all the complexes to ensure that the optimized geometries represent the local minima and there are only positive eigen values. There was a good agreement between the theoretical and experimental structures. On the basis of the optimized ground and excited state geometry structures, the absorption and emission spectra properties in a particular solvent media were calculated by time-dependent density functional theory (TDDFT)[75,76] approach associated with the conductor-like polarizable continuum model (CPCM).[77,78] We computed the lowest 40 singlet – singlet transition and results of the TD calculations were qualitatively very similar. The TDDFT approach had been demonstrated to be reliable for calculating spectra properties of many transition metal complexes.[79,80] Due to the presence of electronic correlation in the TDDFT (B3LYP) method it can yield more accurate electronic excitation energies. Hence TDDFT had been shown to provide a reasonable spectral feature for our complex of investigation. Finally to understand the nature of excited states involved in absorption and emission processes natural transition orbital (NTO) analysis had been performed for all complexes. This approach provides the most compact representation of the electronic transitions in terms of an expansion into single particle orbitals by diagonalizing the transition density matrix associated with each excitation. The spin density difference map calculations were also performed to explain their optical properties.

1.4 Chemicals and Solvents

All commercially available chemicals and solvents utilized in the present work were of analytical grade and were used without further purification. For the preparation of ligands, the solvents were dried in their usual method. Purification steps, where required, will be elaborated in appropriate chapters. The chemicals required for the synthesis of ligands were purchased from MERCK (India) and Sigma Aldrich chemicals limited.

All references in this thesis are given in the following format: Name of the author(s), *Journal*, year, **volume**, page.

References

1) R. D. Costa, E. Ortí, H. J. Bolink, S. Graber, C. E. Housecroft and E. C. Constable, *J. Am. Chem. Soc*., 2010, **132**, 5978-5980.

2) R. D. Costa, E. Ortí, H. J. Bolink, S. Graber, S. Schaffner, M. Neuburger, C. E. Housecroft and E. C. Constable, *Adv. Funct. Mater*., 2009, **19**, 3456-3463.

3) L. He, L. Duan, J. Qiao, G. Dong, L. Wang and Y. Qi, *Chem. Mater*., 2010, **22**, 3535-3542.

4) Z. H. Kafafi, Organic Electroluminescence. CRC Press, Boca Raton, FL: 2005.

5) C. Ulbricht, B. Beyer, C. Friebe, A. Winter and U. S. Schubert, *Adv. Mater.*, 2009, **21**, 4418-4441.

6) Y. Yersin, Highly Efficient OLEDs with Phosphorescent Materials; Wiley-VCH: Weinheim, Germany, 2007.

7) P. T. Chou and Y. Chi, *Chem. Eur. J*., 2007, **13**, 380-395.

8) L. He, J. Qiao, L. Duan, G. Dong, D. Zhang, L. Wang and Y. Qiu, *Adv. Funct. Mater*., 2009, **19**, 2950-2960.

9) S. Reineke, F. Lindner, G. Schwartz, N. Seidler, K. Walzer, B. Lussem and K. Leo, *Nature*, 2009, **459**, 234-238.

10) J. D. Slinker, J. Rivnay, J. S. Moskowitz, J. B. Parker, S. Bernhard, H. D. Abruña and G. G. Malliaras, *J. Mater. Chem*., 2007, **17**, 2976-2988.

11) R. D. Costa, E. Ortí, H. Bolink, F. Monti, G. Accorsi and N. Armaroli, *Angew. Chem., Int. Ed. Engl.* 2012, **51**, 8178-8211.

12) T. Hu, L. He, L. Duan and Y. J. Qiu, *Mater. Chem*., 2012, **22**, 4206-4215.

13) J. Brandel, M. Sairenji, K. Ichikawa and T. Nabeshima, *Chem. Commun*., 2010, **46**, 3958-3960.

14) M. S. Lowry, J. I. Goldsmith, J. D. Slinker, R. Rohl, R. A. Pascal, G. G. Malliaras and S. Bernhard, *Chem. Mater*., 2005, **17**, 5712-5719.

15) R. M. Edkins, S. L. Bettington, A. E. Goeta and A. Beeby, *Dalton Trans*., 2011, **40**, 12765-12770.

16) L. S. Natrajan, A. Toulmin, A. Chewa and S. W. Magennis, *Dalton Trans*., 2010, **39**, 10837-10846.

17) M. Four, D. Riehl, O. Mongin, M. Blanchard-Desce, L. M. Lawson-Daku, J. Moreau, J. Chauvin, J. A. Delairef and G. Lemercier, *Phys. Chem. Chem. Phys*., 2011, **13**, 17304-17312.

18) J. P. Morrall, G. T. Dalton, M. G. Humphrey and M. Samoc, Organotransition Metal Complexes for Nonlinear Optics. *In Advances in Organometallic Chemistry*; Elsevier: Amsterdam, 2007; Vol. 55, 61 − 136.

19) C. Girardot, G. Lemercier, J. C. Mulatier, J. Chauvin, P. L. Baldeck and C. Andraud, *Dalton Trans*., 2007, 3421-3426.

20) E. Baggaley, J. A. Weinstein and J. A. G. Williams, *Coord. Chem. Rev.*, 2012, **256**, 1762−1785.

21) R. G. Balasingham, M. P. Coogan and F. L. Thorp-Greenwood, *Dalton Trans.*, 2011, **40**, 11663−11674.

22) I. S. Butler, R. P. Kengne-Momo, G. Jaouen, C. Policar and A. Vessieres, *Appl. Spectrosc. Rev.*, 2012, **47**, 531−549.

23) V. Fernandez-Moreira, F. L. Thorp-Greenwood and M. P. Coogan, *Chem. Commun.*, 2010, **46**, 186−202.

24) K. K. W. Lo, A. W. T. Choi and W. H. T. Law, *Dalton Trans.*, 2012, **41**, 6021−6047.

25) K. K. W. Lo, K. Y. Zhang and S. P. Y. Li, *Eur. J. Inorg. Chem.* 2011, **2011**, 3551−3568.

26) M. W. Louie, A. W. T. Choi, H. W. Liu, B. T. N. Chan and K. K. W. Lo, *Organometallics*, 2012, **31**, 5844−5855.

27) L. Sacksteder, A. P. Zipp, E. A. Brown, J. Streich, J. N. Demas and B. A. DeGraff, *Inorg. Chem.*, 1990, **29**, 4335−4340.

28) F. L. Thorp- Greenwood, M. P. Coogan, A. J. Hallett, R. H. Laye and S. J. A. Pope, *J. Organomet. Chem.*, 2009, **694**, 1400−1406.

29) R. S. Herrick, I. Wrona, N. McMicken, G. Jones, C. J. Ziegler and J. Shaw, *J. Organomet. Chem.*, 2004, **689**, 4848-4855.

30) K. W. K. Lo, M. W. Louie, K. S. Sze and J. S. Y. Lau, *Inorg. Chem.*, 2008, **47**, 602-611.

31) P. Thanasekaran, R. T. Liao, B. Manimaran, Y. H. Liu, P. T. Chou, S. Rajagopal and K. L. Lu, *J. Phys. Chem. A*, 2006, **110**, 10683-10689.

32) B. Happ, A. Winter, M. D. Hager and U. S. Schubert, *Chem. Soc. Rev.*, 2012, **41**, 2222-2255.

33) A. Coleman, C. Brennan, J. G. Vos and M. T. Pryce, *Coord. Chem. Rev.*, 2008, **252**, 2585-2595.

34) S. M. Fredericks, J. C. Luong and M. S. Wrigthon, *J. Am. Chem. Soc.*, 1979, 7415-7417.

35) R. M. Roat-Malone, Bioinorganic Chemistry: A Short Course; Wiley, 2003.

36) S. K. Mustafa and M. A. AlSharif, *Am. J. Anal. Chem.*, 2018, **9**, 15-26.

37) J. E. Weder, C. T. Dillon, T. W. Hambley, B. J. Kennedy, P. A. Lay, J. R. Biffin, H. L. Regtop and N. M. Davies, *Coord. Chem. Rev.*, 2002, **232**, 95-126.

38) P. Zatta and A. Frank, *Brain Res. Rev.*, 2007, **54**, 19-33.

39) N. E. Hellman and J. D. Gitlin, *Annu. Rev. Nutr.*, 2002, **22**, 439-458.

40) H. Tapiero, D. M. Townsend and K. D. Tew, *Biomed. Pharmacother.*, 2003, **57**, 386-398.

41) J. P. Bach, N. Kumar, C. Depboylu, C. Noelker, T. Klockgether, M. Bacher, M. Balzer-Geldsetzer and R. Dodel, *J. Neurol. Sci.*, 2010, **291**, 95-97.

42) G. Forte, A. Alimonti, N. Violante, M. D. Gregorio, O. Senofonte, F. Petrucci, G. Sancesario and B. Bocca, *J. Trace Elem. Med. Biol*., 2005, **19**, 195-201.

43) T. Kaido, H. Hashimoto, H. Okamura and K. Tsukaguchi, *J. Clin. Neurosci*., 2005, **12**, 205-206.

44) G. J. Brewer, *Chem. Res. Toxicol*., 2010, **23**, 319-326.

45) J. M. Walshe, In *Advances in Clinical Chemistry*; G. S. Makowski, Ed.; Elsevier, Vol. 50, 2010.

46) L. Li, K. D. Karlin and S. E. Rokita, *J. Am. Chem. Soc*., 2005, **127**, 520-521.

47) Y. A. Skorik, C. A. R. Gomes, N. V. Podberezskaya, G. V. Romanenko, L. F. Pinto and Y. G. Yatluk, *Biomacromolecules*, 2005, **6**, 189-195.

48) N. J. Sanghamitra, P. Phatak, S. Das, A. G. Samuelson and K. Somasundaram, *J. Med. Chem*., 2005, **48**, 977-985.

49) S. Sarkar, A. Mondal, J. Ribas, M. G. B. Drew, K. Pramanik and K. K. Rajak, *Inorg. Chim. Acta*, 2005, **358**, 641-649.

50) S. Sarkar, A. Mondal, J. Ribas, M. G. B. Drew, K. Pramanik and K. K. Rajak, *Eur. J. Inorg. Chem*., 2004, **2004**, 4633-4639.

51) J. Mukherjee, R. Gupta, T. Mallah and R. Mukherjee, *Inorg. Chim. Acta*, 2005, **358**, 2711-2717.

52) A. Mukherjee, I. Rudra, S. G. Naik, S. Ramasesha, M. Nethaji and A. R. Chakravarty, *Inorg. Chem.*, 2003, **42**, 5660-5668.

53) R. Balamurugan, M. Palaniandavar and R. S. Gopalan, *Inorg. Chem*., 2001, **40**, 2246-2255.

54) M. Vaidyanathan, R. Balamurugan, S. Usha and M. Palaniandavar, *Dalton Trans.*, 2001, 3498-3506.

55) S. Mohanta, B. Adhikary, S. Baitalik and K. Nag, *New J. Chem*., 2001, **25**, 1466-1471.

56) S. K. Dutta, U. Florke, S. Mohanta and K. Nag, *Inorg. Chem.*, 1998, **37**, 5029-5032.

57) H. Schiff, *Justus Liebigs Ann. Chem*., 1864, **131**, 118-119.

58) S. Patai, The Chemistry of the Carbon-Nitrogen Double Bond, John Wiley & Sons Ltd., New York, 1970.

59) S. K. Raju, A. Settu, A. Thiyagarajan, D. Rama, P. Sekar and S. Kumar, *GSC Biol. Pharm. Sci*., 2022, **21**, 203-215.

60) S. Manzoor, R. A. Tahir, M. A. Younis, W. L. Cao, Q. Tariq, A. Ali, N. Ahmad, C. Qiu, B. Tian and J. G. Zhang, *Bioorg. Chem*., 2023, **140**, 106822.

61) M. M. Sprung, *Chem. Rev*., 1940, **26**, 297-338.

62) P. Y. Sollenberger and R. B. Martin, *J. Am. Chem. Soc*., 1970, **94**, 4261-4270.

63) B. P. Sullivan, D. J. Salmon, T. J. Meyer and J. Peedrin, *Inorg. Chem.*,1979, **18**, 3369-3374.

64) J. V. Houten and R. J. Watts, *J. Am. Chem. Soc.*, 1976, **98**, 4853-4858.

65) SMART; SAINT; SADABS; XPREP; SHELXTL, Bruker AXS Inc., Madison, WI, 1998.

66) G. M. Sheldrick, SHELXTL, v. 6.14, Bruker AXS Inc., Madison, WI, 2003.

67) C. K. Johnson, ORTEP Report ORNL-5138, Oak Ridge National Laboratory, Oak Ridge, TN, 1976.

68) J. Wagler, D. Gerlach and G. Roewer, *Inorg. Chim. Acta*, 2007, **360**, 1935–1942.

69) M. J. Frisch, G. W. Trucks, H. B. Schlegel, G. E. Scuseria, M. A. Robb, J. R. Cheeseman, G. Scalmani, V. Barone, B. Mennucci, G. A. Petersson, H. Nakatsuji, M. Caricato, X. Li, H. P. Hratchian, A. F. Izmaylov, J. Bloino, G. Zheng, J. L. Sonnenberg, M. Hada, M. Ehara, K. Toyota, R. Fukuda, J. Hasegawa, M. Ishida, T. Nakajima, Y. Honda, O. Kitao, H. Nakai, T. Vreven, J. A. Montgomery Jr., J. E. Peralta, F. Ogliaro, M. Bearpark, J. J. Heyd, E. Brothers, K. N. Kudin, V. N. Staroverov, R. Kobayashi, J. Normand, K. Raghavachari, A. Rendell, J. C. Burant, S.

S. Iyengar, J. Tomasi, M. Cossi, N. Rega, J. M. Millam, M. Klene, J. E. Knox, J. B. Cross, V. Bakken, C. Adamo, J. Jaramillo, R. Gomperts, R. E. Stratmann, O. Yazyev, A. J. Austin, R. Cammi, C. Pomelli, J. W. Ochterski, R. L. Martin, K. Morokuma, V. G. Zakrzewski, G. A. Voth, P. Salvador, J. J. Dannenberg, S. Dapprich, A. D. Daniels, O. Farkas, J. B. Foresman, J. V. Ortiz, J. Cioslowski and D. J. Fox, Gaussian 09, (Revision A.1), Gaussian, Inc., Wallingford, CT, 2009.

70) N. M. O'Boyle, A. L. Tenderholt and K. M. Langner, *J. Comput. Chem.*, 2008, **29**, 839-845.

71) E. Runge and E. K. U. Gross, *Phys. Rev. Lett.*, 1984, **52**, 997-1000.

72) A. D. Becke, *J. Chem. Phys.*,1993, **98**, 5648-5652.

73) C. Lee, W. Yang and R. G. Parr, *Phys. Rev. B.*,1988, **37**, 785-789.

74) X. Gao, Y. Wang, Y. Wang, J. Jia and X. Su, *Sci. Sin. Chim.*, 2011, **41**, 1145-1155.

75) M. E. Casida, C. Jamoroski, K. C. Casida and D. R. Salahub, *J. Chem. Phys.*, 1998, **108**, 4439-4449.

76) R. E. Stratmann, G. E. Scuseria and M. J. Frisch, *J. Chem. Phys.*, 1998, **109**, 8218-8224.

77) V. Barone and M. J. Cossi, *Phys. Chem. A*, 1998, **102**, 1995-2001.

78) M. Cossi and V. J. Barone, *Chem. Phys.*, 2001, **115**, 4708-4717.

79) T. Liu, H. X. Zhang and B. H. Xia, *J. Phys. Chem. A*, 2007, **111**, 8724-8730.

80) X. Zhou, H. X. Zhang, Q. J. Pan, B. H. Xia and A. C. Tang, *J. Phys. Chem. A*, 2005, **109**, 8809-8818.

Chapter 2

Synthesis and characterization of blue-violet emitting iridium(III) complex coordinated *via* chlorinated ancillary ligand

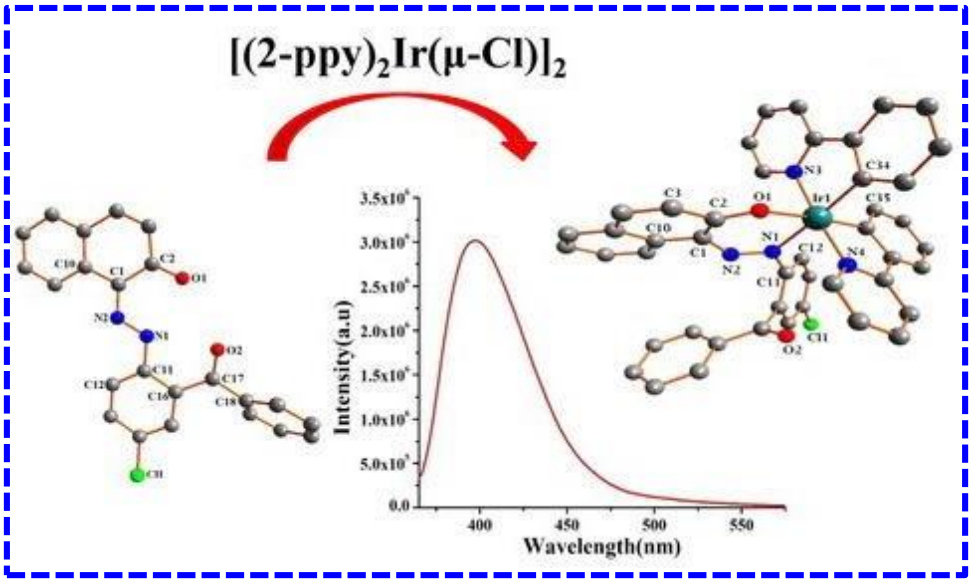

Abstract:

Refluxing HL [5-chloro-2-((2-hydroxynaphthalen-1-yl)diazenyl)phenyl)(phenyl)methanone] with $[(2\text{-ppy})_2Ir(\mu\text{-Cl})]_2$ in ethanol-dichloromethane mixture in the presence of a base (NEt_3) afforded complex of composition $[Ir(2\text{-ppy})_2(L)]PF_6$, where the azo-ligand is coordinated to iridium(III) center as monoanionic bidentate N,O-donors. The ligand and complex were characterized unequivocally. Molecular structures of both the ligand and complex were confirmed by single-crystal X-ray diffraction. The ground and excited-state geometries, absorption, and emission properties of the iridium(III) complex were further examined by DFT and TD-DFT methods. The complex exhibits a blue-violet emission band at 395 nm with quantum yield (Φ) 0.06. Experimental and theoretical studies support the fact that the nature of emission is an admixture of ^{3}IL and ^{3}MLCT state.

2.1 Introduction

Research in the field of cyclometalated iridium(III) complexes have received considerable interest since the last few decades due to their tunable and efficient photoluminescence properties and successive performance in a potential range of photophysical and electronic applications.[1–6] Such cyclometalated complexes are proficient of showing highly intense phosphorescence at room temperature.[7] But, there is also evidence of non emissive iridium(III) complexes that act as non-nucleic acid bonded fluorescence-enhanced nuclear stain, and hence, proved to be an efficient nuclear imaging probe.[8] Very few iridium(III) complexes have been reported with emission at shorter wavelength, which is a consequence of electron-withdrawing property of the attached ligand.[9] As a result, cyclometalated iridium(III) complexes have been found in many applications related to optoelectronics[10], such as electrochemical cells[11–16], photovoltaics[17,18], luminescence imaging[19–23], and as phosphorescence material for fabrication of organic light-emitting diodes (OLEDs).[24] The ability to perform aforementioned role can be facilitated by a finely modulated metal–ligand system, altering the cyclometalated and/or ancillary ligand associated with the iridium center. In this context, the aim of our work is to design and synthesize cyclometalating ancillary ligands with suitable donor sites which induce formation of the stable iridium complex with a concomitant increase in their room temperature luminescence properties.[25–27] 2- Phenylpyridine and its derivatives are among the most widely used ligands due to their efficient coordination to iridium(III), but reports on the studies of heteroleptic iridium(III) complexes with ancillary azo-ligands are limited.

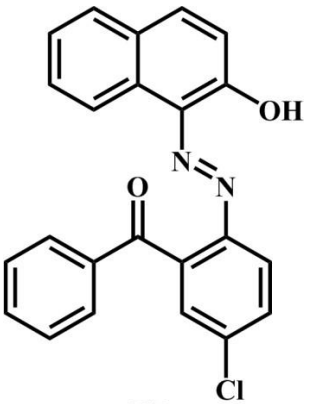

HL

In this present work, we report the synthesis of a heteroleptic iridium(III) complex coordinated with an azo (-N = N-) nitrogen ligand (HL) which is very uncommon. The chelating environment around iridium center is free from steric hindrance as there is no hydrogen present in the vicinity of metal, owing to the fact that the chelating nitrogen of azo- group of the ligand is attached with non-hydrogenated nitrogen. This not only strengthens the metal nitrogen bond but also reduces the HOMO-LUMO energy gap of the complex. This phenomenon creates possibilities for the complex under study to show various applications as mentioned above. The azo-ligand and the complex formation have been authenticated on the basis of single crystal X-ray studies and ^{1}H NMR spectroscopy. The photophysical properties of the cyclometalated iridium(III) complex were also investigated. To get a deeper insight into the geometry and the electronic structure, geometry optimization of the compounds was performed at their ground and excited states with the help of density functional theory (DFT)

and time dependent density functional theory (TD-DFT).

2.2 Experimental Section

2.2.1 Materials and Methods

2-Amino-5-chlorobenzophenone was purchased from Aldrich Chemical Co. $[Ir_2(2\text{-ppy})_4Cl_2]$ was prepared as reported in the literature.[28] All chemicals and solvents were analytically pure and used without purification. Infrared spectra were recorded on a Perkin-Elmer L120-00A FT-IR spectrometer with the samples prepared as KBr pellets. ^{1}H-NMR spectra was recorded on a Bruker FT 400 MHz instrument. For NMR spectra, $CDCl_3$was used as the solvent using TMS as an internal standard. UV–Vis experiments were performed on a Perkin–Elmer LAMBDA 25 spectrophotometer and the fluorescence experiment was performed using a Horiba FluroMax-4 fluorescence spectrometer and a fluorescence cell of 10 mm path length. (ESI-MS) spectra were obtained on a Micromass Qtof YA 263 mass spectrometer. Elemental analyses (C, H, N) were performed on a Perkin-Elmer 2400 series II analyzer.

2.2.2 Computational Details

The geometrical structure of the singlet ground state (S_0) and the lowest lying triplet excited state (T_1) were optimized using the density functional theory (DFT)[29] method at the RB3LYP and UB3LYP levels of theory.[30] The geometry of the iridium(III) complex was fully optimized in solution without any symmetry constraint. The absorption and

photoluminescence spectral properties of the iridium(III) complex based on the optimized ground and excited state geometry structure was computed using the time-dependent DFT (TDDFT)[31] approach in dichloromethane associated with the conductor-like polarizable continuum model (CPCM).[32] Relativistic effective core potential (ECP)[33] on iridium replaced the inner core electrons leaving the outer core [$(5s)^2(5p)^6$] electrons and the ($5d^6$) valence electrons of iridium(III).[34] In the calculation "double- ξ" quality basis set LANL2DZ was adopted as the basis set for iridium atom. The 6-31G basis set was used for the H atom and 6-31 + G(d, p) for C, N, Cl, and O atoms for the optimization of both the ground state and the lowest lying triplet excited state geometries.

2.2.3 Synthesis of ligand HL (5-chloro-2-((2-hydroxynaphthalen-1-yl)diazenyl)phenyl)(phenyl)-methanone)

2-Amino-5-chlorobenzophenone (430 mg, 1.8 mmol) was dissolved in concentrated hydrochloric acid (3.0 mL) and cooled to 0–5 °C. Then, the solution was diazotized with the dropwise addition of (127 mg, 1.8 mmol) sodium nitrite solution (3.0 mL) at 0–5 °C. β- Napthol (267 mg, 1.8 mmol) was dissolved in sodium hydroxide solution (10 mL, 6 M). The solution was then cooled to 0–5 °C. The cold solution of the diazonium salt was added dropwise to this solution at 0–5 °C. The mixture was stirred at 0–5 °C for 1 h. The dark-red precipitation of compound HL (**Scheme 2.1**) that appeared was separated on filtration and recrystallized from dichloromethane-hexane. Yield: 160 mg (41%). Anal. Calc. $C_{23}H_{15}ClN_2O_2$ (387): C, 71.41; H, 3.91; N, 7.24. Found: C, 71.35; H, 3.88; N, 7.31%. IR (KBr pellets, cm^{-1}): ν(C=O) 1672, ν(N=N) 1477 (**Figure 2.1**). ^1H NMR in $CDCl_3$, δ (ppm): 8.39 (d, 1H, J=12 Hz), 8.24 (d, 1H, J=12 Hz), 7.83 (d, 2H, J=8 Hz), 7.64–7.57 (m, 4H), 7.50–7.45 (m, 4H), 7.45(d, 1H, J=8 Hz), 6.73 (d, 1H, J=12 Hz) (**Figure 2.2**).

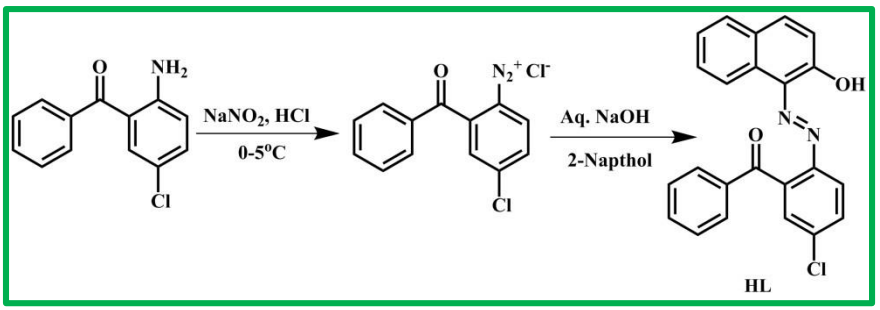

Scheme 2.1 Synthesis of ligand HL.

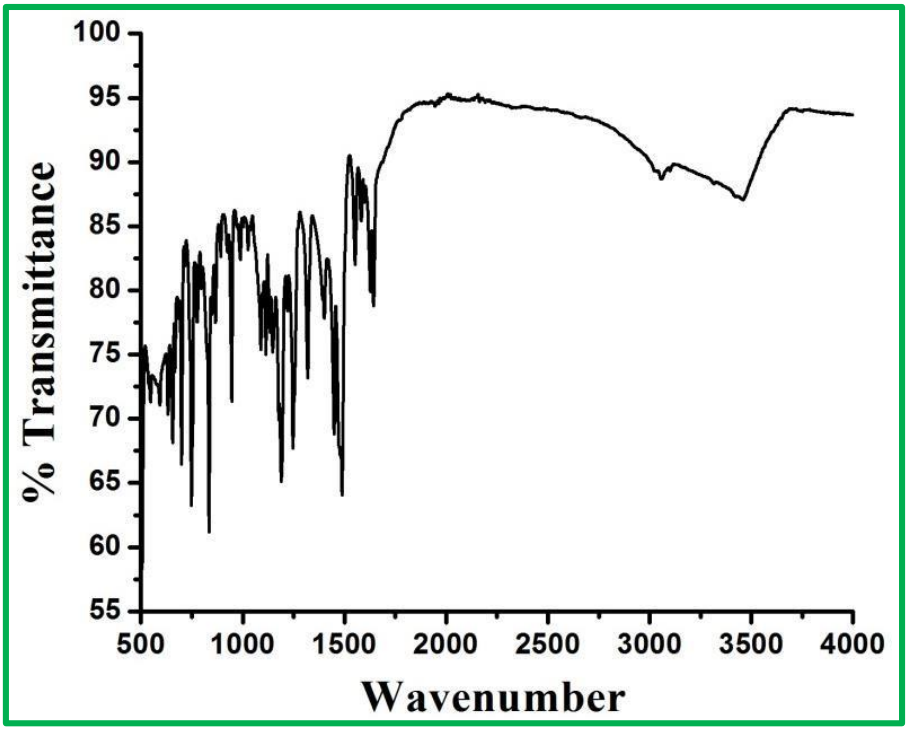

Figure 2.1 IR spectrum of ligand HL.

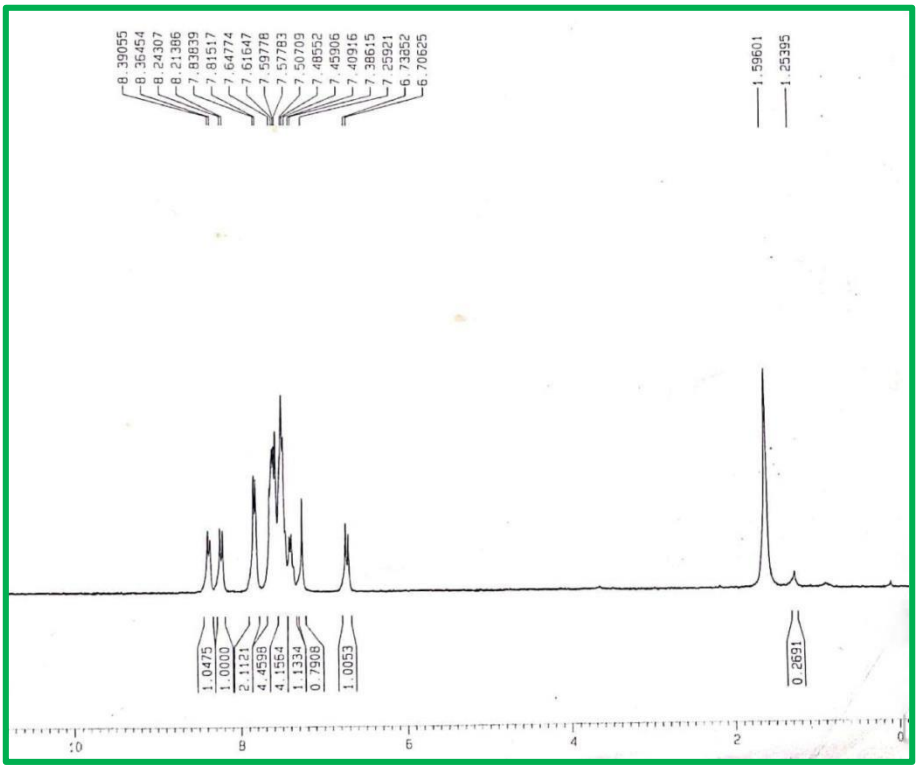

Figure 2.2 ^{1}H-NMR spectrum of ligand HL in $CDCl_3$.

2.2.4 Synthesis of $[Ir(2\text{-}ppy)_2(L)]PF_6$

A mixture of HL (50 mg, 0.129 mmol) and $[(2\text{-}ppy)_2Ir(\mu\text{-}Cl)]_2$ (139 mg, 0.129 mmol) in a mixture of dichloromethane and ethanol (40 mL) and 1-2 drops of triethylamine was refluxed for 4 h. Deep-brown precipitate of $[Ir(2\text{-}ppy)_2(L)]PF_6$ separated out (**Scheme 2.2**) and was collected by filtration and was recrystallized from dichloromethane-hexane. Yield: 125 mg (66%). Elemental Anal. Calcd. for $C_{45}H_{30}ClIrN_4O_2$: C, 60.97; H, 3.41; N, 6.32. Found: C, 60.72; H, 3.45; N, 6.27%. IR (KBr pellets, cm^{-1}): ν(N=N) 1471, ν(C=O) 1642 (**Figure 2.3**). ^1H NMR in $CDCl_3$, δ (ppm): 9.79 (d, 1H, J=6 Hz), 9.52 (d, 1H, J=6 Hz), 8.24–7.98 (m, 5H), 7.57 (t, 1H, J=6 Hz), 7.69 (m, 2H), 7.42 (q, 2H, J=6 Hz), 6.89-6.66 (m, 5H), 6.24 (d, 1H, J=6 Hz), 5.65 (d, 1H, J=9 Hz) (**Figure 2.4**).

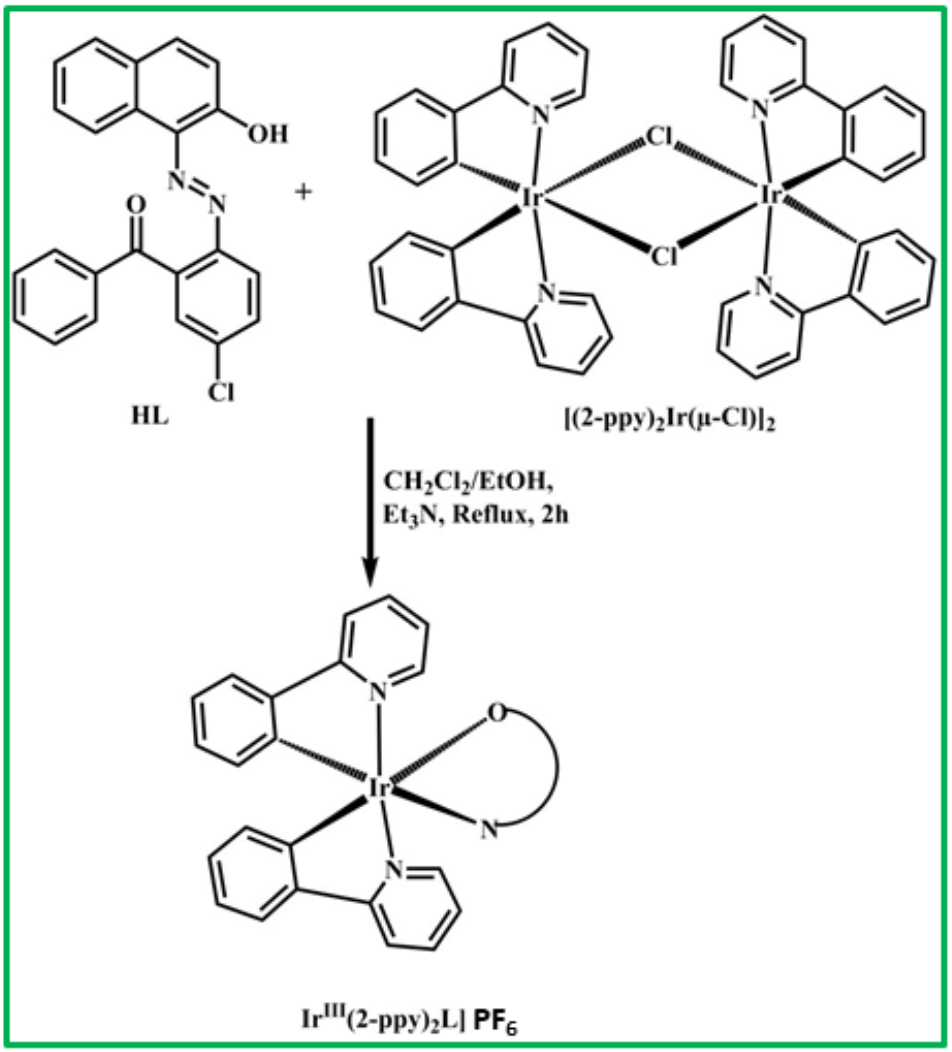

Scheme 2.2 Synthesis of $[Ir(2\text{-}ppy)_2(L)]PF_6$.

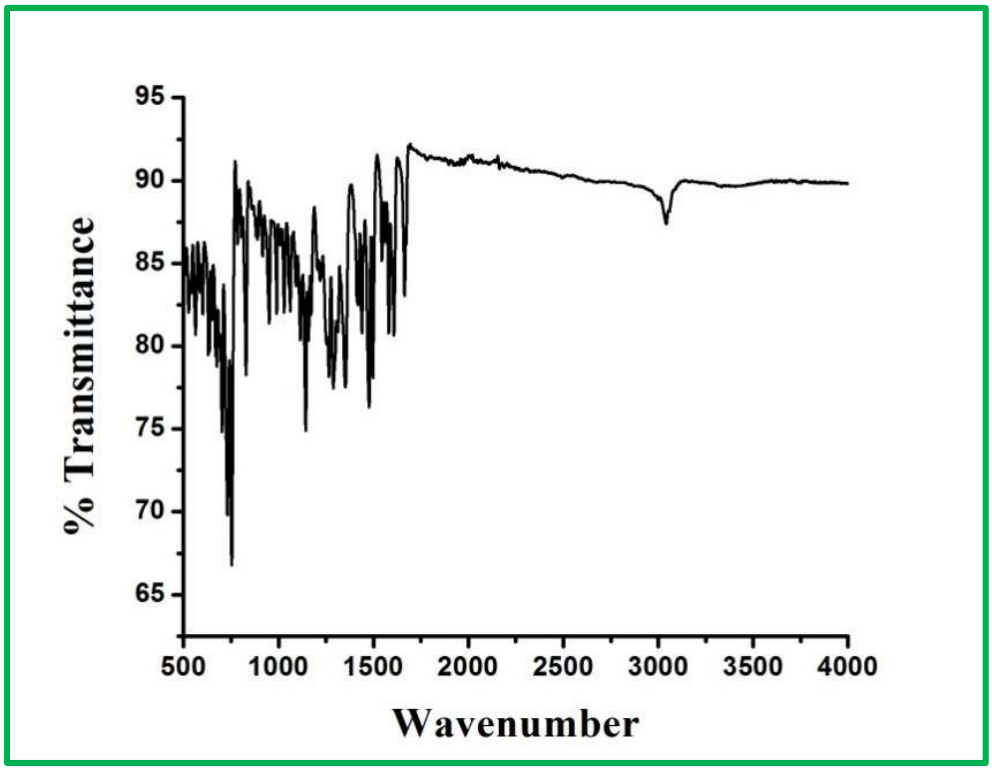

Figure 2.3 IR spectrum of $[Ir(2\text{-}ppy)_2(L)]PF_6$

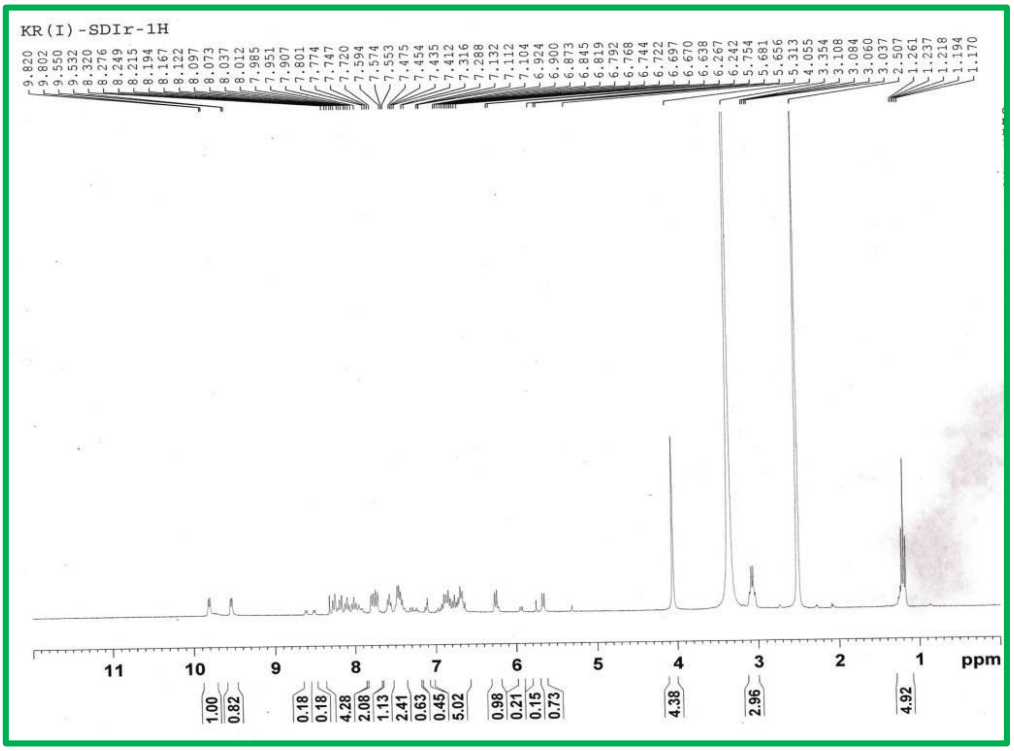

Figure 2.4 ^{1}H-NMR spectrum of $[Ir(2\text{-}ppy)_2(L)]PF_6$ in $CDCl_3$.

Table 2.1 Atomic coordinates and isotropic thermal parameters of HL.

Chemical formula	$C_{23}H_{15}ClN_2O_2$
Formula weight	386.82
Crystal system	Monoclinic
Space group	P21/c
a/Å	17.6345(6)
b/Å	7.1254(2)
c/Å	15.7480(5)
α/deg	90
β/deg	111.898(2)
γ/deg	90
λ /Å	0.71073
V /Å^3	1836.01(10)
F(000)	800
Z	4
T/K	298
D/mg/m^{-3}	1.399
μ /mm^{-1}	0.230
R1(all data)	0.0475
wR2[$I > 2\sigma(I)$]	0.1361
GOF	0.995

2.2.5 Crystallographic Studies

Single-crystals of both the ligand and $[Ir(2\text{-}ppy)_2(L)]PF_6$ complex were grown by slow diffusion of hexane in dichloromethane solution at 25 °C. Data were collected on a Bruker SMART CCD diffractometer using Mo-Kα monochromated (λ = 0.71073) radiation. The solutions of the structures were performed using Shelx 97 PC version program. Full-matrix least-square

refinements on F^2 were performed using SHELXL-97. All non-hydrogen atoms were refined anisotropically using full-matrix least-squares method. Hydrogens were included for structure factor calculations after placing them at calculated positions. Atomic coordinates and isotropic thermal parameters of the ligand and $[Ir(2\text{-}ppy)_2(L)]PF_6$ are given in **Tables 2.1 and 2.2**. The CCDC number is 1954116 for the complex and 1982643 for the ligand.

Table 2.2 Atomic coordinates and isotropic thermal parameters of $[Ir(2\text{-}ppy)_2(L)]PF_6$.

Chemical formula	$C_{45}H_{30}ClN_4O_2Ir$
Formula weight	886.40
Crystal system	Monoclinic
Space group	P21/n (No. 14)
a/Å	9.3437(3)
b/Å	22.4301(7)
c/Å	17.4167(6)
α/deg	90
β/deg	101.284(2)
γ/deg	90
λ /Å	0.71073
V /Å^3	3579.6(2)
F(000)	1752
Z	4
T/K	296
D/mg/m^{-3}	1.645
μ /mm^{-1}	3.850
R1(all data)	0.0393
wR2[$I > 2\sigma(I)$]	0.1351
GOF	0.95

2.3 Results and Discussion

2.3.1 Synthesis

HL was prepared by the diazo-coupling reaction of β-napthol with 2-amino-5-chlorobenzophenone. **Scheme 2.1** shows the steps of diazo-coupling reaction which produced the desired compound HL.

The reaction between HL and $[(2\text{-ppy})_2Ir(\mu\text{-Cl})]_2$ in dichloromethane/ethanol mixture in the presence of triethylamine afforded the brown crystalline complex of composition $[Ir(2\text{-ppy})_2(L)]PF_6$. **Scheme 2.2** represents the synthetic route of $[Ir(2\text{-ppy})_2(L)]PF_6$.

2.3.2 Characterization

The infrared spectra of HL in solid KBr pellet exhibited bands at 1672 cm^{-1} and 1477 cm^{-1} for ν(C=O) and ν(N=N), respectively. The ν(N=N) band of the ligand shifted to lower frequency (near 1471 cm^{-1}) in $[Ir(2\text{-ppy})_2(L)]PF_6$ due to the coordination of azo nitrogen with iridium center.[35] The IR spectra of HL and $[Ir(2\text{-ppy})_2(L)]PF_6$ are given in **Figures 2.1 and 2.3**. The ^{1}H-NMR spectrum of HL shows well-resolved peak within δ = 8.89 – 7.21 ppm which suggests the exact position of aromatic protons. The total count of aromatic protons (δ = 9.79 – 5.65 ppm) matched well with the composition of the complex (**Figures 2.2 and 2.4**). Therefore, the solution structures of the ligand and complex were consistent with the molecular structures in the solid state (see below, X-ray structure).

2.3.3 X-ray Structure

X-ray crystal structure analysis was performed for the unequivocal characterizations of HL and $[Ir(2\text{-ppy})_2(L)]PF_6$. Perspective view of their molecular structures is shown in **Figure 2.5**. $[Ir(2\text{-ppy})_2(L)]PF_6$ crystallizes in the monoclinic system with space group P21/n and the ligand crystallizes also in the monoclinic system but the space group is P21/c. Selected bond distances and angles for $[Ir(2\text{-ppy})_2(L)]PF_6$ and HL are given in **Table 2.3**. In the X-ray structure of metal complex, HL binds Iridium(III) as a bidentate (N,O) fashion. The two 2- phenylpyridine (2-ppy) are arranged mutually trans in position. The complex forms a distorted octahedral structure. The linear bond angles around iridium(III) deviate slightly from 180° and the values roam around 176°. The N1-N2 bond distance in L changes from 1.326 Å to 1.288 Å upon coordination with iridium(III).

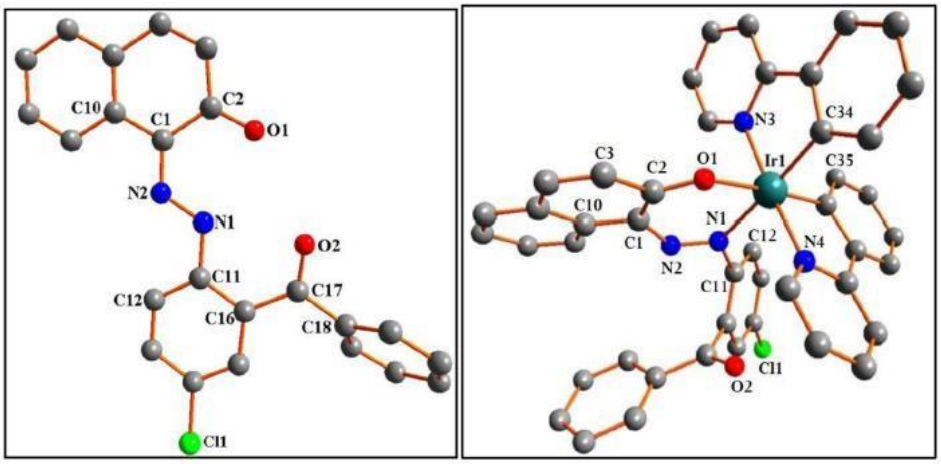

Figure 2.5 Molecular structure of HL (left) and $[Ir(2\text{-}ppy)_2(L)]PF_6$ (right) with the atom numbering scheme. Hydrogens are omitted for clarity.

Table 2.3 Selected bond distances and angles for $[Ir(2\text{-}ppy)_2(L)]PF_6$ and HL.

Bond distance (Å)			
[Ir(2-ppy)2(L)]		HL	
Ir1-O1	2.147(4)	C2-O1	1.235(3)
Ir1-N4	2.034(5)	C1-N2	1.318(2)
Ir1-N1	2.124(4)	N2-N1	1.326(2)
Ir1-N3	2.049(4)	N1-C11	1.393(2)
Ir1-C35	2.008(5)	C17-O2	1.218(2)
Ir1-C34	2.011(5)		
O1-C2	1.284(8)		
N2-N1	1.288(5)		
Bond angle (°)			
O1-Ir1-N1	85.86(15)	O1-C2-C1	121.2(2)
O1-Ir1-N3	87.11(16)	C1-N2-N1	119.64(16)
O1-Ir1-N4	93.55(18)	N2-N1-C11	117.62(16)
O1-Ir1-C34	92.60(19)	C16-C17-O2	121.81(18)
N4-Ir1-N1	89.60(15)		
N4-Ir1-C35	80.1(2)		
N4-Ir1-C34	93.93(19)		
N3-Ir1-C35	98.87(16)		
N3-Ir1-N1	95.49(14)		
C35-Ir1-C34	87.17(18)		
N1-Ir1-C35	94.99(16)		
N3-Ir1-C34	81.0(2)		
N4-Ir1-N3	176.64(14)		
N1-Ir1-C34	176.23(16)		
O1-Ir1-C35	173.70(16)		

2.3.4 Geometry Optimization, Electronic Structure, and Charge Distribution

To understand the molecular structure of iridium(III) complex, geometry optimization (**Figure 2.6**) was performed in the solution phase in both ground singlet (S_0) state and lowest

lying excited triplet (T_1) state. The geometry used for the ground (S_0) and triplet (T_1) state optimization is based on crystal structure parameter of $[Ir(2\text{-}ppy)_2(L)]^+$ without ligand modification. The optimized geometrical parameters for $[Ir(2\text{-}ppy)_2(L)]^+$ in both spin states are given in **Table 2.4**.

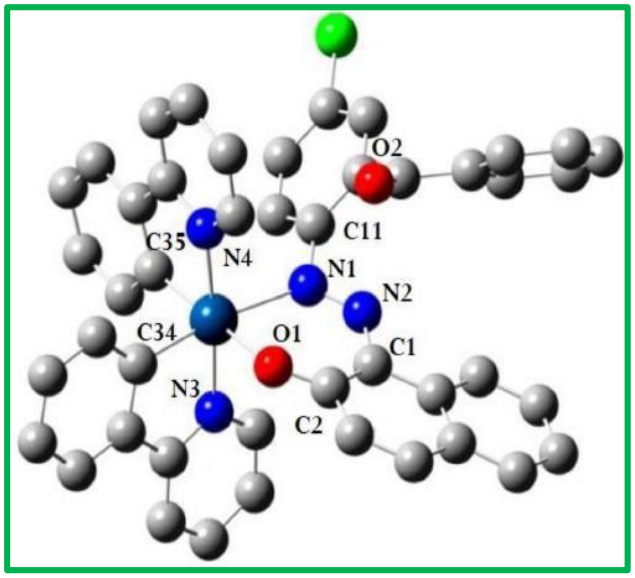

Figure 2.6 Optimized molecular view of $[Ir(2\text{-}ppy)_2(L)]^+$ (Ir: cyan, N: blue, O: red, C: grey). All hydrogens are omitted for clarity.

Table 2.4 The comparison of selected bond distances and bond angles of $[Ir(2\text{-}ppy)_2(L)]^+$ and HL in their singlet ground state (S_0) and excited triplet state (T_1).

Bond Lengths (Å)					
	S_0	**T_1**		**S_0**	**T_1**
Ir1-N4	2.063	2.063	Ir1-C35	2.013	2.011
Ir1-N1	2.242	2.183	Ir1-O1	2.174	2.207
Ir1-N3	2.076	2.082	N1-N2	1.288	1.356
Ir1-C34	2.019	2.028	O1-C2	1.281	1.297
Bond Angles(°)					
	S_0	**T_1**		**S_0**	**T_1**
N4-Ir1-N1	89.42	91.20	C26-Ir1-N1	101.54	106.73
N1-Ir1-N3	94.93	95.72	N4-Ir1-C35	80.36	80.61
N1-Ir1-O1	82.03	78.83	N3-Ir1-O1	87.91	91.35
C35-Ir1-C34	87.84	88.96	N4-Ir1-N3	175.37	172.64
C34-Ir1-O1	88.97	86.34	N1-Ir1-C34	169.99	164.15

The calculated Ir-C and Ir-O bond distances arise at 2.016 Å and 2.17 Å, respectively. The Ir-N (bipy N) and Ir-N (azo N) bond distances occur near 2.07 Å and 2.24 Å for $[Ir(2\text{-}ppy)_2(L)]PF_6$. These values show strong deviation from experimental values which are longer than the experimental values by approximately 0.1 Å. This observation is mainly due to some environmental factors such as crystal packing in solid state and influence of solvents while doing calculations.

In the triplet excited state, the electron that is promoted to the excited state energy level has the same spin orientation to the other unpaired electrons. In $[Ir(2\text{-}ppy)_2(L)]^+$, the bonding electrons get unpaired in the azo group in T_1 state. Because of this reason, the N1-N2 bond length of the complex in T_1 state gets a partial single bond character like the free ligand as there is conjugation between azo group and naphthol moiety (**Scheme 2.3**). Thus, the N1-N2 bond length in T_1 state of the complex differs from S_0 state but become close to the N1-N2 value of HL.

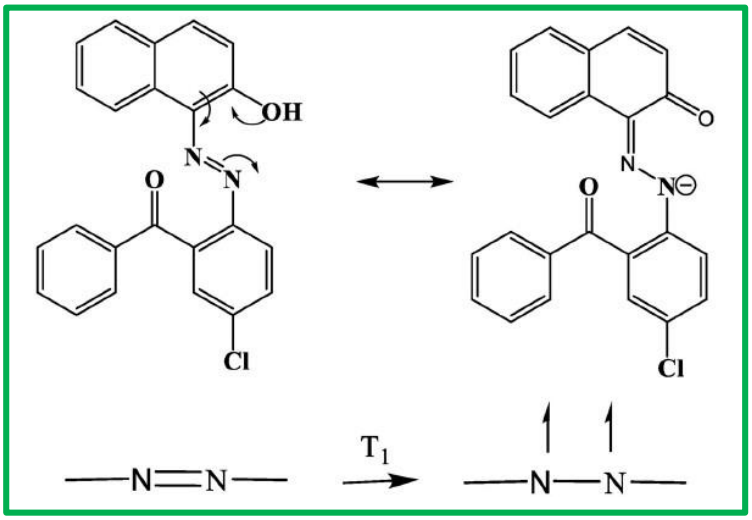

Scheme 2.3 Representation of conjugation of azo group with naphthol moiety in HL showing partial single bond character of azo bond (upper) and unpaired electrons of azo bond in T_1 state of complex (lower).

These results show there are no significant changes of the ligand framework in the octahedral mononuclear iridium(III) complex. The isodensity plots of several optimized frontier molecular orbitals from H-5 to L + 5 for $[Ir(2\text{-}ppy)_2(L)]^+$ are shown in **Figure 2.7**.

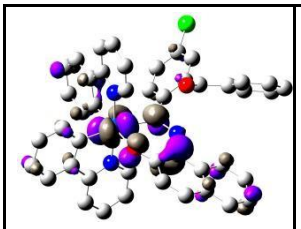	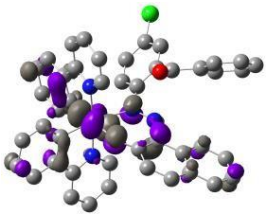	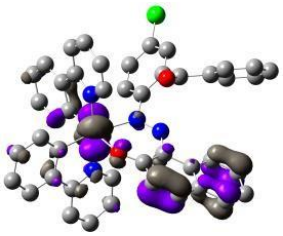	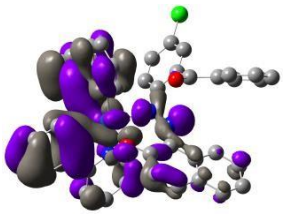
H	H-1	H-2	H-3
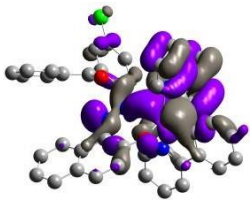	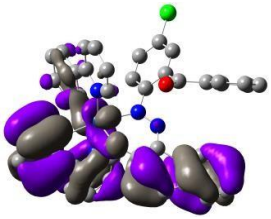	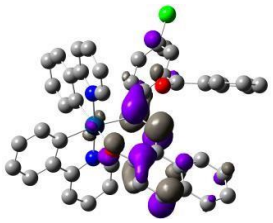	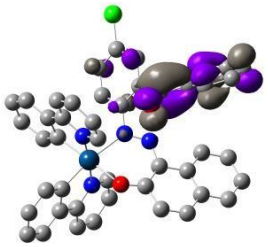
H-4	H-5	L	L+1
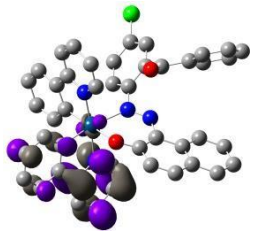	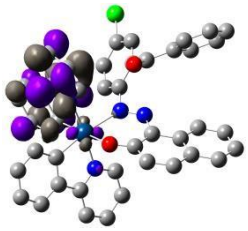	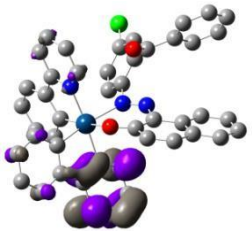	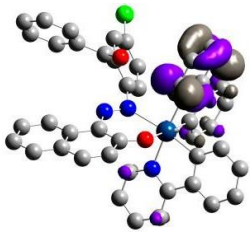
L+2	L+3	L+4	L+5

Figure 2.7 Isodensity plots of frontier orbitals of $[Ir(2\text{-}ppy)_2(L)]^+$

The energy and compositions of selected frontier molecular orbitals of the $[Ir(2\text{-}ppy)_2(L)]^+$ in singlet ground state (S_0) are listed in **Table 2.5**. The value of the energy difference between highest occupied molecular orbital [HOMO (H)] and lowest unoccupied molecular orbital [LUMO (L)] of $[Ir(2\text{-}ppy)_2(L)]^+$ equals to 2.86 eV. **Table 2.5** reveals that in the H and H-1 orbitals the electron density is very high over naphthol moiety and iridium center with respect to other fragments of complex. 2-ppy gives moderate contribution of electron density over the complex. The energy of H-3 and H-4 are almost the same (energy difference ~0.08 eV in the complex). The electron density of the LUMO of $[Ir(2\text{-}ppy)_2(L)]^+$ originates from azo and naphthol π^* orbital of the ligand aromatic system.

Table 2.5 Energy and composition of selected molecular orbitals of $[Ir(2\text{-}ppy)_2(L)]^+$.

MO	Energy (eV)	% of composition						Main bond types
		Ir	2-ppy		Ligand (HL)			
			1	2	Azo	napthol	diphenyl ketone	
L+5	-1.06	0	89	7	0	1	4	л*(2-ppy)
L+4	-1.29	0	7	91	1	0	1	л*(2-ppy)
L+3	-1.57	3	91	3	0	0	3	л*(2-ppy)
L+2	-1.74	3	2	93	0	0	0	л*(2-ppy)
L+1	-1.95	1	2	1	2	0	95	л*(HL)
L	-2.3	2	1	0	39	45	13	л*(HL)
H	-5.16	28	13	10	8	35	6	d(Ir)+л(2-ppy)+л(HL)
H–1	-5.47	30	19	15	6	27	3	d(Ir)+л(2-ppy)+л(HL)
H–2	-6.03	32	12	13	2	39	1	d(Ir)+л(2-ppy)+л(HL)
H–3	-6.08	4	37	41	6	11	0	л(2-ppy)
H–4	-6.16	36	29	10	10	7	9	d(Ir)+л(2-ppy)+л(HL)
H–5	-6.34	8	7	48	0	36	1	л(2-ppy)+л(HL)

2.3.5 Excited State (T_1)

DFT calculations have also been performed for geometry optimization of $[Ir(2\text{-}ppy)_2(L)]^+$ in low lying excited triplet (T_1) spin state at room temperature in solution phase. The optimized geometrical structure of the iridium complex in low lying excited triplet state is given in **Table 2.6** and the geometrical parameters are given in **Table 2.4**. Most interestingly, the geometry around iridium center in S_0 and T_1 states remain almost the same although significant changes have occurred in the ligand frame which corroborated that ligand binds in a similar fashion in the complex. The Isodensity surfaces of HSOMO, LSOMO, and electronic spin density for $[Ir(2\text{-}ppy)_2(L)]^+$ at the relaxed T_1 geometry are shown in **Figure 2.8**. The electron density in HSOMO of $[Ir(2\text{-}ppy)_2(L)]^+$ is mainly due to the major contribution of naphthol moiety and p orbital of chlorobenzene attached with the azo nitrogen of the ligand (**Figure 2.8**). Conversely, the electron density of LSOMO mainly resides on the diphenyl ketone moiety of the ligand and resembles the corresponding L + 1 of the S_0 geometry. The spin density plot of the complex at the triplet state (T_1) displayed that the electron density mainly localized on HL and on the metal center. Thus, the low lying triplet excited state (T_1) in $[Ir(2\text{-}ppy)_2(L)]^+$ is mainly ^{3}MLCT/^{3}LLCT excited state for cyclometalated iridium(III) complex.[36, 37]

Table 2.6 Optimized molecular structure of $[Ir(2\text{-}ppy)_2(L)]^+$ at T_1 state.

Triplet excited state (α spin)	Optimized structure	Spin state	Energy (eV)
L+9	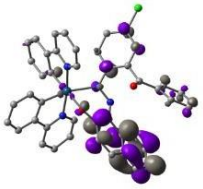	**α**	**-0.518**
L+7	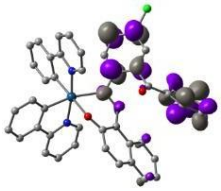	**α**	**-0.696**
L	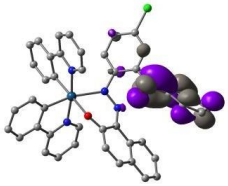	**α**	**-2.115**
H	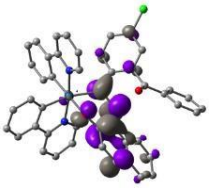	**α**	**-4.432**
H-2	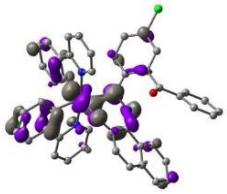	**α**	**-6.096**

2.3.6 TD-DFT Calculation and Electronic Spectra

HL exhibited characteristic UV–Vis spectrum in dichloromethane solution having lowest energy absorption maxima at 485 nm. TD-DFT study displays that the character of transition of HL is intraligand charge transfer (^{1}ILCT) type. The UV–Vis spectra of $[Ir(2\text{-}ppy)_2(L)]PF_6$ were distinctly different from HL. The lowest-energy absorption appeared at 500 nm for $[Ir(2\text{-}ppy)_2(L)]PF_6$. Moreover, such experimental values match well with the theoretical absorption spectra. The lowest energy vertical excitation ($S_0 \rightarrow S_1$) for the complex mainly consists of d$[Ir(2\text{-}ppy)_2(L)]PF_6$ – π^*(2-ppy) π^*(L).[11] Representative UV–Vis spectra of HL and $[Ir(2\text{-}ppy)_2(L)]PF_6$ are shown in **Figure 2.9**.

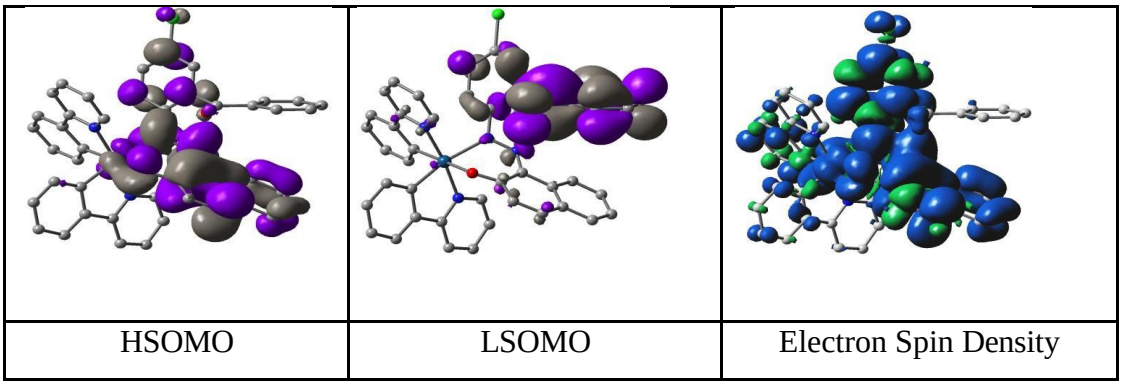

HSOMO	LSOMO	Electron Spin Density

Figure 2.8 Isodensity surface plots of HSOMO, LSOMO, and electron spin density for $[Ir(2\text{-}ppy)_2(L)]^+$ at T_1 state geometry. Blue and green regions represent the positive and negative difference between the alpha and beta electron densities, respectively.

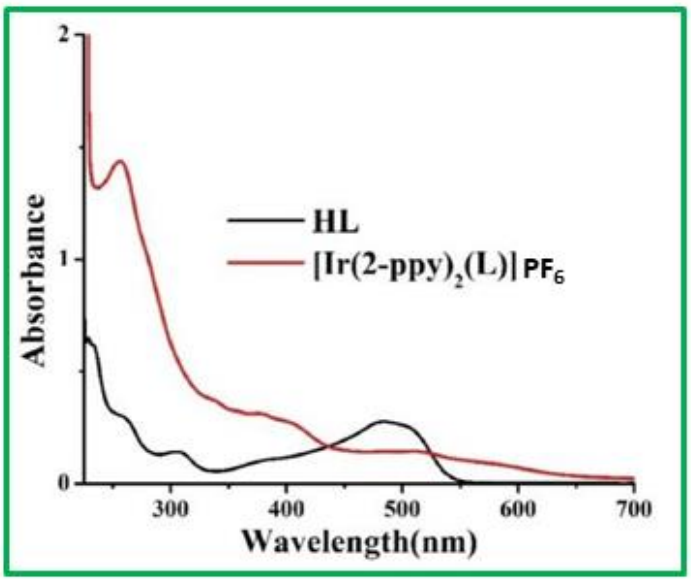

Figure 2.9 UV–Vis spectra of HL (1.5×10^{-5} M) and $[Ir(2\text{-}ppy)_2(L)]PF_6$ (1.5×10^{-5} M) in dichloromethane.

The lowest energy band with maxima at 489 nm for $[Ir(2\text{-}ppy)_2(L)]PF_6$ corresponds to mainly H-1→L (89%) and can rationally be assigned as admixture of metal-to-ligand charge-transfer (^{1}MLCT) and spin-allowed $\pi\rightarrow\pi^*$ (ligand centered, ^{1}ILCT) transitions.[38] **Table 2.7** confirms the usual assignments of all the absorption bands for the complex and HL in acetonitrile at room temperature.

Table 2.7 Main calculated optical transition for $[Ir(2\text{-}ppy)_2(L)]^+$ with composition in terms of molecular orbital contribution of the transition, vertical excitation energies, oscillator strength, and configuration interaction (CI) in dichloromethane.

Compound	Composition	Excitation Energy (eV)	Osc. Strength (*f*)	Assignment	CI	λ_{exp} (nm)
$[Ir(2\text{-}ppy)_2(L)]PF_6$	H-1→L	2.53 (489 nm)	0.0938	^{1}MLCT /^{1}ILCT	0.667	500
$[Ir(2\text{-}ppy)_2(L)]PF_6$	H-2→L	3.04 (407 nm)	0.1322	^{1}MLCT /^{1}ILCT	0.503	400
HL	H-1→L	2.34 (529 nm)	0.9210	^{1}ILCT	0.697	485

2.3.7 Emission Spectral Properties

To investigate the emission property of $[Ir(2\text{-}ppy)_2(L)]PF_6$, photoluminescence measurement in solution state was performed. $[Ir(2\text{-}ppy)_2(L)]PF_6$ exhibited strong photoluminescence near 395 nm on excitation at 350 nm (quantum yield (Φ) ca. 0.06; **Figure 2.10**).

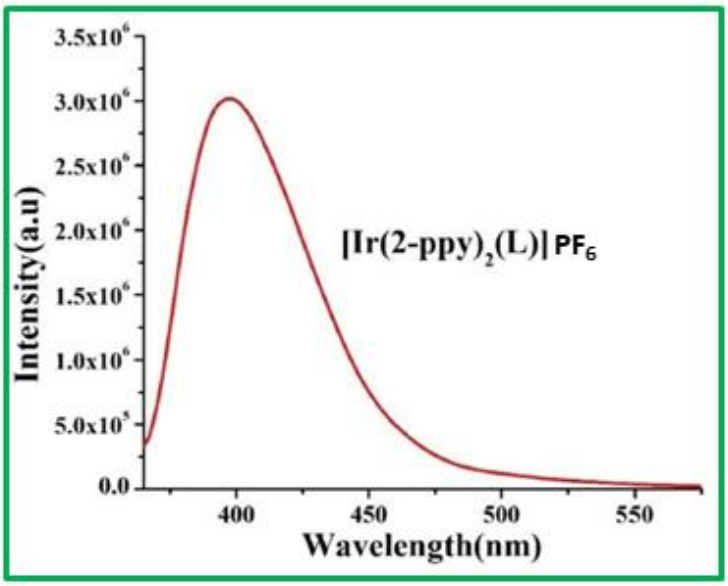

Figure 2.10 Emission spectra of complex in dichloromethane solution ($c=1.5\times10^{-5}$ M) at room temperature (λ_{ex} =350 nm, λ_{em} =395 nm).

Furthermore, the time-resolved luminescence spectra were also recorded to understand the decay process and the emissive nature of the complex. Lifetime data are recorded for $[Ir(2\text{-}ppy)_2(L)]PF_6$ at room temperature in dichloromethane solution when excited at 350 nm. The

observed luminescence decay fit with bi-exponential decay nature of $[Ir(2\text{-}ppy)_2(L)]PF_6$ (**Figure 2.11**). The fluorescence lifetime (τ), radiative (k_r), and nonradiative (k_{nr}) decay rate constant of $[Ir(2\text{-}ppy)_2(L)]PF_6$ are collected in **Table 2.8**.

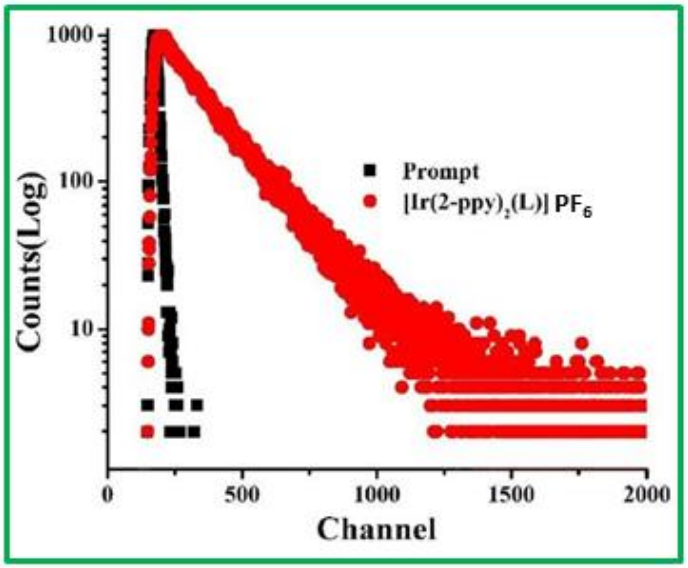

Figure 2.11 Time-resolved fluorescence lifetime decay of $[Ir(2\text{-}ppy)_2(L)]PF_6$.

Table 2.8 Photophysical parameters of $[Ir(2\text{-}ppy)_2(L)]PF_6$. in dichloromethane solution at room temperature.

Sample	τ (ns)	Φ	k_r, $s^{-1}(x10^7)$	k_{nr}, $s^{-1}(x10^8)$
$[Ir(2\text{-}ppy)_2(L)]PF_6$	5.08	0.06	1.18	1.85

In order to analyze the experimental luminescence spectra, unrestricted B3LYP method for the iridium(III) complex in triplet (T_1) state has been performed in dichloromethane. The photoluminescence property mainly originates from triplet state charge transfer transitions and electronic spin density isosurface (**Figure 2.8**) which indicates the ligand centered ^{3}IL nature of the complex. In the complex, spin density isosurfaces are entirely localized on HL and on the metal center. Thus, the lowest-lying triplet excited state is mainly ^{3}MLCT/^{3}LLCT excited state of cyclometalated iridium(III) complexes.[36, 38]

In our earlier work on iridium(III) complexes, the lifetime of the excited state of the previous iridium(III) complex was 3.0 ns. Compared to this, $[Ir(2\text{-}ppy)_2(L)]PF_6$ shows slightly longer excited state lifetime which is 5.08 ns. Although these values are close to each other, the relative value differs about 40%. Such difference is attributed to the newly modulated ligand framework. Previous iridium(III) complexes had a type of ligand where azo group was free from binding, but in the present work the coordination of HL with iridium(III) occurs via azo nitrogen and adjacent phenolic –OH. Presence of the diphenyl keto moiety containing chlorine atom in HL must have influenced the excited state behavior of $[Ir(2\text{-}ppy)_2(L)]^+$.

The calculated emission energy associated with their oscillator strength, the main configurations and their assignments as well as the experimental result of $[Ir(2\text{-}ppy)_2(L)]PF_6$ are listed in **Table 2.9**. TD-DFT study at T_1 state for $[Ir(2\text{-}ppy)_2(L)]^+$ substantiate with the ^{3}ILCT nature for $[Ir(2\text{-}ppy)_2(L)]^+$ transitions.[39, 40]

Table 2.9 Main calculated vertical transitions for complex $[Ir(2\text{-}ppy)_2(L)]^+$ with compositions in terms of molecular orbital contribution of the transition, vertical excitation energies, oscillator strength and configuration interaction (CI) in dichloromethane.

Excitation	Excitation Energy (eV)	Composition	Osc. Strength (*f*)	CI	Assignment	λ_{exp} (nm)
30	3.08 (401 nm)	H→L+9	0.0410	0.6089	^{3}MLCT/ ^{3}LLCT	395
		H→L+7		0.3775	^{3}LLCT	
31	3.15 (394 nm)	H-2→L	0.0207	0.5750	^{3}MLCT	
		H→L+9		0.2186	^{3}LLCT	

2.4 Conclusions

A heteroleptic iridium(III) complex has been prepared with a ligand bearing azo (N=N) linkage. The structures of the ligand and complex $[Ir(2\text{-}ppy)_2(L)]PF_6$ were confirmed by X-ray crystallography. The present study reveals that the complex displays photophysical properties having intense photoluminescence in relatively shorter wavelength region. The bi-exponential decay of the complex and the nature of luminescence suggest that the emitting excited state is an admixture of ^{3}IL and ^{3}MLCT states. The presence of chlorine in the ligand moiety may be crucial for such occurrence. So, this insight shows that there are possibilities to change in strategies for modulating the emission energies of the complexes. Given the ease of functionalization of the complex, our future studies will explore the more effective luminescence properties of iridium(III) complexes.

References

(1) R. D. Costa, E. Ortí, H. J. Bolink, F. Monti, G. Accorsi and N. Armaroli, *Angew. Chem. Int. Ed. Engl*., 2012, **51**, 8178-8211.

(2) A. F. Rausch, H. H. H. Homeier and H. Yersin, *Top. Organomet. Chem*., 2010, **29**, 193-235.

(3) N. M. Shavaleev, F. Monti, R. D. Costa, R. Scopelliti, H. J. Bolink, E. Ortí, G. Accorsi, N. Armaroli, E. Baranoff, M. Grätzel and M. K. Nazeeruddin, *Inorg. Chem*., 2012, **51**, 2263-2271.

(4) A. J. Hallett, N. White, W. Wu, X. Cui, P. N. Horton, S. J. Coles, J. Zhao and S. J. A. Pope, *Chem. Commun*., 2012, **48**, 10838-10840.

(5) J. D. Routledge, A. J. Hallett, J. A. Platts, P. N. Horton, S. J. Coles and S. J. A. Pope, *Eur. J. Inorg. Chem.*, 2012, **2012**, 4065-4075.

(6) A. J. Hallett, B. M. Kariuki and S. J. A. Pope, *Dalton Trans*., 2011, **40**, 9474-9481.

(7) U. Scherf and D. Neher, *Polyfluorenes*, Springer, Berlin, 2008.

(8) C. Li, M. Yu, Y. Sun, Y. Wu, C. Huang and F. Li, *J. Am. Chem. Soc*., 2011, **133**, 11231-11239.

(9) X. L. Zhang, S. J. Liu, L. Y. Guo, C. J. Wang, Y. Tong, B. X. Mi, D. P. Cao, J. Song and Z. Q. Gao, *RSC Adv*., 2016, **6**, 81869-81876.

(10) A. O. Adeloye, *Materials*, 2019, **12**, 2734.

(11) H. C. Su, Y. H. Lin, C. H. Chang, H. W. Lin, C. C. Wu, F. C. Fang, H. F. Chen and K. T. Wong, *J. Mater. Chem*., 2010, **20**, 5521-5526.

(12) L. He, L. Duan, J. Qiao, G. Dong, L. Wang and Y. Qiu, *Chem. Mater*., 2010, **22**, 3535-3542.

(13) C. Rothe, C. J. Chiang, V. Jankus, K. Abdullah, X. Zeng, R. Jitchati, A. S. Batsanov, M. R. Bryce and A. P. Monkman, *Adv. Funct. Mater*., 2009, **19**, 2038-2044.

(14) S. Graber, K. Doyle, M. Neuburger, C. E. Housecroft, E. C. Constable, R. D. Costa, E. Orti, D. Repetto and H. J. Bolink, *J. Am. Chem. Soc*., 2008, **130**, 14944-14945.

(15) R. D. Costa, E. Ortí and H. J. Bolink, *Pure Appl. Chem*., 2011, **83**, 2115-2128.

(16) E. Baranoff, J. H. Yum, I. Jung, R. Vulcano, M. Grätzel and M. K. Nazeeruddin, *Chem. Asian J*., 2010, **5**, 496.

(17) E. Baranoff, J. H. Yum, M. Graetzel and M. K. Nazeeruddin, *J. Organomet. Chem*., 2009, **694**, 2661-2670.

(18) V. F. Moreira, F. L. T. Greenwood and M. P. Coogan, *Chem. Commun*., 2010, **46**, 186-202.

(19) F. L. T. Greenwood, R. G. Balasingham and M. P. Coogan, *J. Organomet. Chem*., 2012, **714**, 12-21.

(20) K. K. W. Lo, S. P. Y. Li and K. Y. Zhang, *New J. Chem*., 2011, **35**, 265-287.

(21) P. K. Lee, W. H. T. Law, H. W. Liu and K. K. W. Lo, *Inorg. Chem*., 2011, **50**, 8570-8579.

(22) F. L. T. Greenwood, *Organometallics*, 2012, **31**, 5686-5692.

(23) S. Abbas, I. D. Din, A. Raheel and A. T. Din, *Appl. Organomet. Chem*., 2020, **34**, e5413.

(24) A. B. Kajjam and S. Vaidyanathan, *Chem. Rec*., 2018, **18**, 293-349.

(25) D. J. Stufkens and A. Vlček. Jr, *Coord. Chem. Rev*., 1998, **177**, 127-179.

(26) A. K. Pal and G. S. Hanan, *Chem. Soc. Rev*., 2014, **43**, 6184-6197.

(27) A. K. Pal, P. K. Mandali, D. K. Chand and G. S. Hanan, *Synlett*, 2015, **26**, 1408-1412.

(28) H. C. Zhao, B. Mello, B. L. Fu, H. Chowdhury, D. J. Szalda, M. K. Tsai, D. C. Grills and J. Rochford, *Organometallics*, 2013, **32**, 1832-1841.

(29) A. S. Polo, M. K. Itokazu, K. M. Frin, A. O. T. Patrocinio and N. Y. M. Iha, *Coord. Chem. Rev*., 2006, **250**, 1669-1680.

(30) M. A. L. Marques and E. K. U. Gross, *Annu. Rev. Phys. Chem*., 2004, **55**, 427-455.

(31) W. Koch and M. C. Holthausen, *A Chemist's Guide to Density Functional Theory*, Wiley-VCH, Weinheim, Germany, 2000.

(32) P. J. Hay and W. R. Wadt, *J. Chem. Phys*., 1985, **82**, 299-310.

(33) G. M. Sheldrick, *Acta Cryst. A*, 2008, **64**, 112-122.

(34) G. M. Sheldrick, SHELEXL-97 and SHELXL-97, *Program for Crystal Structure Solution and Refinement*, University of Gottingen, Gottingen, 1997.

(35) J. L. Pratihar, P. Pattanayak, D. Patra, R. Rathore and S. Chattopadhyay, *Inorg. Chim. Acta*, 2011, **367**, 182-186.

(36) N. G. Park, G. C. Choi, Y. H. Lee and Y. S. Kim, *Curr. Appl. Phys*., 2006, **6**, 620-626.

(37) S. Fantacci and F. De Angelis, *Coord. Chem. Rev*., 2011, **255**, 2704-2726.

(38) A. Maity, R. Sarkar and K. K. Rajak, *RSC Adv*., 2015, **5**, 78852-78863.

(39) K. Nonoyama, *Bull. Chem. Soc. Jpn*., 1974, **47**, 767-768.

(40) R. Czerwieniec, A. Kapturkiewicz, R. A. Ostrowska and J. Nowacki, *J. Chem. Soc., Dalton Trans*., 2001, **19**, 2756-2761.

Chapter 3

Synthesis, structure and effects of an azoimine functionalized iridium complex on cancer cells

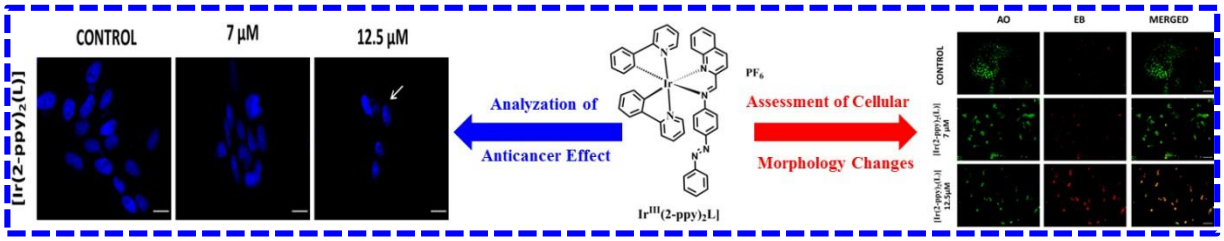

Abstract:

A novel ligand L having azoimine bond with quinoline moiety reacts with $[(2\text{-ppy})_2Ir(\mu\text{-Cl})]_2$ in dichloromethane medium to produce an iridium(III) complex of composition $[Ir(2\text{-ppy})_2(L)]PF_6$. Here, the iridium centre is bound to neutral bidentate N, N donating sites of the ligand (L), where the azo part of L is not involved in chelation. The ligand and complex are characterized by elemental analysis, NMR spectroscopy, ESI-MS mass spectrometry, FTIR, UV–Vis and luminescence spectroscopic techniques. The ligand structure and the geometry around iridium centre of complex $[Ir(2\text{-ppy})_2(L)]PF_6$ is confirmed by the single-crystal X-ray diffraction (XRD) method. DFT studies were also performed to support the experimental aspects of the complex as well as electronic distribution in molecular orbitals of various energy states. The complex exhibits blue emission band at 428 nm with quantum yield (Φ) 0.136. Further, in vitro analysis of the anticancer activity of the complex was studied mainly with the MCF - 7 cell line. The results showed that the complex have good IC_{50} values when compared to the standard drug cisplatin.

3.1 Introduction

Cancer has been a serious illness that puts people's lives in danger since it has been discovered.[1–4] Cancer cells grow abnormally and become uncontrollable as these cells can colonise and disrupt the tissues.[5] Breast cancer is one of the dangerous diseases that have become a global public health challenge among the females because of its high death rate.[6] The MCF - 7 cell line is largely studied as an in vitro model to investigate the biology of breast cancer.[7–10] Due to the number of variants available, it has applications in development of chemotherapeutic drugs and understanding drug resistance. Cancer treatment requires heavy surgery, radiotherapy, chemotherapy and often combination of these.[11–13] But, there are serious adverse effects while using platinum based drugs such as cis-platin, oxaliplatin, Carboplatin etc.[14,15] Recently, numerous metal-based complexes, including those made of palladium, gold, osmium, iridium, rhodium, and ruthenium, have demonstrated superior anti- cancer characteristics to those of platinum-based medications against a variety of cancer cell types.[16–21] Among these metals, Iridium (III) complexes are one of the good choices because of their anticancer activities and potential as anti-tumor drugs.[22,23] The ability to form versatile peripheral structures via coordination with different ligand units having desired functionalities is one of the advantages of using transition metals. The coordination complexes of these metals are proved to be the versatile scaffolds in the field of drug discovery. Iridium coordination compounds have been shown to induce apoptosis, or programmed cell death, in cancer cells, as well as inhibit the growth of tumor cells in both in vitro and in vivo studies.[24] Iridium compounds have also demonstrated the ability to target specific cancer-related pathways, such as the MAPK, PI3K/AKT and NF-κB signalling pathways.[25,26] In addition, they have been shown to modulate the expression of genes involved in cell cycle progression and apoptosis. Finally, iridium coordination compounds have been found to increase the sensitivity of cancer cells to other anti-cancer agents, such as cisplatin. These properties make iridium coordination compounds promising candidates for the development of novel anti-cancer drugs.

All the recent research in this field suggest that the coordinating ligands play a significant role in determining the toxicity of iridium(III) complexes. The chemical nature and the size of the complex affect not only the photophysical properties but also the cytotoxic profiles. Hence, a detail study of the synthesis, structure and characterization is done for the ligand

and the complex. Besides, we intend to investigate how a novel N, N coordinating ligand having azoimine bond would influence the activity of iridium(III) complex towards the cancer cell lines. The complex under this study has shown remarkable anticancer property, particularly in MCF - 7 cell line having lower IC_{50} value as compared to cisplatin.

3.2 Experimental Section

3.2.1 Materials and Methods

The solvents used for all the reactions were of reagent grade (E. Marck, Kolkata, India) and were purified and dried. 4-Aminoazobenzene was purchased from Aldrich Chemical Co. [Ir_2(2-ppy)$_4Cl_2$] was prepared as reported in the literature.[27] Iridium chloride hydrate, 2-Quinolinecarboxaldehyde, and triethyl amine were purchased from Sisco Research Laboratories (SRL), India. Crystal violet solution or Gram's crystal violet and 3-(4, 5-Dimethylthiazol-2-yl)-2, 5-diphenyl tetrazolium bromide (MTT) was purchased from MERCK. DMSO and Methanol was purchased from Sigma. Minimal Essential Media Earl's (MEM) and Fetal Bovine Serum (FBS) was purchased from Gibco Life Technologies, USA. 1% penicillin/streptomycin and Trypsin-EDTA were purchased from Invitrogen. Hoechst 33258 was purchased from Sigma-Aldrich, Acridine Orange was purchased from Sigma-Aldrich and Ethidium Bromide was purchased from HIMEDIA.

3.2.2 Physical Measurements

Elemental analyses (C, H, N) were performed on Perkin–Elmer 2400 series II analyzer. Electrospray ionization mass spectrometry (ESI-MS) spectra were recorded on a Micromass QTOF YA 263 mass spectrometer. IR spectra were observed and obtained with a Perkin– Elmer I-0100 spectrophotometer with KBr disk. ^{1}H NMR spectra were measured on Bruker FT 300 MHz spectrometer in $CDCl_3$ solvent. By Perkin–Elmer LAMBDA 25 spectrophotometer UV–Vis spectra were investigated. The emission data were collected on a Horiba FluroMax-4 fluorescence spectrometer. For all luminescence measurements slit width of 3 nm was used for both excitation and emission. Using freeze-pump-thaw-degassed solutions of the complex by a relative method using quinine sulfate in the same solvent as the standard [Φ_{std}= 0.54 (at 298 K) in 0.1 M H_2SO_4 at λ_{ex}= 350 nm] by usual method quantum yields of the complex was determined.

The quantum yields were calculated using Eq (1):

$$\Phi_r = \Phi_{std} \frac{A_{std}}{A_r} \frac{I_r}{I_{std}} \frac{\eta_r^2}{\eta_{std}^2} \qquad (1)$$

Where, Φ_r and Φ_{std} are the quantum yields of unknown and standard samples, A_r and A_{std} (<0.1) are the solution absorbance's at the excitation wavelength (λ_{ex}), I_r and I_{std} are the integrated emission intensities, and η_r and η_{std} are the refractive indices of the solvent.

3.2.3 Computational Details

The geometrical structures of the ground-state of the selected complex was optimized by the DFT method with B3LYP exchange correlation functional approach.[28,29] The geometry of the complex was fully optimized in solution phase without any symmetry constraints. There was a good agreement between the theoretical and experimental structures. Relativistic effective core potential (ECP)[30] on iridium. replaced the inner core electrons leaving the outer core [$(5s)^2(5p)^6$] electrons and the ($5d^6$) valence electrons of iridium (III).[31] In the calculation basis "double-ξ" quality basis set LANL2DZ was adopted as the basis set for iridium atom. The 6-31G basis set was used for the H atom and 6-31+G(d,p) for C, N, Cl, and O atoms for the optimization of both the ground state and the lowest lying triplet excited state geometries. Figures showing MOs and the difference density plots were prepared by using the Gauss View 5.1 software. All the calculations were performed with the Gaussian 09 W software package.[32]

3.2.4 Synthesis of L

2-Quinolinecarboxaldehyde (157 mg, 1 mmol) was dissolved in 30 ml ethanol. Then the solution was added to the solution of 4-Aminoazobenzene (197 mg, 1 mmol) at room temperature. The mixture was refluxed for 6 h. Brown precipitate was appeared after the mixture was refluxed for 6 h. Then the precipitate of L (**Ssheme 3.1**) was separated on filtration and recrystallized from dichloromethane-hexane layer. Yield: 160 mg (41 %). Anal. Calc. $C_{22}H_{16}N_4$ (336): C, 78.55; H, 4.79; N, 16.66. Found: C, 78.95; H, 4.88; N, 16.31. IR (KBr pellets, cm^{-1}): ν(C=O) 1672, ν(N=N) 1477 (**Figure 3.1**).^{1}H NMR $CDCl_3$: δ 8.39 (d, 1H, *J* = 12), 8.24 (d, 1H, *J* = 12), 7.83 (d, 2H, *J* = 8), 7.64 – 7.57 (m, 4H), 7.50 – 7.45 (m, 4H), 7.45(d, 1H, *J* = 8), 6.73 (d, 1H, *J* = 12) (**Figure 3.2**).

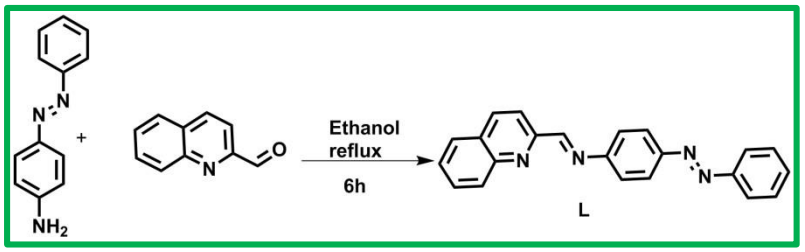

Scheme 3.1 Schematic representation of the synthesis of ligand L.

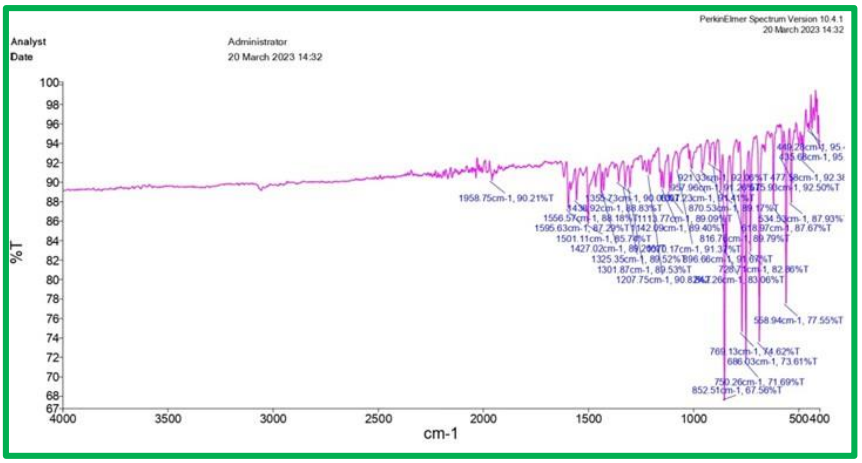

Figure 3.1 IR spectrum of ligand L.

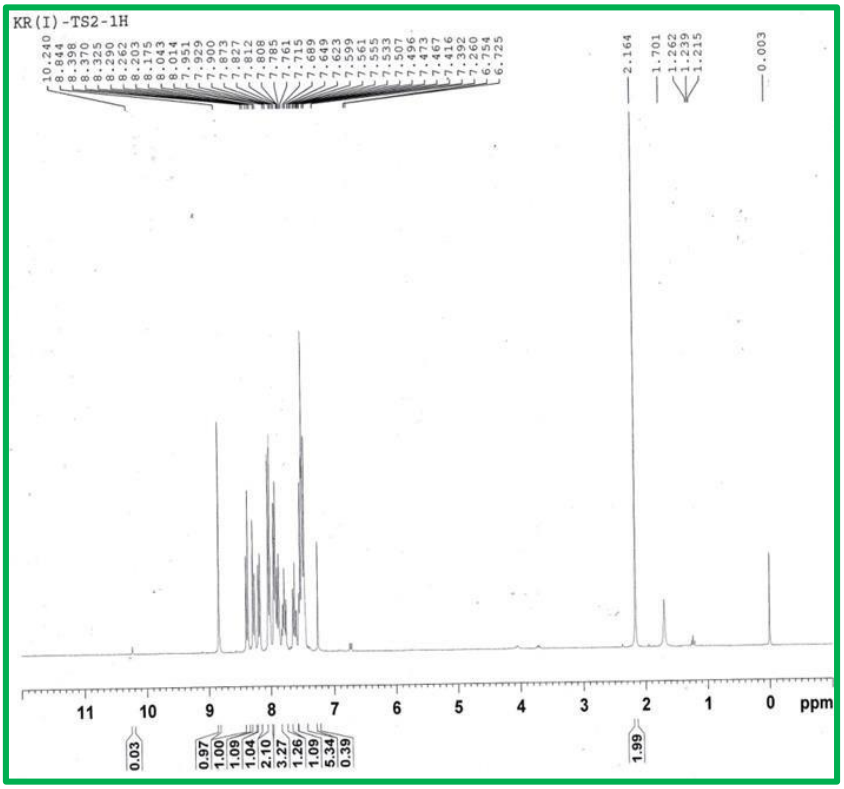

Figure 3.2 ^{1}H-NMR spectrum of ligand L in $CDCl_3$.

3.2.5 Synthesis of $[Ir(2\text{-}ppy)_2(L)]PF_6$ Complex

A mixture of L (10 mg, 0.029 mmol) and $[(2\text{-}ppy)_2Ir(\mu\text{-}Cl)]_2$ (31 mg, 0.029 mmol) was taken in a mixture of dichloromethane and ethanol (40 mL) and it was refluxed for 24 h. Deep brown precipitate of $[Ir(2\text{-}ppy)_2(L)]PF_6$ (**Scheme 3.2**) separated out and was collected by filtration and recrystallized from dichloromethane-hexane. Yield: 125 mg (66 %). Elemental Anal. Calc. for $C_{44}H_{32}IrN_6PF_6$: C, 53.82; H, 3.28; N, 8.56. Found: C, 53.87; H, 3.35; N, 8.61.

IR (KBr pellets, cm^{-1}): ν(N = N) 1471, ν(C=O) 1642 (**Figure 3.3**). ^1H NMR $CDCl_3$: δ (ppm), J (Hz): 9.79 (bs, 1H), 9.52 (bs, 1H), 8.24 – 7.98 (m, 5H), 7.77 – 7.69 (m, 3H), 7.56 – 7.42(m, 4H), 6.89 – 6.66(m, 6H), 6.23(bs, 1H), 5.72(d, 1H) (**Figure 3.4**). *m/z* = 837.16 $[M]^+$ (**Figure 3.5**).

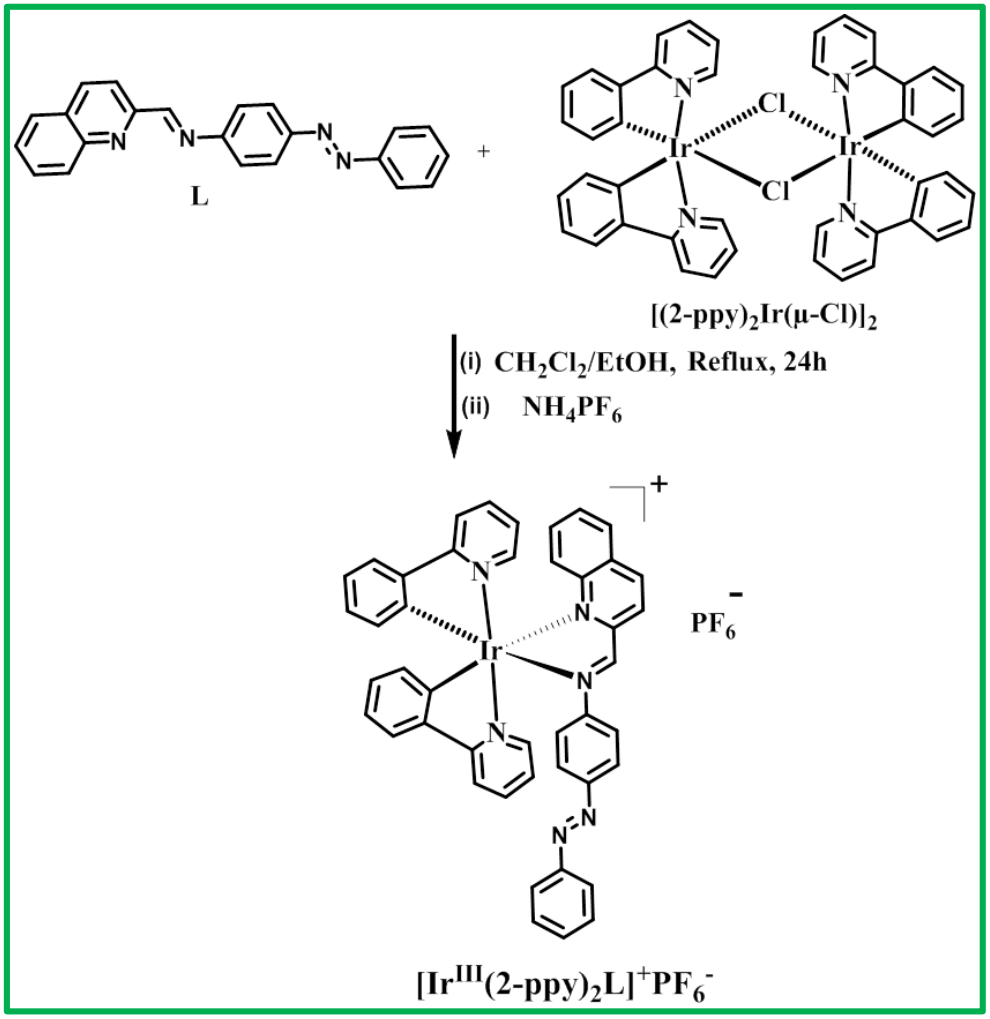

Scheme 3.2 Schematic representation of the synthetic route of complex $[Ir(2\text{-}ppy)_2(L)]PF_6$.

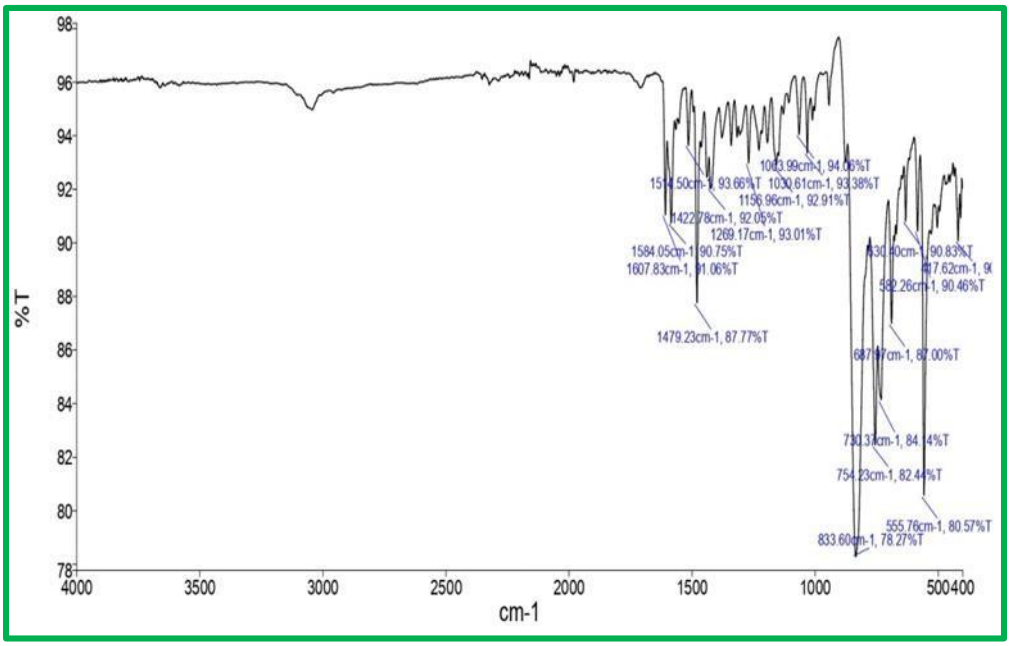

Figure 3.3 IR spectrum of $[Ir(2\text{-}ppy)_2(L)]PF_6$.

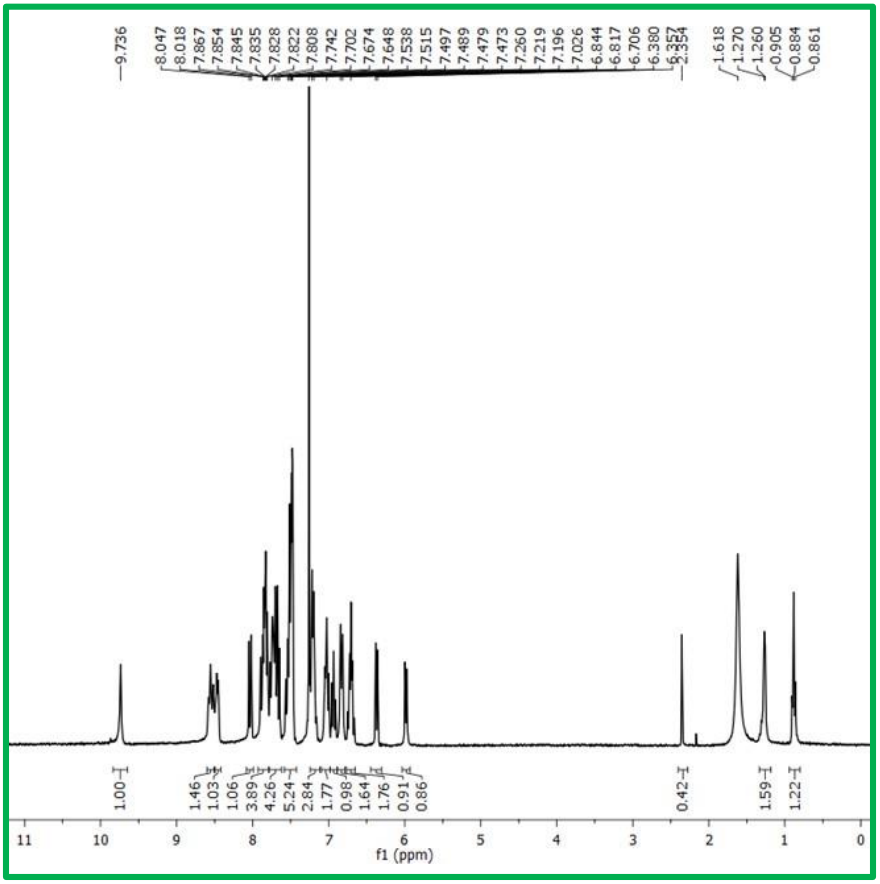

Figure 3.4 ^{1}H-NMR spectrum of $[Ir(2\text{-}ppy)_2(L)]PF_6$ in $CDCl_3$.

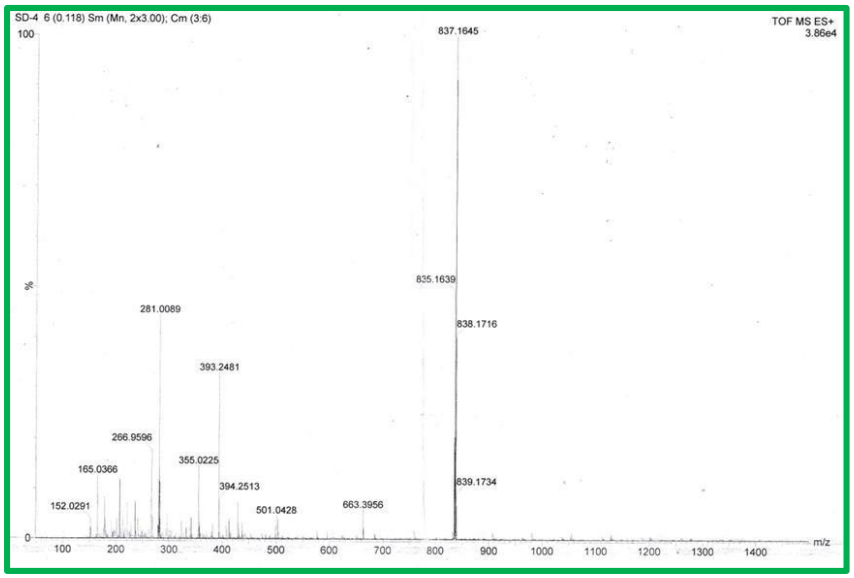

Figure 3.5 Mass spectrum of $[Ir(2\text{-}ppy)_2(L)]PF_6$.

Table 3.1 Crystal data and structure refinement parameters for the complex $[Ir(2\text{-}ppy)_2(L)]PF_6$.

	1
Formula	$C_{44}H_{32}IrN_6PF_6$
M_r	1967.21
Crystal system	Monoclinic
Space group	*C 2/c*
a / Å	32.920(4)
b / Å	22.482(3)
c / Å	24.578(3)
α /°	90
β /°	101.072(4)
γ /°	90
V /Å^3	17851 (4)
Z	8
D_{calcd} /g cm^{-3}	1.464
μ /mm^{-1}	3.090
θ/°	1.903-27.183
T /K	273 K
Reflns collected	10179
R1,[a] wR2[b] [$I > 2\sigma(I)$]	0.1476, 0.3075
GOF on F^2	1.10

$^aR1 = \Sigma \left| \left| F_o \right| - \left| F_c \right| \right| / \Sigma \left| F_o \right|$. $^b wR2 = [\Sigma[w(F_o^2 - F_c^2)^2] / \Sigma[w(F_o^2)^2]]^{1/2}$

3.2.6 Crystallographic Studies

The single crystal suitable for X-ray crystallographic analysis of the complex was obtained by slow evaporation of acetone solution of the complex. The X-ray intensity data were collected on Bruker AXS SMART APEX CCD diffractometer (Mo K_α, $\lambda = 0.71073$ Å) at 293 K. The detector was placed at a distance 6.03 cm from the crystal. Total 606 frames were collected with a scan width of 0.3° in different settings of φ. The data were reduced in SAINTPLUS[33] and empirical absorption correction was applied using the SADABS package.[34] Metal atom was located by Patterson Method and the rest of the non-hydrogen atoms were emerged from successive Fourier synthesis. The structures were refined by full matrix least-square procedure on F^2. All non-hydrogen atoms were refined anisotropically. However, the connectivity and other broad structural features of the complex were refined to a reasonable degree with respect to data quality and are undoubtedly correct. All calculations were performed using the SHELXTL V 6.14 program package.[35] The disorder solvent molecule/(s) has been dealt with "SQUEEZ"[36] command under the above program. Molecular structure plots were drawn using the Oak Ridge thermal ellipsoid plot (ORTEP).[37] The CCDC number of complex $[Ir(2\text{-}ppy)_2(L)]PF_6$ is 2257731. Relevant crystal data is given in **Table 3.1**.

3.2.7 Methods for Cancer Activity

3.2.7.1 Complex Stock Preparation

The Iridium crystals were obtained in powder form. A stock solution of 10 mM was prepared for the complex by weighing them and dissolving them in cell culture grade DMSO. The stock solution was further diluted to 200 µM, 100 µM, 50 µM, 25 µM, and 12.5 µM using media by serial dilution for cell viability assay.

3.2.7.2 Cell Culture

Breast adenocarcinoma cell line MCF-7, triple negative breast cancer cell line MDA - MB - 231 and normal hepatic cell line WRL - 68 were purchased from the National Centre for Cell Science, Pune, India. The MCF - 7 and WRL - 68 cell lines were maintained in Minimal Essential Media Earl's (MEM) supplemented with 10 % Fetal Bovine Serum (FBS) whereas MDA - MB - 231 cell line was maintained in DMEM high glucose media. The cell line was stored in a humidified incubator at 37 °C under an atmosphere of 5 % CO_2.

3.2.7.3 Cell Viability Assay

Cell viability studies of the complex $[Ir(2\text{-}ppy)_2(L)]PF_6$ as well as cis-platin were conducted using 3-(4, 5-Dimethylthiazol-2-yl)-2, 5- diphenyl tetrazolium bromide (MTT) on MCF-7, MDA-MB-231 and WRL-68 cell lines. For this experiment, approximately 1×10^4 cells from different cell lines were used to seed 96 well plates. The cells were further treated with various concentrations of the complex, from 12.5 µM to 200 µM for a period of 24 h at 37 ˚C. 10 µl of MTT at 5 mg/ml concentration was added to each well and incubated for 4 h at 37 ˚C. 100 µl of DMSO: Methanol were added to each well and the absorbance was measured at 570 nm in a Spectramax i3X microtitre plate reader. The IC_{50} for the complex was calculated using Compu Syn software. The statistical significance was evaluated using Graph Pad Prism software.

3.2.7.4 Colony Formation Assay

The effect $[Ir(2\text{-}ppy)_2(L)]PF_6$ complex was further investigated by performing colony formation assay. 6-well plates were used to seed the MCF - 7 cells and incubated at 37 ˚C for 24 h. The cells were treated with $[Ir(2\text{-}ppy)_2(L)]PF_6$ complex at 7 µM and 12.5 µM concentrations. After 24 h of treatment, Methanol was used to fix the cells and 0.5 % Crystal violet was used for staining. The plates were observed under Olympus inverted microscope at 4X magnification.

3.2.7.5 Hoechst Assay

Apoptotic effects of the complex $[Ir(2\text{-}ppy)_2(L)]PF_6$ on MCF - 7 cells were investigated by the Hoechst Staining Assay. The cells were seeded on cover slips placed on 6-well plates. Following adherence, the cells were treated with $[Ir(2\text{-}ppy)_2(L)]PF_6$ at 7 µM and 12.5 µM concentrations and incubated at 37 ˚C for 24 h. PBS was used to wash the cells and 4% formaldehyde was used to fix the cells for 1 h. The wells were further washed with PBS and Hoechst 33,258 was used to stain the cells in the dark. The cover slips were mounted using glycerol on grease-free slides and the cell morphology was visualized at 40X magnification under an Olympus fluorescent microscope.

3.2.7.6 AO/EB Staining

AO/EB staining assay was conducted to find morphological evidence of the incidence of apoptosis. MCF - 7 cells were seeded on sterile cover slips in 6-well plates for AO/EB staining. The cells were treated at 7 µM and 12.5 µM concentrations of $[Ir(2\text{-}ppy)_2(L)]PF_6$

complex. For 24 h, the plates were incubated at 37 ˚C. The cells were washed with PBS and fixed using 4% formaldehyde. 250 µl AO (Acridine Orange) and Ethidium Bromide stains were added to each well to stain the cells and this step was carried out entirely in the dark. After a sequential wash with PBS, the coverslips were mounted on grease-free glass slides using glycerol. Imaging was done with an Olympus fluorescent microscope at 20X magnification.

3.3 Results and Discussion

3.3.1 Synthesis

The Schiff base ligand L was synthesized according to the conventional method by the condensation reaction of 4-aminoazobenzene and 2-quinolinecarboxaldehyde (**Scheme 3.1**) and are used as neutral bidentate N, N donor ligand towards iridium(III) metal centre. It is to be noted that the choice of such ligands helps us to achieve our goal in the context of synthesis of Iridium(III) complex with interesting optical properties. The stoichiometric reaction of $[(2\text{-ppy})_2Ir(\mu\text{-Cl})]_2$ with ligand L in 1:1 ratio in boiling toluene under argon atmosphere afforded yellow coloured complex of composition $[Ir(2\text{-ppy})_2(L)]PF_6$ respectively in excellent yields (54%) (**Scheme 3.2**). The recrystallization of the complex from dichloromethane-hexane layer provided yellow crystals. X-ray crystallographic study reveals the structural parameters of $[Ir(2\text{-ppy})_2(L)]PF_6$. Complex $[Ir(2\text{-ppy})_2(L)]PF_6$ was found to be in cationic form as L acted as N, N donor ligand and the charge was balanced of that complex by hexafluorophosphate anion.

3.3.2 Structural Characterization

The ligand L and the corresponding complex $[Ir(2\text{-ppy})_2(L)]PF_6$ were characterized satisfactorily by IR, ESI-MS and ^1H NMR spectroscopy. The IR spectra of the complex exhibited the characteristic azo bond (*N =N*) stretching frequency at ~ 1475 cm^{-1}. The azomethine (-C = N) stretching frequency usually observed at ~ 1575 cm^{-1} which is present in both the ligand and complex. The IR data of all these compounds are given in the experimental section. The comparison between the IR stretching frequencies of ligands and corresponding complex has shown in **Figure 3.1 and 3.3**. The ^1H NMR spectra of the complex and ligands was recorded in $CDCl_3$. The complex is diamagnetic and display well resolved NMR spectra in $CDCl_3$ solution and the spectral data are given in the experimental section. The assignment of NMR

peaks is based on the intensity and spin-spin splitting pattern. A singlet due to azomethine hydrogen atom observed at 8.844 ppm in ligand which is shifted downfield after chelation with iridium(III) at 9.736 ppm. The ^{1}HNMR spectrum of L reveals the aromatic protons comes under the range of δ 7.26–8.4 ppm whereas for the complex it varies in the range of 6.357–8.047. The overall number of aromatic protons was consistent with the structure of the ligand and complex. **Figure 3.2 and 3.4** provides the spectra of both ligand and complex, respectively.

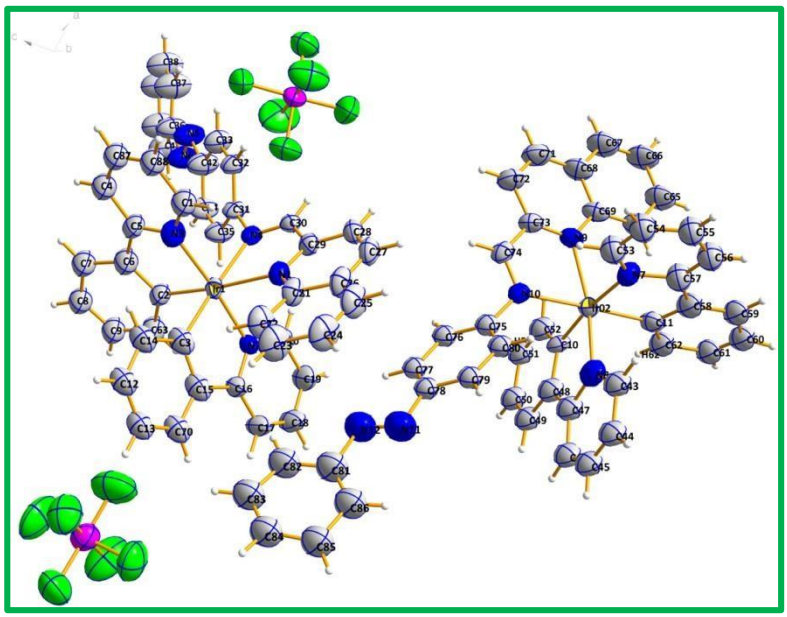

Figure 3.6 Molecular structure of $[Ir(2\text{-}ppy)_2(L)]PF_6$ with atom numbering scheme.

3.3.3 Structure Analysis by X-ray Diffraction Method

The molecular structures of $[Ir(2\text{-}ppy)_2(L)]PF_6$ was determined by using single crystal X-ray diffractometer. Perspective view of the molecular structure is shown in **Figure 3.6**. $[Ir(2\text{-}ppy)_2(L)]PF_6$ crystallized in the monoclinic system with space group C2/c. Selected bond distances and angles for $[Ir(2\text{-}ppy)_2(L)]PF_6$ are given in **Table 3.2**. The X-ray structure reveals that in the complex $[Ir(2\text{-}ppy)_2(L)]PF_6$, iridium centre binds with L through N, N donating site making the complex cationic one. The complex possesses distorted octahedral geometry around the iridium centre. The linear bond angles around iridium centre are not perfectly 180° but it ranges from 174° to 177°. Two phenyl pyridine moieties are arranged in mutually trans in position. The ligand L– iridium bite angle (N1-Ir-N2) was found to be 79.1° which makes a five membered ring with iridium centre. The bond distances between Ir-N1 and Ir-N2 are

2.239 Å and 2.170 Å. The ligand is not planer while coordinating with iridium centre but the azobenzene moiety dangled with the quinolone moiety in L. A PF_6^- ion resides in the unit cell with $[Ir(2\text{-}ppy)_2(L)]PF_6$ molecule to balance the cationic charge.

Table 3.2 Selected bond distances and angles for $[Ir(2\text{-}ppy)_2(L)]PF_6$.

Complex, $[Ir(2\text{-}ppy)_2(L)]PF_6$		
Bond Length (Å)		
	Experimental	Theoretical
Ir1-N1	2.256(17)	2.256
Ir1- N2	2.051(17)	2.075
Ir1- N3	2.06(2)	2.09
Ir1- N4	2.159(17)	2.162
Ir1- C2	1.99(2)	2.01
Ir1- C3	2.01(3)	2.023
Bond Angles(˚)		
N4-Ir1-N2	98.1(6)	100.4
N1-Ir1- N2	87.5(6)	88.8
C3-Ir1- N4	175.2(10)	175.1
N1-Ir1- N4	75.1(7)	76.1
N4-Ir1- N3	85.3(9)	86.3
N3-Ir1- C3	97.4(12)	97.5
N3-Ir1- C2	80.3(10)	80.1
C2-Ir1- N1	174.3(9)	176.05
N1-Ir1- C3	103.7(10)	102.7
N3-Ir1-N1	97.1(8)	97.5
N2-Ir1-C2	95.3(8)	95.3
N4-Ir1-C2	99.5(9)	100.3
N3-Ir1-N2	174.9(8)	175.3
N3-Ir1-C2	80.3(10)	79.1
C3-Ir1-C2	81.8(11)	82.3

3.3.4 DFT Studies

Molecular structures of both ligand and iridium complex were optimized by DFT at their electronic ground state (S_0) using 6–31 G and LANL2DZ basis set respectively. The optimized structures with frontier molecular orbitals showing electron density distribution in their various energy state of the compounds are given in **Table 3.3 and 3.4**.

Table 3.3 Isodensity plots of frontier molecular orbitals of complex with stating energy states.

Energy state	Orbital	Energy (eV)	Frontier Molecular Orbital
182	L+2	-1.562	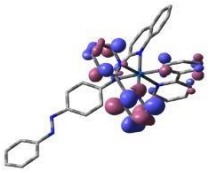
181	L+1	-2.501	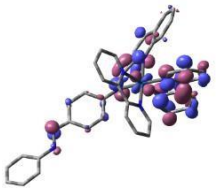
180	L	-2.580	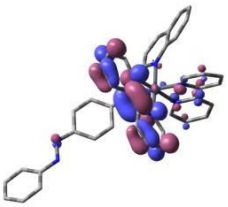
179	H	-3.318	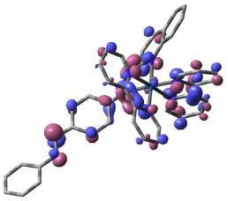
178	H-1	-4.055	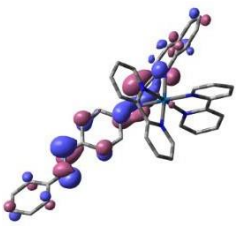
177	H-2	-0.557	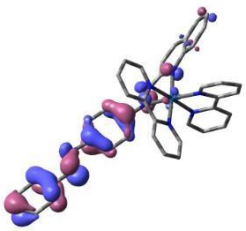

Table 3.4 Isodensity plots of frontier molecular orbitals of ligand with stating energy states.

Energy state	Orbital	Energy (eV)	Frontier Molecular Orbital
91	L+2	-1.380	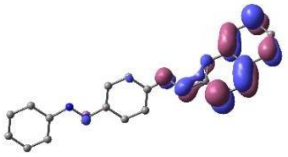
90	L+1	-2.309	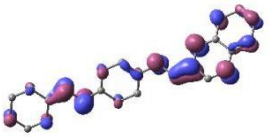
89	L	-2.921	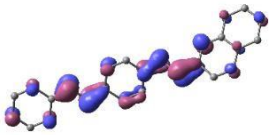
88	H	-6.244	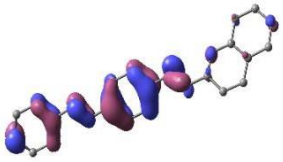
87	H-1	-6.647	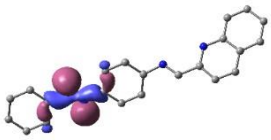
86	H-2	-6.751	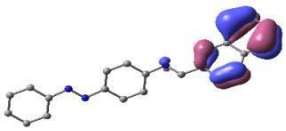

As no suitable single crystal was not obtained for ligand L, DFT study can give an idea about its structural parameters and orientation of electron density around atoms in molecular level. The optimized ground state structures of the complex at its singlet (S_0) state, possesses distorted octahedral geometry around iridium(III) metal centre which is accordance with the experimental values. In this complex all the Ir-N lies in the range of 2.0 to 2.2 Å. Bond angles of the optimized structure are close to the experimental values. All these values deviate from the experimental parameters faintly, which is dependent on the errors originated from the environmental factors such as crystal packing and the impact of the medium.

It is very interesting to compare the HOMO (Highest occupied molecular orbital) LUMO (Lowest unoccupied molecular orbital) energy gap between the ligand and the complex. The HOMO LUMO energy gap of the ligand is 3.333 eV whereas 0.738 eV for the complex. Because of this low energy gap, the complex is more stable and there is a possibility of the enhancement of mobility of π electrons over the aromatic moieties of the ligand part of the iridium complex. This phenomenon makes the complex a potential semiconductor since its small conduction band gap. From the frontier molecular orbitals, it is observed that the electrons are dense in one of the phenyl pyridine moiety of the iridium complex in LUMO whereas in HOMO, electrons density is dispersed over the entire molecule. **Figure 3.7** represents partial molecular orbital diagram of L and $[Ir(2\text{-}ppy)_2(L)]^+$ showing HOMO LUMO energy levels.

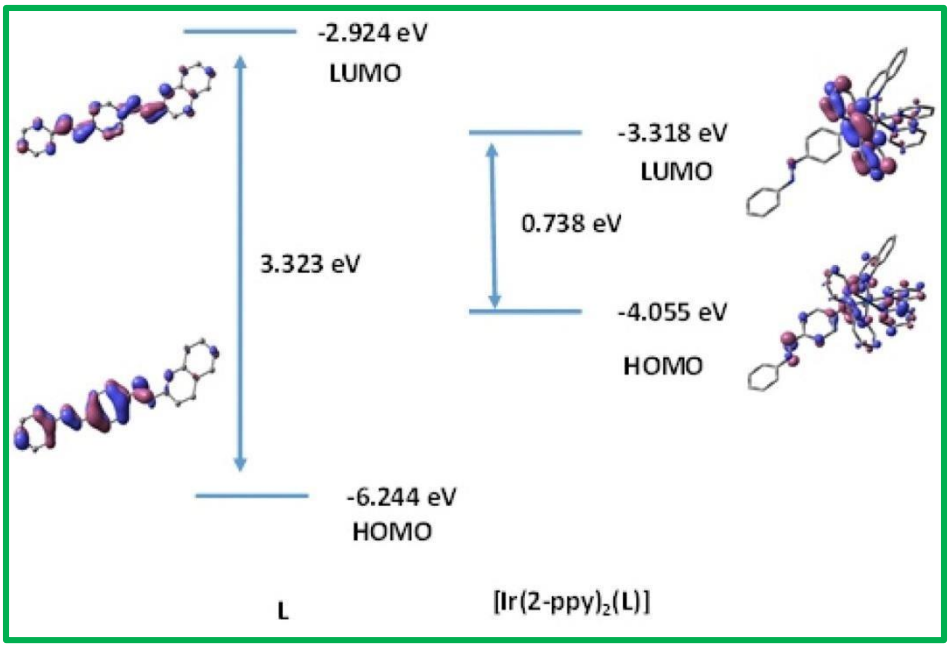

Figure 3.7 Partial molecular orbital diagram of L and $[Ir(2\text{-}ppy)_2(L)]^+$.

3.3.5 Photophysical Properties of the Complex

The absorption spectral behaviour of the ligand and iridium(III) complex is recorded in acetonitrile at room temperature. The relevant electronic spectra are given in **Figure 3.8**. Complex $[Ir(2\text{-}ppy)_2(L)]PF_6$ shows three distinct absorbance peak at 264 nm (ε = 88,300 M^{-1} cm^{-1}), 317 nm (ε = 58,535 $M^{-1}cm^{-1}$), 385 nm respectively. Low energy absorption at 385 nm (ε = 32,428 $M^{-1}cm^{-1}$) is assigned as MLCT transition and other high energy absorptions are

assigned as intraligand charge transfer (ILCT) transition. As the ligand is non-emissive in nature the emission of the complex may arises due to ^{3}MLCT. The emission property of the complex was measured in acetonitrile solution keeping the concentration at 2×10^{-5} M. Emission occurs at 428 nm, with little shoulder peak at 406 nm and 470 nm when $[Ir(2\text{-}ppy)_2(L)]PF_6$ was excited at 380 nm. It is found that the Stokes shifts for $[Ir(2\text{-}ppy)_2(L)]PF_6$ complex are very less ~40 nm. The quantum yield was found to be 0.136 for $[Ir(2\text{-}ppy)_2(L)]PF_6$. The relevant emission spectra are given in **Figure 3.9**.

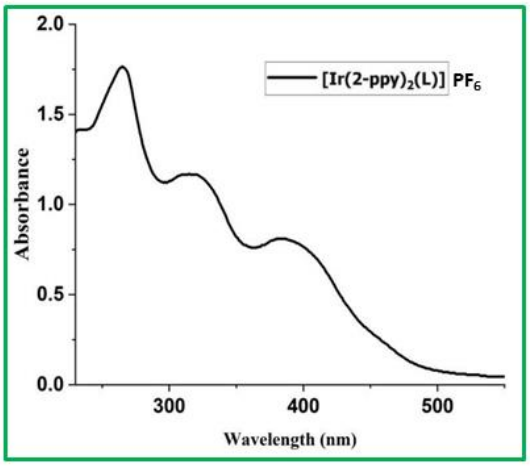

Figure 3.8 Absorption spectra of complex $[Ir(2\text{-}ppy)_2(L)]PF_6$ in acetonitrile at room temperature keeping concentration ($c = 2 \times 10^{-5}$ M).

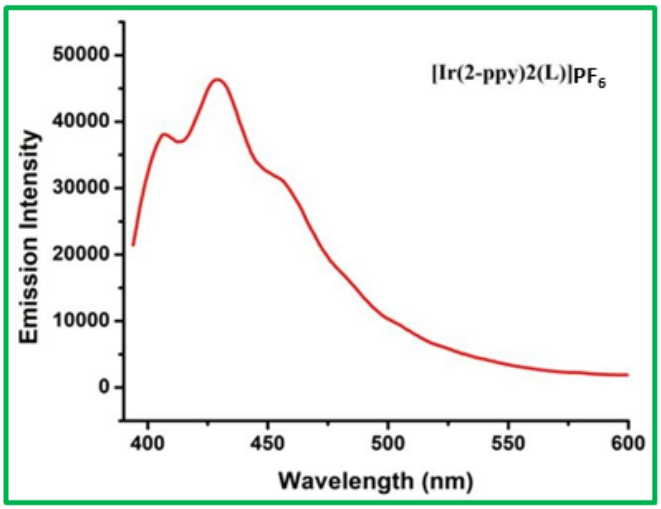

Figure 3.9 Emission spectra of complex $[Ir(2\text{-}ppy)_2(L)]PF_6$ in acetonitrile at room temperature keeping concentration ($c = 2 \times 10^{-5}$ M).

Table 3.5 IC * value of $[Ir(2\text{-}ppy)_2(L)]PF_6$ and Cisplatin against various cell lines. *IC is the concentration required to inhibit 50 % of cellular growth. The values are the mean of triplicate determinations.

Compounds	IC_{50}		
	MCF-7	MDA-MB-231	WRL68
$[Ir(2\text{-}ppy)_2(L)]PF_6$	9.15±1.5	45.38±2.5	53.4±1.3
Cisplatin	16.57±1.4	92.1±2.2	41.05±1.2

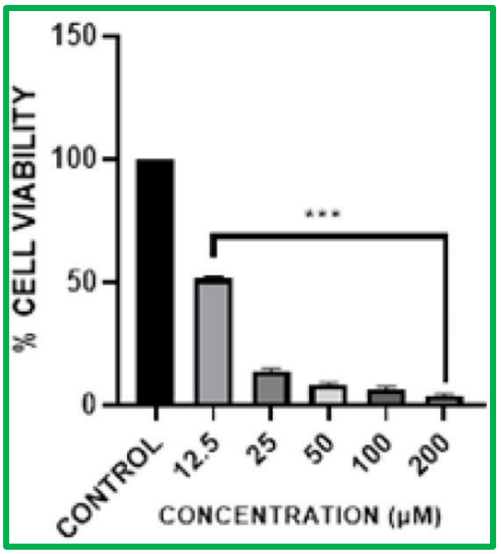

Figure 3.10 The Bar Diagram showing the cytotoxic effects of Iridium complex (from 12.5 to 100 μM) was analysed using MTT Assay on MCF-7 cells in-vitro. All the experiments are performed independently three times where $*P < 0.05$, $**P < 0.01$ and $***P < 0.001$.

3.3.6 Cell Viability Assay

MTT assay was performed to analyse the cytotoxic effect of $[Ir(2\text{-}ppy)_2(L)]PF_6$ and Cisplatin on various cell lines {MCF-7 (breast adenocarcinoma), MDA-MB-231 (breast carcinoma), WRL 68 (human cervix carcinoma)} for 24 h. The result is shown in **Table 3.5**. After 24 h of treatment, the IC_{50} values were calculated which was 9.15 ± 1.5 μM for $[Ir(2\text{-}ppy)_2(L)]PF_6$ on MCF - 7 cell line. So from the table of IC_{50} values of different cell lines, it can be concluded that in comparison to other cell lines, $[Ir(2\text{-}ppy)_2(L)]PF_6$ show the most effective antiproliferative activity in MCF - 7 cell line. That is why MCF - 7 cell line was used for further experiments. It is important to note that complex $[Ir(2\text{-}ppy)_2(L)]PF_6$ with quinoline and azobenzene group is

more effective in antiproliferation activity. The cause behind such result can be assumed that as the increment of the lipophilic character of the complex with the aid of azoimine moiety. This further enhance the penetration across the lipid cell membrane. It is also noteworthy that the iridium(III) complex under this study outperformed cisplatin with low cytotoxicity especially complex $[Ir(2\text{-}ppy)_2(L)]PF_6$. A one-way ANOVA test was used to examine the statistical significance of the individual treatment groups with respect to the untreated control. The experiment was performed in triplicate. **Table 3.5** represents the IC50 values of the complex in comparison to *cis* platin (**Figures 3.10 – 3.13**).

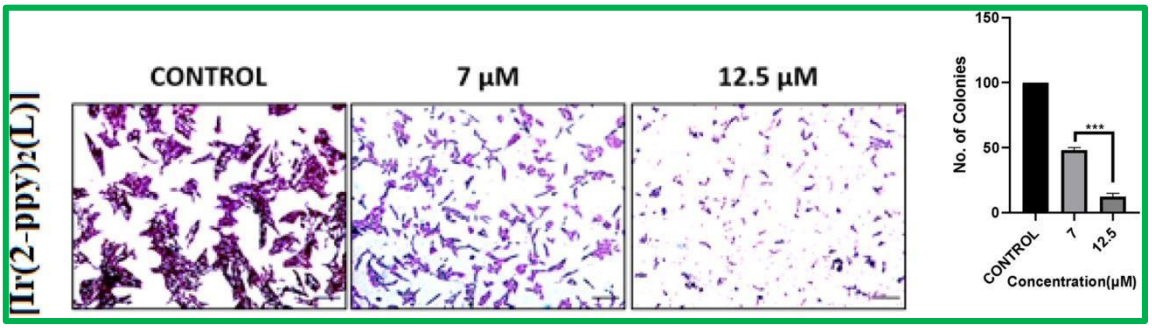

Figure 3.11 MCF7 cells were treated with $[Ir(2\text{-}ppy)_2(L)]PF_6$ for 24 h at different concentrations. The treated cells were observed under 4X magnification. The experiments were performed thrice (***$P < 0.001$).

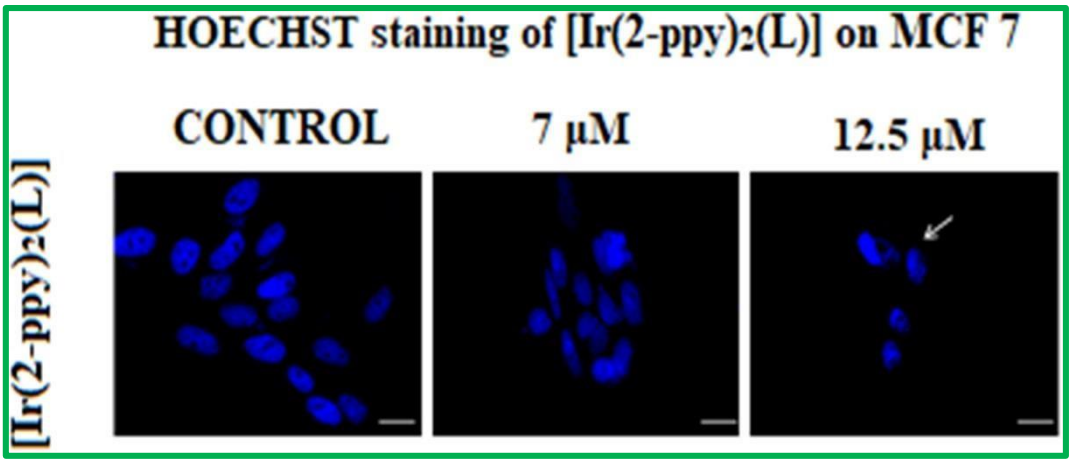

Figure 3.12 The Iridium complex was used to treat MCF-7 cells in vitro to analyze anticancer effects of the complex for a period of 24 h. The arrows indicate nuclear fragmentation. The experiments were performed three times.

3.3.7 Colony Formation Assay

MCF-7 was treated with different concentrations of $[Ir(2\text{-}ppy)_2(L)]PF_6$ complex for 24 h. The cells were observed in bright field at 4X magnification. The colony numbers and sizes were analyzed and found to decrease for both the concentrations of each complex, which decreased further at higher doses of treatment. Each experiment was performed three times and the statistical significance was calculated by Graph Pad Prism version 8.0 (One-way ANOVA $p < 0.001$).

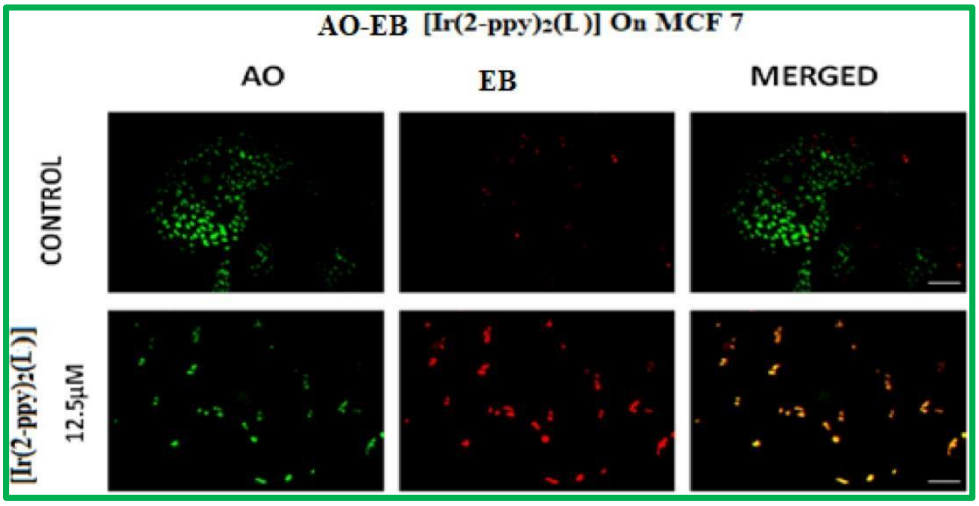

Figure 3.13 Effect of $[Ir(2\text{-}ppy)_2(L)]PF_6$ on MCF7 cells. MCF7 cells were treated with $[Ir(2\text{-}ppy)_2(L)]PF_6$ complex at different concentrations. The cellular morphology was assessed under microscope immediately after at 20X magnification.

3.3.8 HOECHST Assay

To further examine the anti-cancer effect of the $[Ir(2\text{-}ppy)_2(L)]PF_6$ complex on breast cancer cells, Hoechst staining assay, which is sensitive to DNA, was conducted. Alterations in nuclear morphology was observed in the MCF-7 cells after treatment with the Iridium complex for 24 h. Clear evidences of nuclear fragmentation were observed in the treated cells, indicating the occurrence of cellular apoptosis with shrinkage of the nucleus, cytoplasmic vacuolation, and blebbing and chromatin condensation whereas in the untreated control the nucleus appeared blue with a distinct structure and no morphological changes. These results demonstrated potent effect of $[Ir(2\text{-}ppy)_2(L)]PF_6$ complex on inducing apoptosis. The experiment was performed in triplicate.

3.3.9 AO/EB Staining

AO/EB staining is a standardized procedure to investigate incidence of cellular apoptosis in cells which is characterized by distinct changes in cellular morphology and DNA fragmentation. Viable cells with organized cellular structure stain green which indicates no occurrence of apoptosis. Cells that retain a yellow stain are indicative of early apoptosis, where the cell membrane is intact but there is evident initiation of DNA fragmentation whereas cells that stain red indicates cellular apoptosis along with chromatin condensation or fragmentation. On treatment with different doses of $[Ir(2\text{-}ppy)_2(L)]PF_6$ complex, MCF-7 cells showed an increase in red staining, which is indicative of apoptosis with cellular morphological changes like distortion of nuclear morphology, membrane blebbing, fragmentation, and shrinkage. The experiment was performed in triplicate.

3.4 Conclusions

In conclusion, a novel quinolone based Schiff base ligand and corresponding tris-cyclometalated iridum complex have been synthesized and investigated. The Iridium(III) complex is produced by chelation through N, N donor atoms of ligand. X-ray crystal structure of the complex suggests the proper orientation of the ligand with the iridium centre. DFT study has been done to support the experimental results. The photophysical property of the complex shows MLCT transition at 385 nm and blue emission near 428 nm having weak emission intensity. The complex shows lower toxicity compared to cisplatin and very effective in treating MCF-7 cells through apoptosis with cellular morphologic changes. On the basis of this findings, future works with variations of polydentate ligand will likely yield complex with even more enhanced optical and cytotoxic properties for cancer diagnostic and therapeutic applications.

References

(1) V. Ganapathy, M. Thangaraju and P. D. Prasad, *Pharmacol. Ther*., 2009, **121**, 29–40.

(2) R. L. Siegel, K. D. Miller and A. Jemal, *CA A Cancer J. Clin*., 2018, **68**, 7–30.

(3) D. P. Rose, E. M. Gilhooly and D. W. Nixon, *Int. J. Oncol*., 2002, **21**, 1285–1292.

(4) R. L. Fernandez, J. Leal, A. Gray and R. Sullivan, *Lancet Oncol*., 2013, **14**, 1165–1174.

(5) P. F. Iqbal, M. A. Malik and W. A. Wani, *World J. Pharm. Pharm. Sci*., 2018, **7**, 654–664.

(6) C. T. Kuo, C. L. Chiang, C. H. Chang, H. K. Liu, G. S. Huang, R. Y. Huang, H. Lee, C. S. Huang and A. M. Wo, Biomaterials, 2014, **35**, 1562–1571.

(7) D. Terefinko, A. Dzimitrowicz, A. B. Pohl, A. Klimczak, P. Pohl and P. Jamroz, *Int. J. Mol. Sci*., 2021, **22**, 3855.

(8) Y. E. Hadisaputri, U. Habibah, F. F. Abdullah, E. Halimah, M. Mutakin, S. Megantara, R. Abdulah and A. Diantini, *Breast Cancer*, 2021, **13**, 447–457.

(9) E. B. Jahromi, L. Jafaarnejad, M. Vahdani and S. Zolghadri, *Iran. Quart. J. Breast Dis*., 2020, **13**, 37–48.

(10) (a) S. Zolghadri, A. Ghanbariasad, F. Fallahian, M. Rahban, M. Kalavani, E. Bahman Jahromi, A. Asadzadeh and M. Hajiani, *Mol. Biol. Rep*., 2022, **49**, 363–372; (b) Y. Li, B. Liu, H. Shi, Y. Wang, Q. Sun and Q. Zhang, *Dalton Trans*., 2021, **50**, 14498–14512.

(11) X. Qu, D. Zhou, J. Lu, D. Qin, J. Zhou and H. J. Liu, *Bioact. Mater*., 2023, **24**, 136–152.

(12) M. Jain, A. Mishra, V. Yadav, H. Shyam, S. Kumar, S. K. Mishra and P. Ramakant, *Support. Care Cancer*, 2023, **31**, 6.

(13) C. Bailly, *Chem. Rev*., 2012, **112**, 3611–3640.

(14) M. Demaria, M. N. O'Leary, J. Chang, L. Shao, S. Liu, F. Alimirah, K. Koenig, C. Le, N. Mitin, A. M. Deal, S. Alston, E. C. Academia, S. Kilmarx, A. Valdovinos, B. Wang, A. de Bruin, B. K. Kennedy, S. Melov, D. Zhou, N. E. Sharpless, H. Muss and J. Campisi, *Cancer Discov*., 2017, **7**, 165–176.

(15) S. Hoelder, P. A. Clarke and P. Workman, *Mol. Oncol*., 2012, **6**, 155–176.

(16) G. Sahu, S. A. Patra, S. Lima, S. Das, H. Gorls, W. Plass and R. Dinda, *Chem. Eur. J*., 2023, **29**, e202202694.

(17) P. Zhang and H. Huang, *Dalton Trans*., 2018, **47**, 14841–14854.

(18) A. Sharma, P. Sudhindra, N. Roy and P. Paira, *Inorgan. Chim. Acta*, 2020, **513**, 119925.

(19) Y. Q. Gu, K. Yang, Q. Y. Yang, H. Q. Li, M. Q. Hu, M. X. Ma, N. F. Chen, Y. H. Liu, H. Liang and Z. F. Chen, *J. Med. Chem*., 2023, **66**, 9592–9606.

(20) H. Farhangian and A. N. Kharat, *J. Mol. Struct*., 2023, **1294**, 136373.

(21) M. Lv, X. Qian, S. Li, J. Gong, Q. Wang, Y. Qian, Z. Su, X. Xue and H. K. Liu, *J. Inorg. Biochem*., 2023, **238**, 112057.

(22) F. X. Wang, M. H. Chen, Y. N. Lin, H. Zhang, C. P. Tan, L. N. Ji and Z. W. Mao, *ACS Appl. Mater. Interfaces*, 2017, **9**, 42471–42481.

(23) Z. Liu, A. Habtemariam, A. M. Pizarro, S. A. Fletcher, A. Kisova, O. Vrana, L. Salassa, P. C. A. Bruijnincx, G. J. Clarkson and V. Brabec, *J. Med. Chem*., 2011, **54**, 3011–3026.

(24) D. L. Ma, C. Wu, K. J. Wu and C. H. Leung, *Molecules*, 2019, **24**, 2739.

(25) S. K. Tripathy, U. Deb, N. Dehury, P. Laha, M. K. Panda, H .S. Kim and S. Patra, *Dalton Trans*., 2016, **45**, 15122–15136.

(26) R. Cao, J. Jia, X. Ma, M. Zhou and H. Fei, *J. Med. Chem*., 2013, **56**, 3636–3644.

(27) H. C. Zhao, B. Mello, B. L. Fu, H. Chowdhury, D. J. Szalda, M. K. Tsai, D. C. Grills and J. Rochford, *Organometallics*, 2013, **32**, 1832.

(28) A. D. Becke, *J. Chem. Phys*., 1993, **98**, 5648–5652.

(29) C. Lee, W. Yang and R. G. Parr, *Phys. Rev. B*, 1988, **37**, 785–789.

(30) G. M. Sheldrick, *Acta Cryst. A*, 2008, **64**, 112-122.

(31) G. M. Sheldrick, SHELEXL-97 and SHELXL-97, *Program for Crystal Structure Solution and Refinement*, University of Gottingen, Gottingen, 1997.

(32) G. Scalmani, V. Barone, B. Mennucci, G. A. Petersson, H. Nakatsuji, M. Caricato, X. Li, H. P. Hratchian, A. F. Izmaylov, J. Bloino, G. Zheng, J. L. Sonnenberg, M. Hada, M. Ehara, K. Toyota, R. Fukuda, J. Hasegawa, M. Ishida, T. Nakajima, Y. Honda, O. Kitao, H. Nakai, T. Vreven, J. A. Montgomery Jr, J. E. Peralta, F. Ogliaro, M. Bearpark, J. J. Heyd, E. Brothers, K. N. Kudin, V. N. Staroverov, R. Kobayashi, J. Normand, K. Raghavachari, A. Rendell, J. C. Burant, S. S. Iyengar, J. Tomasi, M. Cossi, N. Rega, J. M. Millam, M. Klene, J. E. Knox, J. B. Cross, V. Bakken, C. Adamo, J. Jaramillo, R. Gomperts, R. E. Stratmann, O. Yazyev, A. J. Austin, R. Cammi, C. Pomelli, J. W.

Ochterski, R. L. Martin, K. Morokuma, V. G. Zakrzewski, G. A. Voth, P. Salvador, J. J. Dannenberg, S. Dapprich, A. D. Daniels, O. Farkas, J. B. Foresman, J. V. Ortiz, J. Cioslowski and D. J. Fox, Gaussian09, (RevisionA.1), Gaussian, Inc., Wallingford, CT, 2009.

(33) SMART; SAINT; SADABS; XPREP; SHELXTL, BrukerAXSInc., Madison, WI, 1998.

(34) G. M. Sheldrick, SHELXTL, v.6.14, Bruker AXS Inc., Madison, WI, 2003.

(35) C. K. Johnson, ORTEP Report ORNL-5138, Oak Ridge National Laboratory, TN, Oak Ridge, 1976.

(36) A. L. Spek, *Acta Cryst. C*, 2015, **71**, 9–18.

(37) J. Wagler, D. Gerlach and G. Roewer, *Inorg. Chim. Acta*, 2007, **360**, 1935–1942.

Chapter 4

Synthesis, structure and, photophysical and catalytic properties of a copper(II) complex containing bidentate (N,O) Schiff base ligand

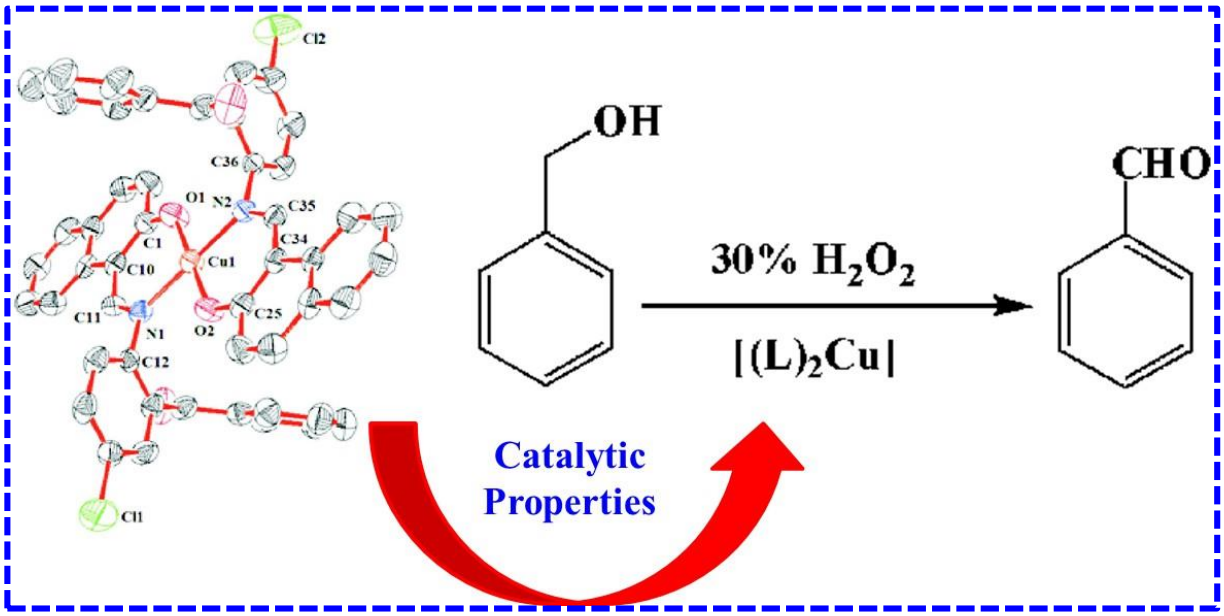

Abstract:

The bidentate ligand HL was prepared by the condensation of 2-naphthaldehyde with 2- amino-5-chlorobenzophenone. The reaction of HL with $Cu(OAc)_2.H_2O$ afforded the new complex of composition $[(L)_2Cu]$. The ligand HL binds the Cu(II) centre in bidentate (N,O) fashion being uni-negative anion by the way of phenolic proton dissociation during chelation. The complex was characterized by spectroscopic studies. X-Ray structures of $[(L)_2Cu]$ was determined to confirm the molecular species unequivocally. The photoluminescence properties of the ligand and complex were studied. Oxidation of benzyl alcohol using the newly synthesized complex as catalyst has been studied.

4.1 Introduction

The chemistry of transition metal complexes incorporating Schiff base ligands have been explored considerably during the last few decades due to their multifunctional properties in luminescence,[1–3] magnetism,[4–7] catalysis[8–10] and electro-chemistry,[11,12] host-guest chemistry,[13] sensors[14] and biological activity[15]. Schiff bases have been significantly active in metal coordination chemistry over the years due to their facile syntheses. The high affinity for the complexation of the Schiff base ligands towards the transition metal ions, especially copper ions, is utilized in preparing their complexes. The chemistry of copper complexes is of interest due to their significance in biological and industrial processes.[16,17] The copper complexes derived from Schiff base ligands has received enormous attention due to their wide application in the field of catalyst[18,19] including asymmetric epoxidations, oxidation of sulphides and Lewis acid assisted organic transformation. The biological relevance of transition metal complexes containing imine-nitrogen donor ligands and the rich catalytic activity of copper complexes encouraged us to prepare the Cu^{II} complexes of the Schiff base ligands.[20–27] Herein, we report the synthesis of the bidentate ligand HL and its mononuclear bis copper complex $[(L)_2Cu]$. The ligand and complex have been characterized by spectroscopic techniques. The crystal structure of complex $[(L)_2Cu]$ has been determined, confirming the molecular structure. The fluorescence properties of both the ligand and the complex have been studied. The catalytic oxidation of benzyl alcohol to benzaldehyde has been investigated using H_2O_2 as oxidant.

4.2 Experimental Section

4.2.1 Materials and Methods

The solvents used for all the reactions were of reagent grade (E. Merck, India) and were purified and dried by reported procedure.[28] Copper acetate monohydrate was purchased from Sisco Research Laboratories (SRL), India. Microanalysis (C, H, N) was performed using a Perkin-Elmer 2400 C, H, N, S/O series II elemental analyzer. Infrared spectra were recorded on a Perkin-Elmer L120-00A FT-IR spectrometer with the samples prepared as KBr pellets. Electronic mspectra were recorded on a Shimadzu UV-1800 PC spectrophotometer.

4.2.2 Synthesis of ligand HL

2-Naphthaldehyde (200 mg, 1.28 mmol) and 2-amino-5-chlorobenzophenone (296 mg, 1.28 mmol) were heated to reflux in ethanol (40 ml) for 4 h. The bright yellow solid product was obtained as micro crystals which were collected by filtration and thoroughly washed with ethanol and diethyl ether and dried under vacuum (**Scheme 4.1**). Yield: 370 mg (75%). Anal. Calcd. $C_{24}H_{16}ClNO_2$ (385): C, 74.71; H, 4.18; N, 3.63. Found: C, 74.81; H, 4.25; N, 3.58%; UV-Vis spectrum (CH_3CN) λ_{max} (ε, M^{-1} cm^{-1}): 385 (695094), 326 (50635); IR: ν(C=N) 1621, ν(C=O) 1658; ^{1}H NMR $CDCl_3$: δ 13.19 (s, -OH, 1H), 9.34 (s, HC=N, 1H), 8.37 (d, 1H), 7.85 (d, 2H), 7.77–7.68 (q, 2H), 7.58 (d, 2H), 7.48 (t, 4H), 7.38 (d, 2H), 7.00 (d, 1H) (**Figure 4.1**). HRMS (ESI-TOF): *m/z* Calcd: 385.0870, Found: 385.9864 [M+H$^+$].

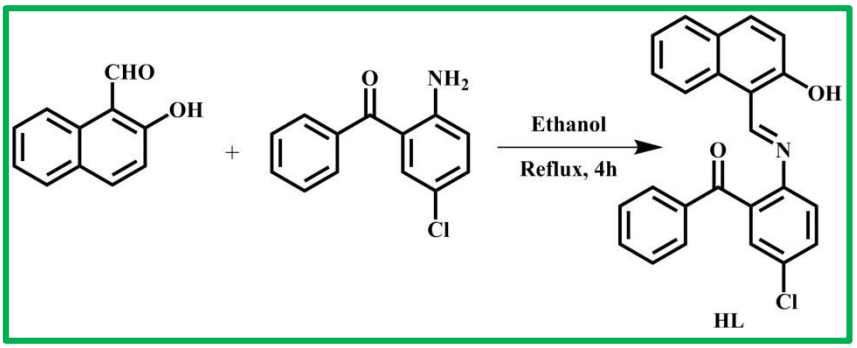

Scheme 4.1 Synthesis of ligand HL.

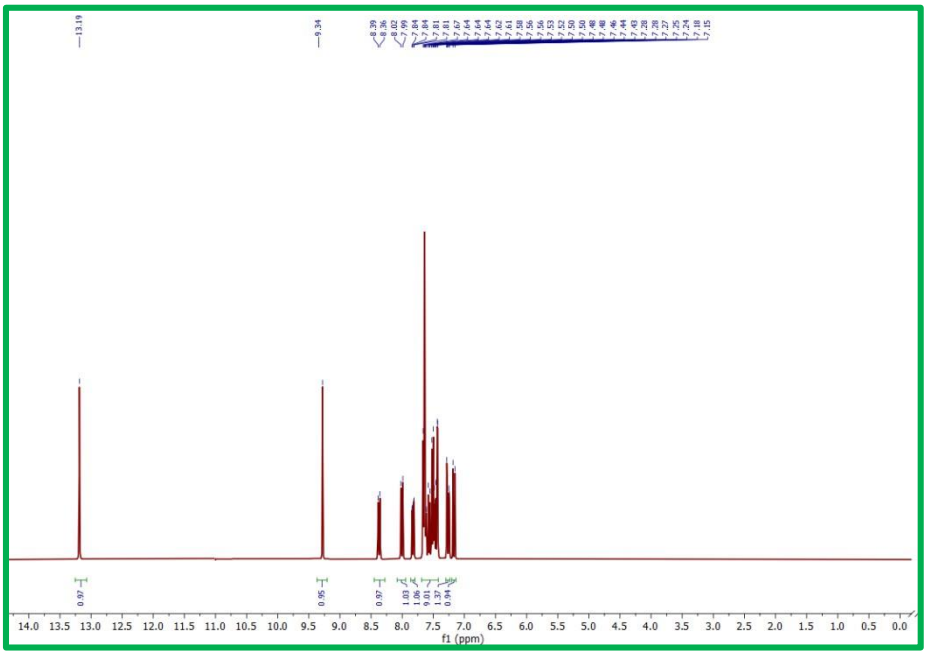

Figure 4.1 ^{1}H-NMR spectrum of ligand HL in $CDCl_3$.

4.2.3 Synthesis of $[(L)_2Cu]$ complex

5 ml methanolic solution of 45 mg (0.247 mmol) $Cu(OAc)_2$. H_2O, 10 ml methanol solution of 200 mg (0.519 mmol) of HL was added and the mixture was stirred for 2 h. Dark brown product was precipitated which was collected by filtration and was washed with petroleum ether and hexane. The precipitate then recrystallized from a dichloromethane-hexane solvent Mixture (**Scheme 4.2**). Yield: 180 mg (73%). Anal. Calcd. $C_{48}H_{30}Cl_2CuN_2O_4$ (833): C, 69.19; H, 3.63; N, 3.36. Found: C, 69.25; H, 3.67; N, 3.42%; UV-Vis spectrum (CH_3CN) λ_{max} (ε, M^{-1} cm^{-1}): 410 (86712), 316 (127491); IR: ν(C=N) 1616,ν(C=O) 1659.

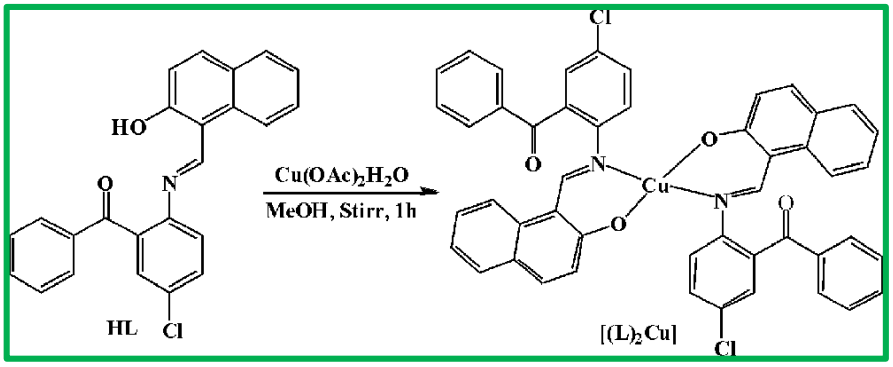

Scheme 4.2 Synthesis of $[(L)_2Cu]$ complex.

4.2.4 X-Ray structure determination of $[(L)_2Cu]$:

Single crystals of $[(L)_2Cu]$ was grown by slow diffusion of hexane in dichloromethane solution at 25ºC. Data were collected on a Bruker SMART CCD diffractometer using Mo-Kα monochromator (λ = 0.71073). Structure solutions were performed using Shelx 97 PC version program.[29] Full matrix least square refinements on F^2 were performed using SHELXL-97 program.[30] All the non-hydrogen atoms were refined anisotropically using full-matrix least squares method. Hydrogen atoms were included for structure factor calculations after placing them at calculated positions. Atomic coordinates and isotropic thermal parameters of $[(L)_2Cu]$ are given in **Table 4.1**.

4.2.5 Procedure for the catalytic oxidation of benzyl alcohol

To an acetonitrile solution of benzyl alcohol (5 mmol), the catalyst $[(L)_2Cu]$ (4 mol%) or and 30% H_2O_2 (5 equiv.) were added and the mixture was vigorously stirred at 70 ºC for 1 h. The

reaction was monitored by TLC. After completion of the reaction, the mixture was poured into water and the product was extracted with dichloromethane and dried over Na_2SO_4. The solvent was removed and the product was purified by column chromatography. Yields were determined by weighing the isolated product. The product was characterized by IR and ^1H NMR spectra.

Table 4.1 Crystallographic data for the complex $[(L)_2Cu]$.

Formula	$C_{48}H_{30}Cl_2CuN_2O_4$
M_r	833.19
Crystal system	Triclinic
Space group	P-1
a / Å	14.7980(7)
b / Å	10.7176(6)
c / Å	24.7174(13)
α /°	90.013(4)
β /°	100.772(4)
γ /°	89.993(4)
V /Å^3	3851.1(4)
Z	4
F(000)	1832.0
D_{calcd} /mg m^{-3}	1.437
μ /mm^{-1}	0.756
R1 (all data)	0.0695
wR2 [$I > 2\sigma(I)$]	0.2252
GOF	0.931

4.3 Results and Discussion

4.3.1 Synthesis of ligand and complex

The HL, ligand was prepared by the condensation reaction of 2-naphthaldehyde with 2- amino-5-chlorobenzophenone in 1:1 M ratio in refluxing ethanol (**Scheme 4.1**). The reaction of the HL ligand with $Cu(OAc)_2.H_2O$ in methanol afforded brown complex of composition $[(L)_2Cu]$ (**Scheme 4.2**). The complex $[(L)_2Cu]$ was paramagnetic matching with one unpaired electron as expected for Cu^{II} metal ion. The suitable crystal of $[(L)_2Cu]$ complex for X-ray studies were grown from dichloromethane-hexane solvent mixture.

4.3.2 Characterization

The UV-Vis spectra of $[(L)_2Cu]$ is distinctly different from the ligand HL the lowest energy absorption appeared near 385 nm and 410 nm, respectively.[31] Representative UV-Vis spectra of HL and $[(L)_2Cu]$ are shown in **Figure 4.2**. The ν(C=N) of $[(L)_2Cu]$ complex appear in the lower range (1616 cm^{-1}) compared to the ligand signifying the coordination to the metal centre. The ν(C=O) band of the ligand (~1658 cm^{-1}) almost remain similar after the formation of the $[(L)_2Cu]$ complex (1659 cm^{-1}), that clearly indicating that carbonyl group did not coordinated. The ligand HL afforded satisfactory ^1H NMR spectral data in $CDCl_3$. The sharp singlet near δ 13.19 was assigned to phenolic (-OH) proton for the ligand HL. The ^1H NMR spectra of HL showed resonances of proton belonging to the Schiff base group at δ 9.34. The ^1H NMR spectral features for the aromatic protons of the ligand HL matched well with the composition and structure. The electrospray mass spectrum of HL exhibited the most significant peak at *m/z* 385.9864 which was consistent with the molecular MH^+ ion.

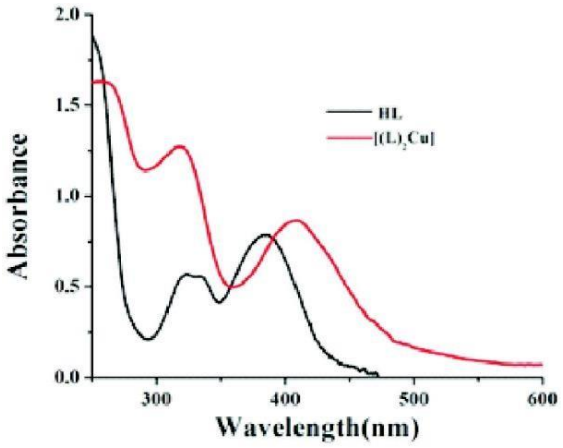

Figure 4.2 UV-Vis spectra of the ligand HL and complex in acetonitrile.

4.3.3 X-Ray structure of $[(L)_2Cu]$

Suitable crystals of $[(L)_2Cu]$ was grown by slow diffusion of hexane into dichloromethane solution. The X-ray structure of $[(L)_2Cu]$ was determined and described below. The perspective view of $[(L)_2Cu]$ complex is shown in **Figure 4.3**. Selected bond parameters of $[(L)_2Cu]$ complex is listed in **Table 4.1** and **Table 4.2**, respectively. In the $[(L)_2Cu]$ complex, the Cu centre is coordinated by two phenolato oxygens (O1 or O_{ph}), two imine nitrogen (N_{im}). The central Cu^{II} ion in this complex is four-coordinate and is slightly distorted square planar geometry.

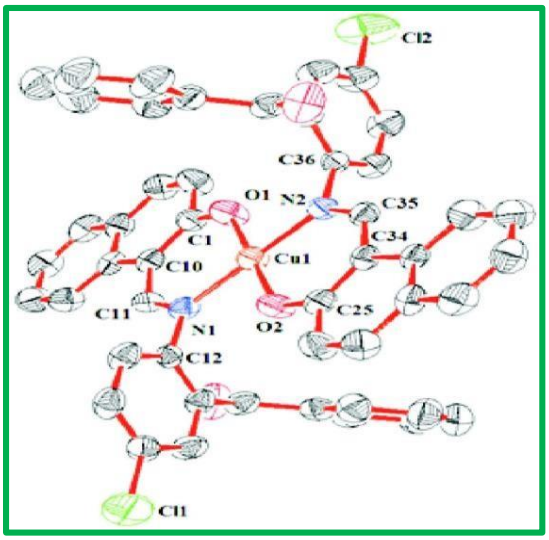

Figure 4.3 ORTEP and atom-numbering scheme for $[(L)_2Cu]$ complex. Hydrogen atoms are omitted for clarity.

Table 4.2 Selected bond distances (Å) and angles (deg) for $[(L)_2Cu]$.

Atoms	**Distance**	**atoms**	**Distance**
Cu1-N1	1.981(4)	C10-C11	1.428(7)
Cu1-N2	1.977(5)	C25-C34	1.397(8)
Cu1-O1	1.880(3)	C34-C35	1.406(7)
Cu1-O2	1.875(3)	N1-C11	1.306(6)
O1-C1	1.301(6)	N1-C12	1.449(7)
O2-C25	1.309(6)	N2-C35	1.309(6)
C1-C10	1.396(8)	N2-C36	1.447(7)
Atoms	**Angles**	**Atoms**	**Angles**
O1-Cu1-N1	90.6(2)	Cu1-N1-C11	125.6(3)
O1-Cu1-N2	89.9(2)	Cu1-N1-C12	120.4(3)
O2-Cu1-N1	88.9(2)	C1-C10-C11	120.9(4)
O2-Cu1-N2	90.7(2)	N1-C11-C10	126.7(5)
Cu1-O1-C1	130.6(4)	N2-C35-C34	127.3(4)

The asymmetric unit of $[(L)_2Cu]$ complex consist of half molecule where Cu^{II} occupies the special position. The Cu-O and Cu-N_{im} distances are 1.873(2) Å and 1.297(4) Å and consistent with the coordination of phenolato oxygen to Cu^{II} square planar.[31]

4.3.4 Selective oxidation of benzyl alcohol

Selective oxidation of benzyl alcohols to the benzaldehyde is a significant and widely used reaction in laboratory scale organic synthesis as well as in large scale in chemical industry[32–35]. The complex $[(L)_2Cu]$ have been scrutinized for the per oxidative oxidation of benzyl alcohol with H_2O_2 (30%) as the oxidant in aqueous acetonitrile mixture.

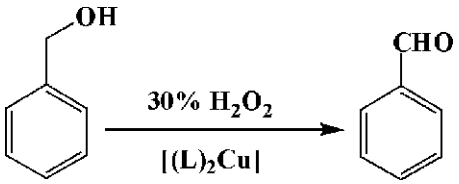

The reaction has been optimized by varying the relative proportions of hydrogen peroxide with respect to the catalyst and also by varying the reaction time and temperature. The isolated yield of the benzaldehyde after one hour of reaction time was 60% using $[(L)_2Cu]$ catalyst.

4.3.5 Fluorescence spectral studies

The photoluminescence properties of the ligand HL and the $[(L)_2Cu]$ complex were investigated in acetonitrile (**Figure 4.4**). The ligand HL exhibited moderate intensity emission near 500 nm upon excitation at 385 nm.

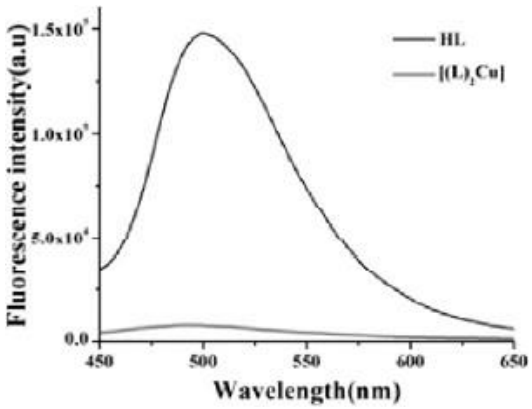

Figure 4.4 Emission spectra of HL and $[(L)_2Cu]$ in CH_3CN.

The peak at 595 nm is arises due to the excited state intramolecular proton transfer (ESIPT) followed by excited state intramolecular charge transfer (ESICT) from the phenol -OH to the imine nitrogen atom (**Scheme 4.3**).[36–38] On the other hand, $[(L)_2Cu]$ complex exhibited quenched emission at 500 nm in acetonitrile. Coordination of Cu^{2+} involving the imine nitrogen atom inhibits the ESIPT which resulted in decrease in the emission at 500 nm.

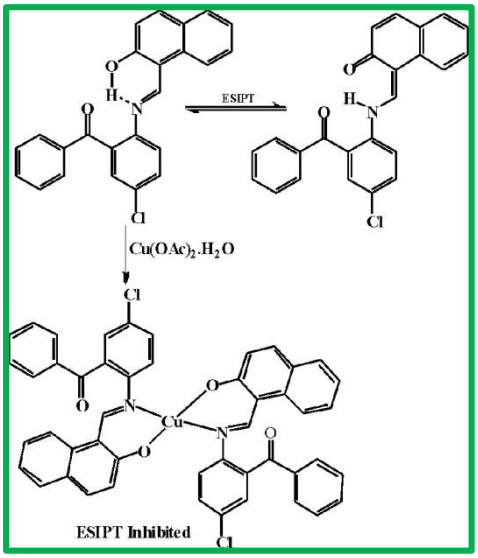

Scheme 4.3 Possible emission mechanism of HL to Cu^{2+}.

4.4 Conclusions

In summary, we have successfully synthesized and characterized Schiff base copper(II) complex incorporating N,O donor ligand. The structure of the complex $[(L)_2Cu]$ was confirmed by X-ray crystallography. As application, the synthesized $[(L)_2Cu]$ complex have been used as catalyst in the oxidation of benzyl alcohol to benzaldehyde. In addition we have also examined the fluorescence properties of the ligand and complex. The ligand exhibited photoluminescence property due to the excited state intramolecular proton transfer (ESIPT).

References

(1) H. Achira, Y. Hoga, I. Yoshikawa, T. Mutai, K. Matsumura and H. Houjou, *Polyhedron*, 2016, **113**, 123-131.

(2) Z. P. Zheng, Q. Wei, W. X. Yin, L. T. Wan, X. Huang, Y. Yu and Y. P. Cai, *RSC Adv.*, 2015, **5**, 27682- 27689.

(3) A. E. Vaughn, D. B. Bassil, C. L. Barnes, S. A. Tucker and P. B. Duval, *J. Am. Chem. Soc*., 2006, **128**, 10656-10657.

(4) F. X. Shen, W. Huang, X. C. Huang, S. Peng and D. Y. Wu, *Transition Met. Chem*., 2015, **40**, 681-689.

(5) D. N. Woodruff, R. E. P. Winpenny and R. A. Layfield, *Chem. Rev*., 2013, **113**, 5110-5148.

(6) D. Y. Wu, O. Sato, Y. Einaga and C. Y. Duan, *Angew. Chem*., 2009, **48**, 1475-1478.

(7) R. Ruamps, L. J. Batchelor, R. Maurice, N. Gogoi, P. Jimenez-Lozano, N. Guihery, C. de Graaf, A. L. Barra, J. P. Sutter and T. Mallah, *Chem. Eur. J*., 2013, **19**, 950-956.

(8) K. C. Gupta and A. K. Sutar, *Coord. Chem. Rev*., 2008, **252**, 1420-1450.

(9) R. Drozdzak, B. Allaert, N. Ledoux, I. Dragutan, V. Dragutan and F. Verpoort, *Coord. Chem. Rev*., 2005, **249**, 3055-3074.

(10) E. Tsuchida and K. Oyaizu, *Coord. Chem. Rev*., 2003, **237**, 213-228.

(11) B. Sarkar, S. Konar, C. J. Gomez-Garcia and A. Ghosh, *Inorg. Chem*., 2008, **47**, 11611-11619.

(12) F. C. Frederick, W. M. Coleman and L. T. Taylor, *Inorg. Chem*., 1983, **22**, 792-795.

(13) T. Kitazawa, S. Nishikiori, R. Kuroda and T. Iwamoto, *J. Chem. Soc., Dalton Trans*., 1994, 1029-1036.

(14) D. N. Dybtsev, H. Chun, S. H. Yoon, D. Kim and K. Kim, *J. Am. Chem. Soc*., 2004, **126**, 32-33.

(15) L. Pan, M. B. Sander, X. Y. Huang, J. Li, M. Smith, E. Bittner, B. Bochrath and J. K. Johnson, *J. Am. Chem. Soc*., 2004, **126**, 1308-1309.

(16) L. Que (Jr.) and W. B. Tolman, *Angew. Chem*., 2002, **114**, 1160-1185.

(17) B. Dede, I. Ozmen and F. Karipcin, *Polyhedron*, 2009, **28**, 3967-3974.

(18) M. Fujita, Y. J. Kwon, S. Washizu and K. Ogura, *J. Am. Chem. Soc*., 1994, **116**, 1151-1152.

(19) (a) Z. H. Chohan and S. K. A. Shorazi, *Synth. React. Inorg. Metal-Org. Chem*., 1999, **29**, 105-118; (b) R. Parrey and A. A. Hashmi, *Mor. J. Chem*., 2015, **3**, 147-151.

(20) R. Lontie, "Copper Proteins and Copper Enzymes", CRC Press, Boca Raton, 1984, **3**.

(21) G. Evano, N. Blanchard and M. Toumi, *Chem. Rev.*, 2008, **108**, 3054-3131.

(22) I. Bertini, "Bioinorganic Chemistry", University Science Books, Mill Valley, 1994.

(23) E. I. Solomon, M. J. Baldwin and M. D. Lowery, *Chem. Rev*., 1992, **92**, 521-542.

(24) J. March, "Advanced Organic Chemistry", John Wiley, New York, 1992.

(25) M. Hudlicky, "Advanced Organic Chemistry", ACS, Washington, DC, 1990.

(26) A. Rezaeifard, M. Jafarpour, A. Naeimi and R. Haddad, *Green Chem*., 2012, **14**, 3386-3394.

(27) J. U. Ahmad, P. J. Figiel, M. T. Räisänen, M. Leskelä and T. Repo, *Appl. Catal. A: Gen.*, 2009, **371**, 17-21.

(28) K. K. Sarker, S. Saha Halder, D. Banerjee, T. K. Mondal, A. R. Paital, P. K. Nand, P. Raghavaiah and C. Sinha, *Inorg. Chim. Acta*, 2010, **363**, 2955-2964.

(29) G. M. Sheldrick, *Acta Cryst. A*, 2008, **64**, 112-122.

(30) G. M. Sheldrick, SHELEXL-97 and SHELXL-97, *Program for Crystal Structure Solution and Refinement*, University of Gottingen, Gottingen, 1997.

(31) S. P. Parua, P. Mondal, P. Pattanayak and S. Chattopadhyay, *Polyhedron*, 2015, **89**, 142-148.

(32) A. Antinolo, F. C. Hermosilla, V. Cadierno, J. Alvarez and A. Otero, *Chem.Cat.Chem*, 2012, **4**, 123-128.

(33) B. Singaram, M. V. Rangaishenvi and H. C. Brown, *J. Org. Chem*., 1991, **56**, 1543-1549.

(34) A. Abad, C. Almela, A. Corma and H. Garcia, *Tetrahedron*, 2006, **62**, 6666-6672.

(35) R. R. Fernandesa, J. Lasri, M. F. C. Guedes da Silva, J. A. L. Silva, F. J. J. R. Silva and A. J. L. Pombeiro, *J. Mol. Catal. A: Chem*., 2011, **351**, 10.

(36) S. Basu Roy, A. Maity and K. K. Rajak, *Inorg. Chem. Commun.*, 2017, **76**, 81-86.

(37) S. Goswami, S. Maity, A. C. Maity, A. K. Das, B. Pakhira, K. Khanra, N. Bhattacharyya and S. Sarkar, *RSC Adv.*, 2015**, 5**, 5735-5740.

(38) A. Jana, B. Das, S. K. Mandal, S. Mabhai, A. R. Khuda-Bukhshe and S. Dey, *New J. Chem.*, 2016, **40**, 5976-5984.

Chapter 5

Synthesis, characterization and DFT studies of a Cu (II) complex bearing O, N coordinating azo appended Schiff base ligand

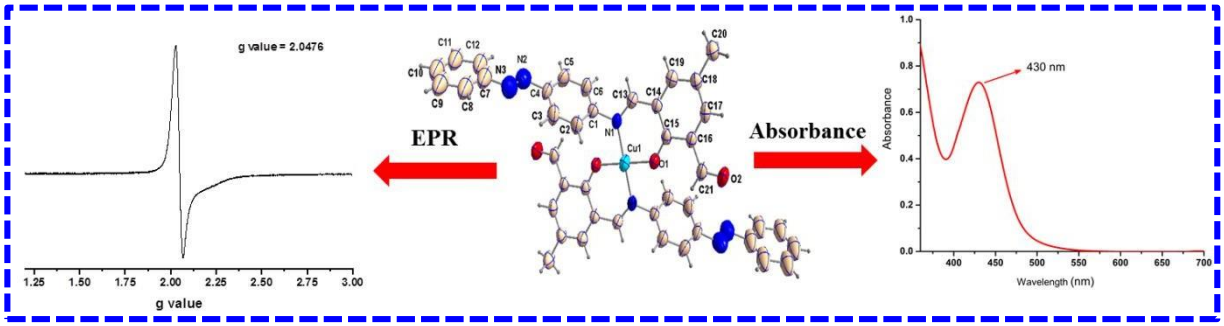

Abstract:

2-hydroxy-5-methyl-3-(((4-((E)-phenyldiazenyl)phenyl)imino)methyl) ligand (HL_1) was synthesized in this chapter. The ligand reacted with copper acetate to afford the new complexes of composition $[(L_1)_2Cu]$ where it binds the Cu(II) centres in bidentate (N, O) fashion. The complexes were characterized by analytical and spectroscopic studies. X-ray structure of $[(L_1)_2Cu]$ was determined to confirm the molecular species unequivocally.

5.1 Introduction

Synthesis of metal organic hybrid core having distinct photophysical properties has garnered considerable attention in recent years due to their importance in designing sensors and optical materials.[1] On the other hand, the azo compounds often show very reach photochromic properties. Although, a few azo ligands have been utilised as chemosensor for anions and cations.[2-10] 2,6-Diformyl-4-methylphenol is one of the important aromatic aldehydes that has been used to synthesize various compartmental Schiff base ligands[11, 12] to explore their metal complexes. It exhibited fascinating fluorescence properties due to formation of keto tautomer upon excitation. Therefore, we contemplated to synthesize new fluorescent azo ligand system (HL_1) by the condensation of 2-hydroxy-5-methylisophthalaldehyde with (E)-4-(phenyldiazenyl) aniline. It was presumed that the studies on photoluminescence properties of ligand and its metal complexes would be interesting. Again, there is a scope of further extending the delocalization within the ligand framework exploiting the reactivity of free formyl functionality of ligand. Copper ion was chosen to study the coordination chemistry incorporating ligand system with the objectives to unfold the structure, coordination mode and photoluminescence behavior of the ligand and the complex. Herein, the synthesis and structure of a new ligand system HL_1 and its Cu(II) complex have been described. Redox, absorption properties of new copper complex have also been reported.

5.2 Experimental Section

5.2.1 Materials and Methods

The solvents used for all the reactions were of reagent grade (E. Merck, India) and were purified and dried by reported procedure. Copper acetate monohydrate was purchased from Sisco Research Laboratories (SRL), India. Infrared spectra were recorded on a Perkin-Elmer L120-00A FT-IR spectrometer with the samples prepared as KBr pellets. Electronic mspectra were recorded on a Shimadzu UV-1800 PC spectrophotometer.

5.2.2 Synthesis of ligand HL_1

2-hydroxy-5-methylisophthalaldehyde (0.328 g, 2 mmol) and (E)-4-(phenyldiazenyl)aniline (0.394 g, 2 mmol) were heated to reflux in diethyl ether (40 ml) for 6 h. The bright yellow solid product was obtained as micro crystals which were collected by filtration and thoroughly washed diethyl ether and dried under vacuum (**Scheme 5.1**).

^{1}H NMR (300 MHz), $CDCl_3$, δ (ppm): 10.515 (1H, s, –CHO), 8.716 (1H, s, –N=CH), 8.009 (1H, s, –OH), 7.988−6.078 (11H, m, Ar–H), 2.143 (3H, s, $–CH_3$) (**Figure 5.1**). (ESI –MS (positive) in MeOH: The base peak was detected at *m/z* = 344, corresponding to $[L_1 + H]^+$ (**Figure 5.2**). IR (KBr, ν_{max} / cm^{-1}): 3031 (broad from bound OH moiety), 1672 (C=O), 1569 (imine C=N) (**Figure 5.3**).

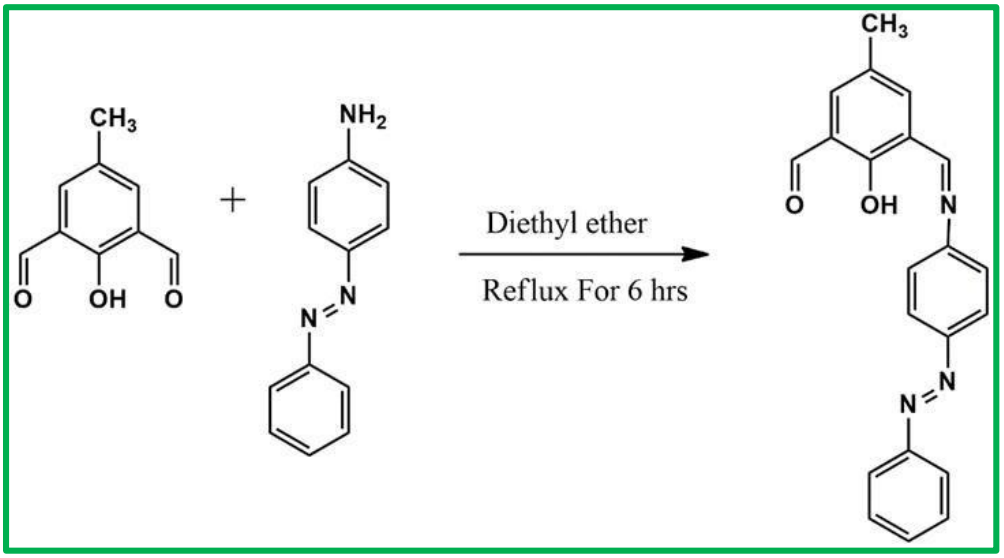

Scheme 5.1 Synthesis of ligand HL_1.

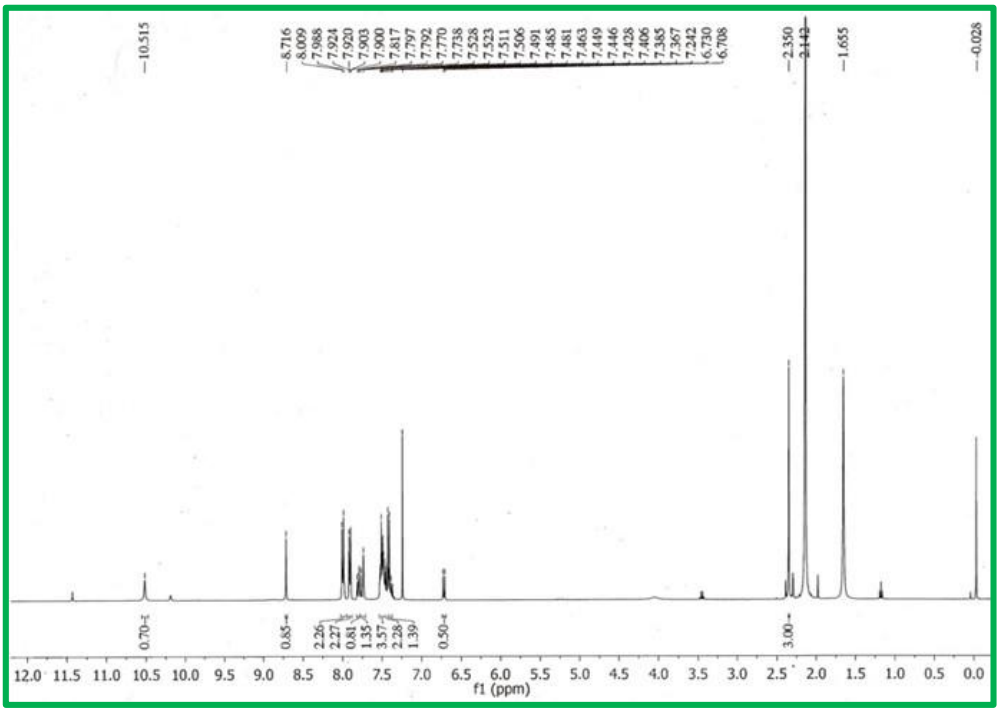

Figure 5.1 ^{1}H-NMR spectrum of ligand HL_1 in $CDCl_3$.

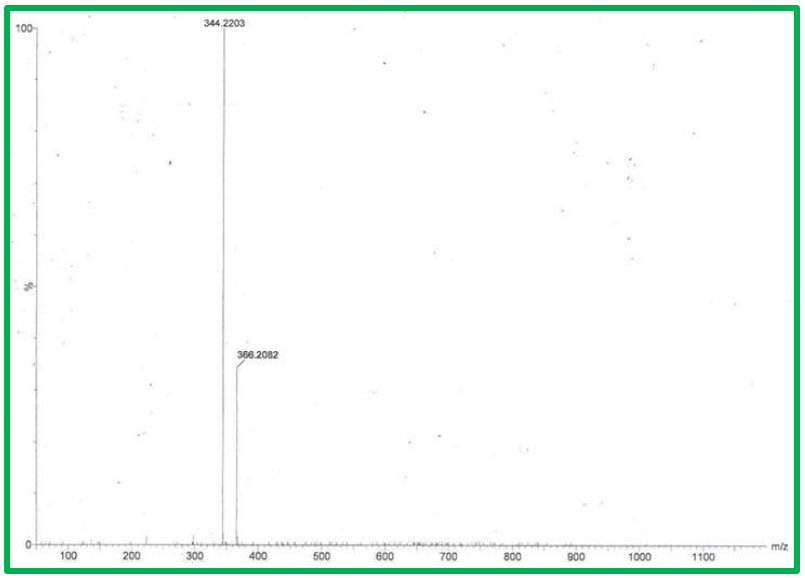

Figure 5.2 Mass spectrum of ligand HL_1 in MeOH.

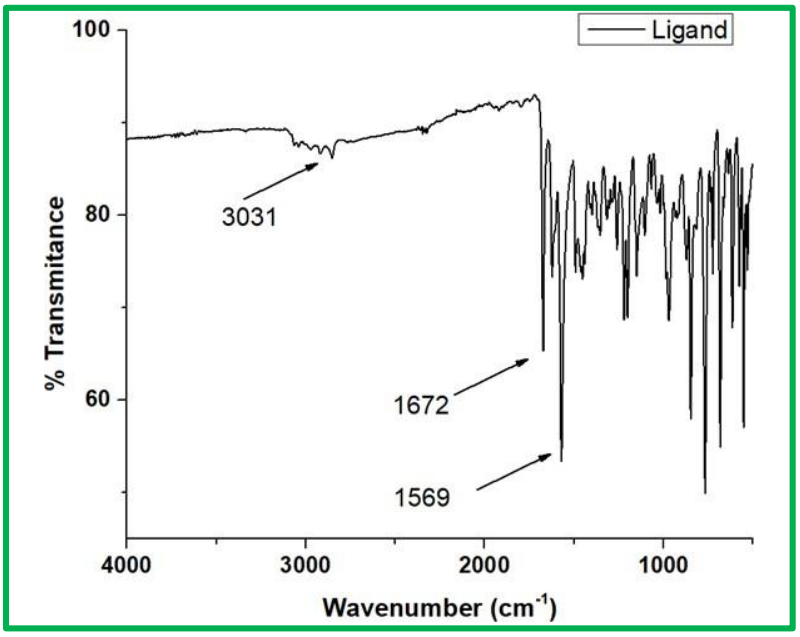

Figure 5.3 IR spectrum of ligand HL_1.

5.2.3 Synthesis of $[(L_1)_2Cu]$ complex

5 ml ethanolic solution of 45 mg (0.247 mmol) $Cu(OAc)_2$. H_2O, 10 ml ethanol solution of 0.519 mmol of HL_1 was added and the mixture was stirred for 6 h. Then the product was precipitated which was collected by filtration and was washed with petroleum ether and hexane. The precipitate then recrystallized from a dichloromethane-hexane solvent mixture (**Scheme 5.2**).

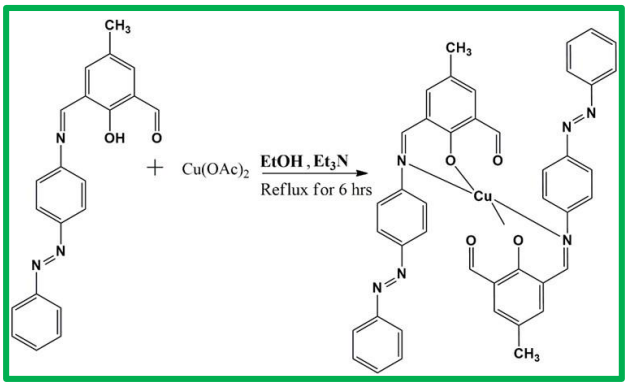

Scheme 5.2 Synthesis of $[(L_1)_2Cu]$ complex.

5.2.4 X-Ray structure determination of $[(L_1)_2Cu]$:

Single crystals of $[(L_1)_2Cu]$ was grown by slow diffusion of hexane in dichloromethane solution at 25ºC. Data were collected on a Brucker SMART CCD diffractometer using Mo-Kα monochromator (λ = 0.71073). Structure solutions were performed using Shelx 97 PC version program. Full matrix least square refinements on F^2 were performed using SHELXL-97 program. All the non-hydrogen atoms were refined anisotropically using full-matrix least squares method. Atomic coordinates and isotropic thermal parameters of $[(L_1)_2Cu]$ are given in **Table 5.1**.

Table 5.1 Crystallographic data for the complex $[(L_1)_2Cu]$.

Empirical formula	$C_{42}H_{32}N_6CuO_4$
Formula weight	749.97
Temperature/K	296
Crystal system	Monoclinic
Space group	C2/c
a/Å	30.300(3)
b/Å	6.9012(6)
c/Å	20.180(2)
α/°	90
β/°	120.461(5)
γ/°	90
Volume/$Å^3$	3637.3(6)
Z	8
$\rho_{calc}g/cm^3$	1.370
μ/mm^{-1}	0.652
F(000)	1551.4
Goodness-of-fit on F^2	1.084
R_1	0.0577
wR_2	0.01811

5.3 Results and Discussion

5.3.1 Synthesis of ligand and complex

The HL_1, ligand was prepared by the condensation reaction of 2-hydroxy-5-methylisophthalaldehyde with (E)-4-(phenyldiazenyl)aniline in 1:1 M ratio in diethyl ether (**Scheme 5.1**). The reaction of the HL_1 ligand with $Cu(OAc)_2.H_2O$ in ethanol afforded complex $[(L_1)_2Cu]$ (**Scheme 5.2**). The complex $[(L_1)_2Cu]$ was paramagnetic matching with one unpaired electron as expected for Cu^{II} metal ion. The suitable crystal of $[(L_1)_2Cu]$ complex for X-ray studies were grown from dichloromethane-hexane solvent mixture.

5.3.2 Electronic absorption spectra

The UV-vis absorption spectra of the ligand HL_1 (**Figure 5.4A**) and complex $[(L_1)_2Cu]$ (**Figure 5.4B**) were recorded in CH_2Cl_2 at 298 K by employing concentrations in the range ~60 µM. A broad band in the range 380 nm was observed for ligand.

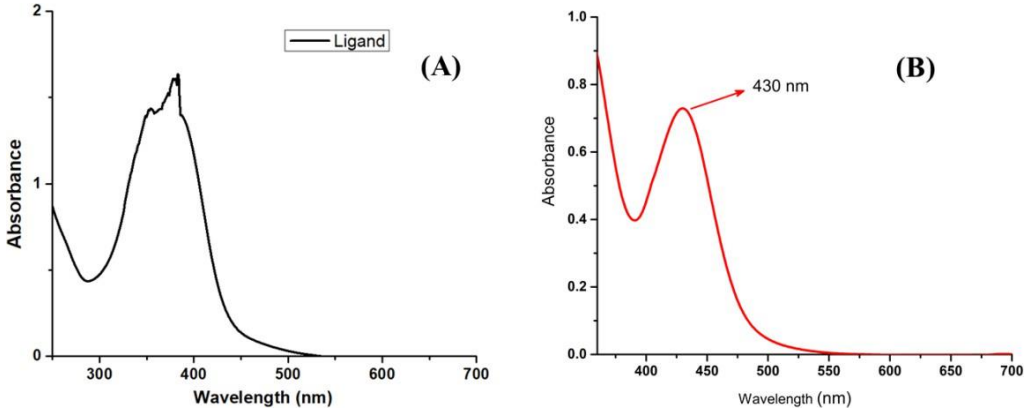

Figure 5.4 UV-Vis spectra of (A) ligand HL_1 and (B) complex $[(L_1)_2Cu]$ in CH_2Cl_2.

5.3.3 X-Ray structure of $[(L_1)_2Cu]$

Single crystals suitable for X-ray diffraction were obtained by diffusion of hexane into dichloromethane solution at ambient temperature. The complexes appeared as dark orange hexagonal shaped crystals. Complex $[(L_1)_2Cu]$ crystallized with C2/c space group in monoclinic crystal system. In the complex the ligand bonded to the metal centre as O, N coordinating monoanionic ligand. The N2–N3 distance is 1.166(6) Å suggesting free azo moiety. The Cu–O bonds are in the trans configuration and the Cu–O distances are shorter than the Cu–N distances. The Cu1–N1 and Cu1–O1 bond emerge at 1.997(3) Å and 1.890(2) Å respectively. The central Cu(II) atom has distorted square planar coordination. The

molecular views of the crystals are shown in **Figure 5.5** and selected bond parameters are listed in **Table 5.2** and **Table 5.3**.

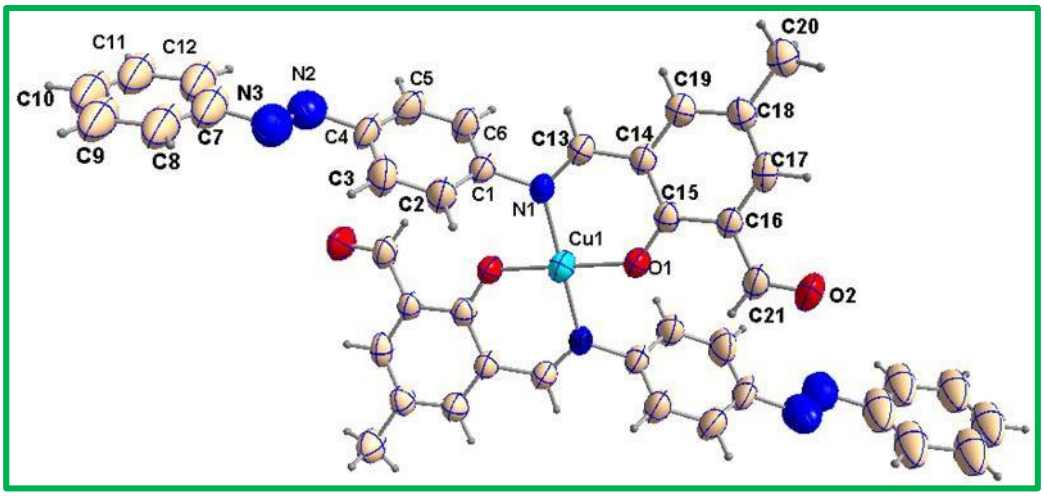

Figure 5.5 Ortep view of complex $[(L_1)_2Cu]$. Atoms are shown as 30% thermal ellipsoids.

Table 5.2 Selected bond distances (Å) for $[(L_1)_2Cu]$.

Atoms	Distance	Atoms	Distance
Cu1-O1	1.890(2)	O1-C15	1.295(4)
Cu1-N1	1.997(3)	N1-C13	1.293(4)
N1-C1	1.446(4)	C14-C13	1.438(4)
O2-C21	1.208(4)	N2-N3	1.166(6)
N2-C4	1.487(6)	N3-C7	1.511(7)

Table 5.3 Selected bond angles (deg) for $[(L_1)_2Cu]$.

O1 Cu1 O1	180.0	C1 N1 Cu1	121.7(2)	O1 Cu1 N1	91.45(10)
O1 Cu1 N1	88.55(10)	O1 C15 C16	119.3(3)	C13 N1 Cu1	123.3(2)
C15 O1 Cu1	128.8(2)	C6 C1 N1	120.6(3)	O1 C15 C14	123.9(3)
C13 N1 C1	115.0(3)	N1 C13 C14	126.5(3)	C2 C1 N1	119.0(3)
C5 C4 N2	114.2(4)	O2 C21 C16	123.9(4)	N2 N3 C7	107.0(5)
C8 C7 N3	109.9(6)	N3 N2 C4	109.0(5)	C12 C7 N3	127.8(6)

5.3.4 EPR Spectra

The ligand was redox innocent in nature, hence EPR silent. The complex was found to be paramagnetic in nature. The EPR spectrum was recorded in CH_2Cl_2 solution at ambient temperature. The EPR spectrum of the

complex exhibited characteristic (g = 2.0476) single line spectrum[13] due to presence of extra one unpaired electron spin (S = ½) ^{63}Cu (I = 3/2). **Figure 5.6** suggested the presence of unpaired electron in the system. The X-band EPR spectra were collected using a Magnettech GmbH MiniScope MS400 spectrometer (fitted with a TC H03 temperature controller), and the microwave frequency was measured with an FC400 frequency counter.

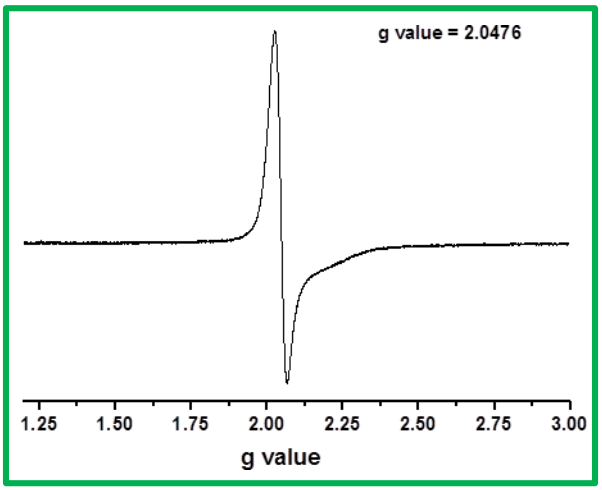

Figure 5.6 EPR spectra of Complex $[(L_1)_2Cu]$ at RT.

5.3.5 Theoretical Calculation

The geometrical structure of the singlet ground state (S_0) were optimized using the density functional theory (DFT)[14] method at the RB3LYP levels of theory. The geometry of the mononuclear Cu(II) complex was fully optimized in solution phase. The absorption spectral properties of the mononuclear Cu(II) complex based on the optimized ground state geometry structure was computed using the time dependent density functional theory (TDDFT)[15] approach in dichloromethane associated with the conductor-like polarizable continuum model (CPCM).[16] In the calculation, the 6-31G+g basis set was used for the C, H, N and O atoms for the optimization of both the ground state geometries. All the calculations were performed using the Gaussian 09W software package.[17] The geometry of the mononuclear Cu(II) complex was fully optimized in solution phase with imposing centre of symmetry constraint. The ground state geometry optimization was performed assuming a doublet ground state (S = 2, $t_{2g}^6e_g^3$). The geometry utilized for the ground state optimization is based on crystal structure parameter of the complex $[(L_1)_2Cu]$ with ligand modification. The optimized bond distances and bond angles of the complex $[(L_1)_2Cu]$ are given in **Table 5.4** and **Table 5.5**. The

optimized geometrical structure of the $[(L_1)_2Cu]$ complex at doublet ground (S_0) state is shown in **Figure 5.7**.

Table 5.4 Calculated bond angles (°) for the complex $[(L_1)_2Cu]$.

Bond Angles (°)		
O1 Cu1 O1 179.97	C1 N1 Cu1 121.21	O1 Cu1 N1 90.51
O1 Cu1 N1 90.50	O1 C15 C16 119.98	C13 N1 Cu1 122.24
C15 O1 Cu1 130.28	C6 C1 N1 121.12	O1 C15 C14 123.27
C13 N1 C1 116.23	N1 C13 C14 128.06	C2 C1 N1 119.19
C5 C4 N2 115.69	O2 C21 C16 123.78	N2 N3 C7 115.32
C8 C7 N3 115.38	N3 N2 C4 115.05	C12 C7 N3 124.66

Table 5.5 Calculated bond lengths (Å) for the complex $[(L_1)_2Cu]$.

Bond lengths (Å)	
Cu1-O1 1.9337	O1-C15 1.2983
Cu1-N1 2.0543	N1-C13 1.3054
N1-C1 1.4286	C14-C13 1.4309
O2-C21 1.2244	N2-N3 1.2583
N2-C4 1.4169	N3-C7 1.4180

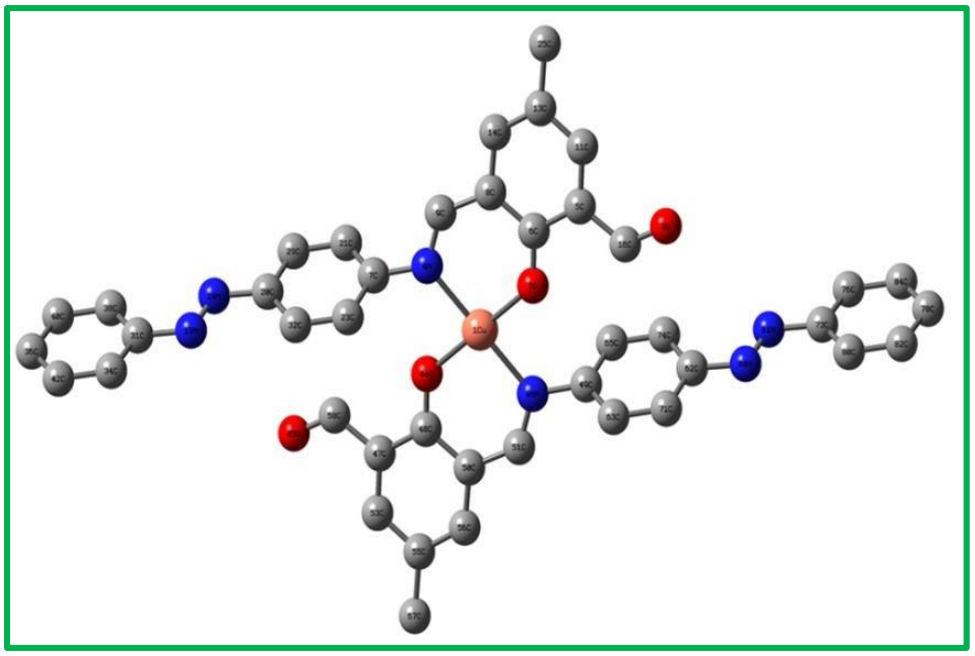

Figure 5.7 Optimised structure of the complex $[(L_1)_2Cu]$.

As depicted, the Cu(II) center of $[(L_1)_2Cu]$ complex displays the distorted square planar geometry with respect to the ligand binding sites at each center. The optimized parameters of the complex $[(L_1)_2Cu]$ matched well with the X-ray crystal structure data. These results clearly represent that there are no significant changes of the ligand framework in the Cu(II) complex. The electron density in HSOMO of $[(L_1)_2Cu]$ complex is mainly due to the major contribution of *p*-cresol moiety and π orbital of phenyl azo fragment of the ligand **(Figure 5.8)**. On the other hand the electron density of LSOMO mainly resides on the metal centre along with small contribution of the π orbital of the ligand.

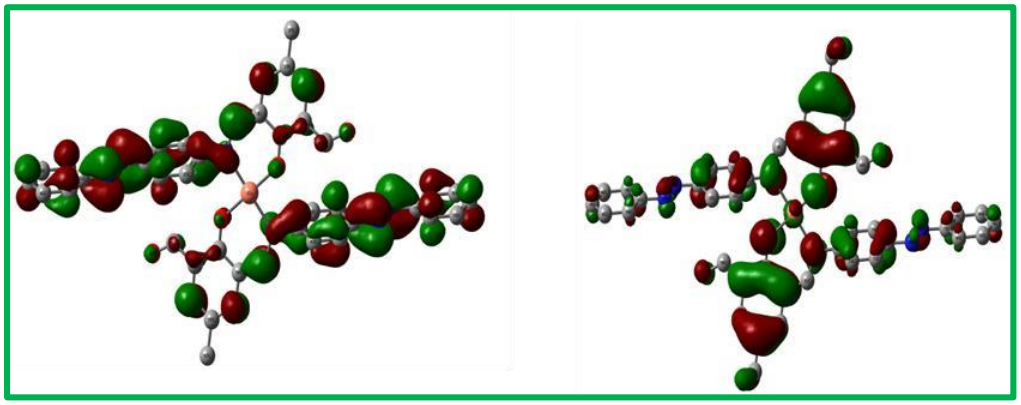

Figure 5.8 Isodensity plot of frontier orbitals of $[(L_1)_2Cu]$ complex.

The electronic spectra of both the ligand and complex $[(L_1)_2Cu]$ were recorded in dichloromethane solution at room temperature. The ligand displayed intense peak at 370 nm. The $[(L_1)_2Cu]$ complex exhibited strong intense peak at 430 nm (**Figure 5.4**).

Table 5.6 Main calculated optical transition for the complex $[(L_1)_2Cu]$ with composition in terms of molecular orbital contribution of the transition, vertical excitation energies, and oscillator strength in acetonitrile.

Composition	Excitation Energy(eV)	Osc. Strength (*f*)	Assign	CI	λ_{exp} (nm)
H-1→ L H-1→ L+4	2.46(502 nm)	0.2765	^{1}MLCT/^{1}ILCT ^{1}MLCT/^{1}ILCT	0.68	475
H→ L+5	4.00(309 nm)	0.0110	^{1}ILCT	0.52	300

In order to elucidate the electronic transitions from a theoretical perspective, TDDFT/B3LYP/CPCM calculation on the optimized geometry of the complex $[(L_1)_2Cu]$ has been performed in dichloromethane. In the TDDFT calculation we have found highly intense

transition at 502 nm (f = 0.2765) corresponds to HOMO-1→ LUMO having ^{1}MLCT character with little ^{1}ILCT (**Table 5.6**). The highest energy band with maxima at 430 nm for complex $[(L_1)_2Cu]$ can rationally be assigned to an admixture of metal-to-ligand charge transfer (^{1}MLCT) transition and spin-allowed π→ π* (ligand-centered, ^{1}ILCT) transitions.

5.4 Conclusions

In summary, a versatile ligand pocket was synthesised and with the ligand mono nuclear Cu(II) complex was reported. The complex showed considerable absorbance characteristics. The redox behaviour was determined using EPR spectroscopy. Theoretical calculation was employed to support the experimental data.

References

(1) J. Shinar (Ed.), Organic Light-Emitting Devices: A Survey, Springer-Verlag, NY, 2004.

(2) A. Hens, P. Mondal and K. K. Rajak, *Polyhedron*, 2015, **85**, 255-266.

(3) J. Wang and C. S. Ha, Tetrahedron, 2010, **66**, 1846-1851.

(4) Y. F. Cheng, D. T. Zhao, M. Zhang, Z. Q. Liu, Y. F. Zhou, T. M. Shu, F. Y. Li, T. Yi and C. H. Huang, *Tetrahedron Lett*., 2006, **47**, 6413-6416.

(5) A. Misra and M. Shahid, *J. Phys. Chem*., 2010, **114**, 16726-16739.

(6) M. Kumar, J. Nagendra Babu, V. Bhalla and A. Dhir, *Inorg. Chem. Commun*., 2009, **12**, 332-335.

(7) X. Lou, J. Qin and Z. Li, *Analyst*, 2009, **134**, 2071-2075.

(8) R. Arabahmadi, M. Orojloo and S. Amani, *Anal. Methods*, 2014, **6**, 7384-7393.

(9) T. Gunnlaugsson and J. P. Leonard, *J. Chem. Soc., Perkin Trans*., 2002, **2**, 1980-1985.

(10) R. Arabahmadi and S. Amani, *J. Coord. Chem*., 2013, **66**, 218-226.

(11) U. Panda and C. Sinha, *J. Indian Chem. Soc*., 2016, **93**, 703–709.

(12) Y. Nakane, T. Takeda, N. Hoshino, K. Sakai and T. Akutagawa, *J. Phys. Chem. A*, 2015, **119**, 6223–6231.

(13) P. S. Subramanian, E. Suresh and D. Srinivas, *Inorg. Chem*., 2000, **39**, 2053–2060.

(14) J. V. Houten and R. J. Watts, *J. Am. Chem. Soc*., 1976, **98**, 4853-4858.

(15) (a) M. E. Casida, C. Jamoroski, K. C. Casida and D. R. Salahub, *J. Chem. Phys*., 1998, **108**, 4439-4449; (b) R. E. Stratmann, G. E. Scuseria and M. J. Frisch, *J. Chem. Phys*., 1998, **109**, 8218-8224; (c) R. Bauernschmitt and R. Ahlrichs, *Chem. Phys. Lett*., 1996, **256**, 454-464.

(16) (a) V. Barone and M. Cossi, *J. Phys. Chem. A*, 1998, **102**, 1995-2001; (b) M. Cossi and V. Barone, *J. Chem. Phys*., 2001, **115**, 4708-4717; (c) M. Cossi, N. Rega, G. Scalmani and V. Barone, *J. Comput. Chem*., 2003, **24**, 669-681.

(17) G. Scalmani, V. Barone, B. Mennucci, G. A. Petersson, H. Nakatsuji, M. Caricato, X. Li, H. P. Hratchian, A. F. Izmaylov, J. Bloino, G. Zheng, J. L. Sonnenberg, M. Hada, M. Ehara, K. Toyota, R. Fukuda, J. Hasegawa, M. Ishida, T. Nakajima, Y. Honda, O. Kitao, H. Nakai, T. Vreven, J. A. Montgomery Jr, J. E. Peralta, F. Ogliaro, M. Bearpark, J. J. Heyd, E. Brothers, K. N. Kudin, V. N. Staroverov, R. Kobayashi, J. Normand, K. Raghavachari, A. Rendell, J. C. Burant, S. S. Iyengar, J. Tomasi, M. Cossi, N. Rega, J. M. Millam, M. Klene, J. E. Knox, J. B. Cross, V. Bakken, C. Adamo, J. Jaramillo, R. Gomperts, R. E. Stratmann, O. Yazyev, A. J. Austin, R. Cammi, C. Pomelli, J. W. Ochterski, R. L. Martin, K. Morokuma, V. G. Zakrzewski, G. A. Voth, P. Salvador, J. J. Dannenberg, S. Dapprich, A. D. Daniels, O. Farkas, J. B. Foresman, J. V. Ortiz, J. Cioslowski and D. J. Fox, Gaussian09, (RevisionA.1), Gaussian, Inc., Wallingford, CT, 2009.

List of Publications

1. **S. Debnath**, T. Das, S. P. Parua and K. K. Rajak, Synthesis, structure and, photophysical and catalytic properties of a copper(II) complex containing bidentate (N,O) Schiff-base ligand, ***J. Indian Chem. Soc.,*** 2018, **95**, 1-6.
2. **S. Debnath**, T. Das, S. P. Parua and K. K. Rajak, Synthesis and characterization of blue-violet emitting iridium(III) complex coordinated via chlorinated ancillary ligand, ***J. Coord. Chem.,*** 2021, **74**, 1399–1413.
3. **S. Debnath**, T. Das, M. Majumder, A. Bhattacharjee, N. Murmu and K. K. Rajak, Synthesis, structure and effects of an azoimine functionalized iridium complex on cancer cells, ***J. Organomet. Chem.,*** 2024, **1011**, 123121.